IChF
Instytut Chemii Fizycznej PAN

PhD Thesis

Nanoarchitectonics of Adaptive Colloidal Langmuir Films at the Air-Water Interface

Rafał Zbonikowski

Instytut Chemii Fizycznej
Polskiej Akademii Nauk

ul. Kasprzaka 44/52

www.ichf.edu.pl

IChF
Institute of Physical Chemistry PAS

Living
Materials
Institute of Physical Chemistry PAS

The doctoral thesis

“Nanoarchitectonics of Adaptive Colloidal Langmuir Films at the Air-Water Interface”

„Nanoarchitektonika adaptacyjnych koloidalnych filmów Langmuira na granicy faz powietrze-woda”

prepared by

Rafał Zbonikowski

within

Warsaw Doctoral School in Natural and BioMedical Sciences
Warsaw-4-PhD

at the Institute of Physical Chemistry, Polish Academy of Sciences,
ul. Kasprzaka 44/52, 01-224 Warszawa
Living Materials Group,

supervised by

dr hab. Jan Jakub Paczesny, prof. IChF

Warsaw,

March 2026

Warsaw-4-PhD
Warsaw Doctoral School
in Natural and BioMedical Sciences

Acknowledgement

Niniejszą pracę dedykuję moim Rodzicom. To dzięki Ich wsparciu, cierpliwości i latom wyrzeczeń mogłem dojść do tego miejsca. Bez Nich nie byłoby to możliwe. Dziękuję całej rodzinie za to, że zawsze mogę na Was liczyć.

Serdeczne podziękowania składam mojemu Promotorowi, dr hab. Janowi Paczesnemu, prof. IChF, za wspólną przygodę, jaką był doktorat w Instytucie Chemii Fizycznej. Dziękuję za wiedzę, zaufanie, wsparcie i za to, jak wiele mogłem się nauczyć – nie tylko w sprawach naukowych.

Chciałbym również podziękować koleżankom i kolegom z Instytutu Chemii Fizycznej PAN za wsparcie i pomoc na różnych etapach mojej pracy. Dziękuję współautorom publikacji za wartościowe dyskusje i wkład w wyniki, które znalazły się w tej rozprawie.

Szczególnie dziękuję wszystkim członkom grupy Living Materials, z którymi miałem przyjemność pracować przez te wszystkie lata. Dzięki Wam czas spędzony w Instytucie nie był tylko pracą, ale również źródłem wielu dobrych wspomnień, do których z całą pewnością będę wracał z uśmiechem. Dziękuję wszystkim za wytrzymywanie ze mną w jednym pokoju/laboratorium, rozmowy na najbardziej niedorzeczne i pokręcone tematy, za szalone pomysły, a jeszcze bardziej za ich wspólną realizację. Dziękuję za wspólne przejazdy koleją dużych prędkości, za Punjabi Tadka, testowanie granic cierpliwości INTP, zdobywanie galaktyk, degustacje papryki i wiele, wiele innych.

I dedicate this thesis to my Parents. It is thanks to their support, patience, and everything they have done for me over the years that I was able to come this far. Without them, this would not have been possible. Thank you to the whole family for always being there for me.

I would like to sincerely thank my supervisor, Professor Jan Paczesny, for his guidance, trust, and support throughout my PhD at the Institute of Physical Chemistry. I am grateful for how much I have learned from him, not only in science but also beyond it.

I would also like to thank my colleagues at the Institute of Physical Chemistry of the Polish Academy of Sciences for their support and help at different stages of my work. I am also grateful to my co-authors for valuable discussions and for their contribution to the results included in this dissertation.

I would especially like to thank all members of the Living Materials group, with whom I have had the pleasure of working over the years. Thanks to you, my time at the Institute was not just about work, but also about many good memories that I will always look back on with a smile. Thank you all for putting up with me in the same room/lab, for conversations on the most absurd and bizarre topics, for the crazy ideas, and even more for bringing them to life together. Thank you for our high-speed train journeys, for Punjabi Tadka, for testing the limits of INTP patience, for conquering galaxies, for pepper testing sessions, and for many, many other things.

This thesis was funded within the OPUS 18 research grant 2019/35/B/ST5/03229 entitled „Dynamic and Responsive Langmuir-Blodgett Films”, funded by the National Science Centre, Poland (Narodowe Centrum Nauki).

NARODOWE CENTRUM NAUKI

Streszczenie

Materiały reagujące na bodźce zewnętrzne, materiały adaptujące się do warunków zewnętrznych oraz interaktywne materiały stanowią zyskujący na znaczeniu kierunek w rozwoju nanotechnologii. Umiejętność konstruowania złożonych układów funkcjonalnych i ich integracja, zwłaszcza z układami biologicznymi, została w 2025 roku zidentyfikowana przez grupę ponad 100 wiodących naukowców, z Chadem A. Mirkinem na czele, jako jedno z głównych wyzwań stojących przed współczesną nanonauką. Podczas gdy takie układy operujące w trzech wymiarach są intensywnie badane, dwuwymiarowe i pseudo-dwuwymiarowe warstwy na granicy faz pozostają wciąż słabo poznane. Cienkie filmy, takie jak błony komórkowe – są kluczowymi elementami kompartmentalizacji i funkcjonalizacji organizmów żywych, jednakże względnie niewiele jest prób stworzenia sztucznych i responsywnych układów tego typu. Zmniejszanie grubości użytej warstwy materiału jest z kolei istotne z punktu widzenia przemysłu, zwłaszcza w takich obszarach jak powłoki funkcjonalne, fotowoltaiki czy kataliza.

Niniejsza rozprawa doktorska ma na celu wyjść naprzeciw wyżej wymienionym problemom, wnosząc wkład w rozwój nanoarchitektoniki koloidalnych filmów Langmuira reagujących na bodźce zewnętrzne.

Praca przedstawia aktualny obraz nanotechnologii jako dziedziny nauki oraz po krótce omawia ją w ujęciu makroekonomicznym. W dalszej kolejności wprowadza i omawia realia tworzenia responsywnych, adaptujących się dwuwymiarowych oraz pseudo-dwuwymiarowych układów, ze szczególnym naciskiem na zasady ich działania oraz kluczowe aspekty projektowania.

Część eksperymentalna skupia się na opisie układu w opartego o nanocząstki pokryte krótkimi polimerami termoresponsywnymi (PNIPAM, 24 mery). Badania podzielono na dwie części: pierwsza z nich dotyczy opisu właściwości układu działającego na granicy faz powietrze-woda; druga natomiast analizuje wzrost złożoności układ, przez zwiększenie siły jonowej subfazy (zmieniając wodę na roztwór KCl).

Badane układy wykazywały szereg nietypowych zachowań, m. in. spadek ciśnienia powierzchniowego przy wzroście temperatury, agregację nanocząstek poniżej ich dolnej krytycznej temperatury roztworu (odwrotnie niż ma to miejsce dla użytego wolnego polimeru) oraz wzrost odległości miedzy nanocząstkami przy tym samym ciśnieniu powierzchniowych, pomimo ekranowania oddziaływań elektrostatycznych i skrócenia promienia Debye'a.

Celem wyjaśnienia powyższych obserwacji, w rozprawie analizowane są właściwości fizykochemiczne prezentowanych układów, w tym reologia powierzchniowa. Uzyskane w ten sposób dane nie tylko dają wgląd w działanie układu, ale stanowią wkład w rozwój nanoarchitektoniki filmów Langmuira.

Abstract

Stimuli-responsive, adaptive, and interactive materials are an increasingly important direction in nanotechnology. The capability to construct complex functional systems and integrate them with biological systems, in particular, was identified by over 100 prominent nanoscientists, led by Chad A. Mirkin, as one of the main challenges in modern nanotechnology (2025). While three-dimensional systems are being intensively developed, two-dimensional systems operating at fluid-fluid interfaces remain comparatively underexplored. Thin films, such as membranes, are key components of compartmentalisation and functionalisation of living organisms; examples of artificial responsive structures of this type are limited. On the other hand, reducing the material's thickness is of interest to industry in fields such as functional coating, photovoltaics, and catalysis.

This thesis aims to address the abovementioned issues by developing nanoarchitectonics of stimuli-responsive colloidal Langmuir films. Nanoarchitectonics refers to the rational design of the properties and functions of nanomaterials by tuning the interactions and nanoscale phenomena within a system. In parallel, the Langmuir trough is a well-defined platform for investigating interactions and interfacial phenomena in nanoparticle monolayers.

The thesis first outlines the current outlook on nanotechnology as a branch of science and briefly presents its macroeconomic perspective. Then, stimuli-responsive and adaptive 2D and pseudo-2D systems are introduced, with emphasis on their principles and key design aspects.

The experimental part focuses on a system based on nanoparticles capped with short thermoresponsive oligomers (PNIPAM, 24 monomer units). The study is divided into two parts: the first examines the properties of a system operating at the air-water interface, and the second investigates the increased complexity introduced by increasing ionic strength in the subphase (replacing the subphase with a KCl solution).

The investigated systems exhibit several counterintuitive behaviours, including a decrease in surface pressure upon heating, aggregation of nanoparticles below their lower critical solution temperature (opposite to the behaviour of the used thermoresponsive polymer), and increased interparticulate distances at the same surface pressures despite electrostatic screening and a decrease in the Debye length.

To rationalise these observations, the thesis investigates physicochemical properties, including surface rheology, to explain them and provide data useful for further development in nanoarchitectonics of Langmuir films.

List of Achievements

† equal contribution
* corresponding author

Publications Included in this Thesis

(1) **Zbonikowski, R.**†; Mente, P.†; Bończak, B.†; Paczesny, J.* Adaptive 2D and Pseudo-2D Systems: Molecular, Polymeric, and Colloidal Building Blocks for Tailored Complexity. *Nanomaterials* **2023**, *13* (5), 855. https://doi.org/10.3390/nano13050855.

(2) **Zbonikowski, R.**; Iwan, M.; Paczesny, J.* Stimuli-Responsive Langmuir Films Composed of Nanoparticles Decorated with Poly(N-Isopropyl Acrylamide) (PNIPAM) at the Air/Water Interface. *ACS Omega* **2023**, *8* (26), 23706–23719. https://doi.org/10.1021/acsomega.3c01862.

(3) **Zbonikowski, R.***; Aryanfar, A.; Iwan, M.; Presselt, M.; Paczesny, J.* Langmuir Nanoarchitectonics of Thermoresponsive Adaptive System of PNIPAM-Decorated Nanoparticles Induced by the Ionic Strength of the Subphase. *The Journal of Physical Chemistry C* **2025**. https://doi.org/10.1021/acs.jpcc.5c02555.

Other Publications

(4) Stasiewicz, K. A.*; Jakubowska, I.; Moś, J. E.; Marć, P.; Paczesny, J.; **Zbonikowski, R.**; Jaroszewicz, L. R. Optical Properties of a Tapered Optical Fiber Coated with Alkanes Doped with Fe_3O_4 Nanoparticles. *Sensors* **2022**, *22* (20). https://doi.org/10.3390/s22207801.

(5) Wdowiak, M.; Mierzejewski, P. A.; **Zbonikowski, R.**; Bończak, B.; Paczesny, J.* Congo Red Protects Bacteriophages against UV Irradiation and Allows for the Simultaneous Use of Phages and UV for Membrane Sterilization. *Environ. Sci.: Water Res. Technol.* **2023**, *9* (3). https://doi.org/10.1039/d2ew00913g.

(6) Ochirbat, E.†; **Zbonikowski, R.**†; Sulicka, A.; Bończak, B.; Bonarowska, M.; Łoś, M.; Malinowska, E.; Hołyst, R.; Paczesny, J.* Heteroaggregation of Virions and Microplastics Reduces the Number of Active Bacteriophages in Aqueous Environments. *J Environ Qual* **2023**, *52* (3), 665–677. https://doi.org/10.1002/jeq2.20459.

(7) Niewczas, M.; Stasiewicz, K. A.*; Przybysz, N.; Pakuła, A.; Paczesny, J.; **Zbonikowski, R.**; Dziaduszek, J.; Kula, P.; Jaroszewicz, L. R. Technology and Research on the Influence of Liquid Crystal Cladding Doped with Magnetic Fe_3O_4 Nanoparticles on Light Propagation in an Optical Taper Sensor. *Advanced Optical Technologies* **2024**, *13* (July), 1–14. https://doi.org/10.3389/aot.2024.1422695.

(8) Maleki-Ghaleh, H.*; Kamiński, B.; Moradpur-Tari, E.; Raza, S.; Khanmohammadi, M.; **Zbonikowski, R.**; Shakeri, M. S.; Siadati, M. H.; Akbari-Fakhrabadi, A.; Paczesny, J.* Visible Light-Sensitive Sustainable Quantum Dot Crystals of Co/Mg Doped Natural Hydroxyapatite Possessing Antimicrobial Activity and Biocompatibility. *Small* **2024**. https://doi.org/10.1002/smll.202405708.

(9) **Zbonikowski, R.*** What Influences the Number of Citations of Scientific Articles? Study on Colloid and Interface Science. *Scientometrics* **2025**, https://doi.org/10.1007/s11192-025-05311-4.

This article is based on the Bachelor's thesis entitled "*Co wpływa na liczbę cytowań artykułów naukowych?*" defended at the Faculty of Economic Sciences, University of Warsaw in 2023.

(10) Wdowiak, M.; Raza, S.*; Grotek, M.; **Zbonikowski, R.**; Nowakowska, J.; Doligalska, M.*; Cai, N.; Luo, Z.; Paczesny, J.* Phage/Nanoparticle Cocktails for a Biocompatible and Environmentally Friendly Antibacterial Therapy. *Appl Microbiol Biotechnol* **2025**, *109* (1), 129. https://doi.org/10.1007/s00253-025-13526-x.

(11) Ochirbat, E.†; **Zbonikowski, R.**†; Folga, M.; Bonarowska, M.; Paczesny, J.* Microplastics of Broad Size Range Reduce Bacteriophage Activity in Aqueous Environments. *J Phys Chem B* **2025**, *129* (24), 6100–6110. https://doi.org/10.1021/acs.jpcb.5c01316.

(12) Borkenhagen, A.; Wolska-Pietkiewicz, M.*; Binkiewicz, I.; Richter, Ł.; **Zbonikowski, R.**; Paczesny, J.*; Lewiński, J.* Unraveling the Influence of the Anchored Headgroup and Ligand Tail Group Length on the Self-Assembly of ZnO NCs at the Air–Water Interface. *ACS Appl Mater Interfaces* **2025**, *17* (24), 36212–36225. https://doi.org/10.1021/acsami.5c07324.

(13) Korec-Kosturek, J.*; Niewczas, M.; Dziaduszek, J.; Kula, P.; **Zbonikowski, R.**; Paczesny, J.; Stasiewicz, K. A. Investigation of the Ability to Manipulate Light Polarization Properties in a Liquid Crystal Cell Filled with Ferronematic Material through Electric and Magnetic Fields. *Bulletin of the Polish Academy of Sciences Technical Sciences* **2025**, 154724–154724. https://doi.org/10.24425/bpasts.2025.154724.

(14) Maleki-Ghaleh, H.*; Paczesny, J.; Shahriyari, F.; Khanmohammadi, M.; Swieszkowski, W.; Volpic, M.; Fallah, A.; Dargahi, Z.; Khademi-Azandehi, P.; **Zbonikowski, R.**; Zarrabi, A.; Siadati, M. H.; Akbari-Fakhrabadi, A.; Adibkia, K.* Bioactive Copper-Doped Natural Hydroxyapatite Quantum Dots/Graphene Oxide Nanocomposites in 3D-Printed PCL Scaffolds for Superior Osteogenic and Angiogenic Performance in Bone Tissue Engineering. Accepted in *Advanced Healthcare Materials.*

Submitted Manuscripts

(15) Dargahi, Z.*; Marynowski, W.; Moradpur-Tari, E.; Raza, S.; **Zbonikowski, R.**; Akbari-Fakhrabadi, R.; Lewiński, J.; Maleki-Ghaleh, H.; Paczesny, J.* Sonochemical synthesis of cobalt-doped barium titanate nanoparticles for visible-light applications: catalytic and antimicrobial properties. Submitted to *Surfaces and Interfaces*.

Patent Applications

(16) **Zbonikowski R.**; Adamkiewicz W.; Paczesny J.; Polish patent application P.450044: „*Waga i koryto Langmuira, zestaw zawierający wagę i koryto Langmuira, sposób badania albo organizacji warstwy typu warstwy Langmuira i zastosowanie zestawu do badania albo organizacji warstw typu Langmuira na granicy faz w polu elektrycznym z kontrolą powierzchni i jednoczesnym pomiarem ciśnienia powierzchniowego*". Submitted on 26.10.2024.

Table of Contents

Acknowledgement 3
Streszczenie 7
Abstract 8
List of Achievements 9
Publications Included in this Thesis 9
Other Publications 9
Submitted Manuscripts 10
Patent Applications 10
Preface 15
Introduction 17
Literature Review 21
1. Nanotechnology 21
1.1. Did Nanotechnology Deliver on Its Expectations? 22
2. Adaptive 2D and Pseudo-2D Systems 29
2.1. Introduction 29
2.2. Dynamic, Adaptive, or Stimuli-Responsive? 30
3. Design Principles of Adaptive 2D and Pseudo-2D Systems 33
3.1. Classification of 2D Systems Based on a Type of Building Blocks 34
3.2. Adaptive Colloidal Langmuir Films 40
3.3. Interfacial Phenomena and Interactions between Particles at Interfaces 42
4. Langmuir Trough and Interfacial Phenomena 44
4.1. A Brief History of Langmuir Films 44
4.2. Nanoarchitectonics in Langmuir Films 45
4.3. Historical and Modern Construction of a Langmuir Trough 45
4.3.1. Langmuir, Langmuir-Blodgett, Langmuir-Schaefer Method of Monolayer Formation 47
4.4. Theory of Langmuir Monolayers 50
4.4.1. Surface Pressure 50
4.4.2. Surface Rheology 50
4.4.3. Surface Potential 51
4.4.4. Brewster Angle Microscopy 53
4.4.5. Other Methods 54
The Aim of the Study 55

Experimental 57
1. The Design of the Nanoparticles 57
2. Materials and Methods 61
2.1. Synthesis of PSiFeNPs 61
2.2. Synthesis of Fe_xO_y@SiO_2NPs 61
2.3. Functionalisation of Fe_xO_y@SiO_2NPs (Synthesis of PSiFeNPs) 61
2.4. Purification of PSiFeNPs 61
2.5. Characterisation of Nanoparticles 62
2.6. Sample Preparation 62
2.7. Langmuir Systems 62
2.8. Preparation of the Langmuir Trough 63
2.9. Deposition of PSiFeNPs at the Air-Water Interface 63
2.10. Preparation of KCl Solutions 64
2.11. Langmuir Experiments 64
2.12. Relaxation Experiments 65
2.13. Transfer of the Samples onto Solid Substrates 65
2.14. Preparation of Solid Substrates 65
2.15. Other Instrumentation 66
3. Results and Discussion – Pure-Water-Based System 68
3.1. Langmuir Films of PSiFeNPs at Pure Water 68
3.2. Surface Compressional Modulus 73
3.3. Surface Rheology 74
3.4. Relaxation Experiments 76
3.5. Brewster Angle Microscopy 77
3.6. Scanning Electron Microscopy of Langmuir-Blodgett films 79
3.7. PSiFeNPs at the Pure Water Surface – Discussion 80
3.8. Summary – Pure-Water System 86
4. Results and Discussions – KCl-Solution-Based System 88
4.1. PSiFeNPs in Suspensions (ζ-potential, Electrophoretic Mobility and Hydrodynamic Diameters) 88
4.2. Langmuir Films 90
4.3. Brewster Angle Microscopy 92
4.4. PSiFeNPs Films Transferred onto Solid Substrates 93
4.5. Spacing between Nanoparticles 96
4.6. Interactions between Nanoparticles 98

4.7. Summary – KCl-Solution-Based System 103
Summary 105
Appendix 1 108
Appendix 2 114
Appendix 3 115
Appendix 4 119
Appendix 5 120
Appendix 6 123
References 124

Preface

Equilibrium is a term that has accompanied me throughout most of my scientific career, from high school to my current research work. Equilibrium describes chemical processes, colloid aggregation, and interfacial phenomena. It is present in economics, where it appears in the context of the classical free market (Adam Smith's "invisible hand")[1,2] and neoclassical economics,[3] through Le Chatelier's principle to the Nash equilibrium in game theory.[4]

Antoine-Laurent Lavoisier, the famous chemist and tax collector, popularised accounting in analysing the balance of chemical reactions. Later in the 19th century, applying thermodynamics to study chemical reactions shed new light on the balance of the reagents and the description of chemical equilibrium.[5] Then, in 1884, and in a more concise form in 1888, Le Chatelier formulated his principle, which can nowadays be expressed as follows, according to the Merriam-Webster Dictionary:[6]

"If the equilibrium of a system is disturbed by a change in one or more of the determining factors (as temperature, pressure, or concentration) the system tends to adjust itself to a new equilibrium by counteracting as far as possible the effect of the change".

In 1947, Paul A. Samuelson[a], a future Nobel Memorial Prize winner, introduced the concept of adapting this rule to economic analysis, later known as the Le Chatelier-Samuelson principle.[7] The same economist showed that adapting the chemical principle is not only an intuitive analogy but is driven by mathematical isomorphism.[8]

Despite that, it is not the equilibrium that fascinates people the most; it is the change. Nonetheless, equilibrium is not the most interesting phenomenon; the change is. The change that distinguishes two equilibrium states or that prevents the system from being in equilibrium. The change can be long-term or even permanent, aiming to force certain phenomena to occur (e.g., by taxes and subsidies)[9] or temporal (ineffectiveness at the market,[10] "black swans"[11]).

[a] Paul Samuelson was awarded the Nobel Memorial Prize In Economic Sciences in 1970 as he "has done more than any other contemporary economist to raise the level of scientific analysis in economic theory". He is known for development of e.g. revealed preference approach to consumer theory, welfare economics, international trade theories and many other fundamentals of modern-day neoclassical economics.

Similarly, engine-powered machinery requires an energy supply to perform work. Depending on the type of engine, the machine can be powered with petrol, electricity or other less conventional sources. In other words, to sustain the “working mode”, the system is kept out of equilibrium due to the energy flow/charge. Analogically, living organisms are systems of a chemical network working out of equilibrium, powered by nourishment or processes like light harvesting (photosynthesis).[12]

Therefore, changing equilibrium or moving out of equilibrium is a common thread in this work.

Introduction

The importance of self-assembly was raised by George Whitesides and Bartosz Grzybowski in their viewpoint published in "Science" in 2002.[13] While the article focused on typical static self-assembly, the authors mentioned two visionary points. The first was the rise of dynamic self-assembly, a term they introduced two years earlier in their pioneering work on an energy-dissipative self-organising system.[14] The second was a perspective on designing netted systems. The authors wrote:

"*At the outer limits of self-assembly, at least as it is currently defined in the physical and biological sciences, are netted systems: computers, sensors, and controllers that interact with one another only through the flow of bits and configure (or self-assemble) themselves based on that flow into functional systems. These netted information systems will be entirely different in their realization from self-assembled aggregates of material components, but will share underlying concepts of design and architecture*."

Now, almost 25 years later, complex, networked systems of stimuli-responsive, self-regulating, adaptive, and interactive materials are in the spotlight of nanotechnology. In 2025, Mirkin, leading a group of over 100 top-tier nanotechnology researchers from around the world, published a prospectus formulating 33 unresolved questions in nanoscience and nanotechnology.[15] The authors emphasised that such complex, interconnected systems, especially when integrated with biological systems, are crucial to the field's further development. What is still missing, in particular, is a fundamental understanding of the structure-function relationship in nanomaterials, their precise design, synthesis, and functionalisation, especially to create hierarchical structures with real-life applications.

This change is supported by the bibliography research by Hughes et al. (2025). Nanoscience primarily focused on the synthesis of materials in the 1990s. Currently observed is a strong emphasis on understanding and applying nanoscale phenomena, as well as the functional aspects of nanomaterials. Interdisciplinary studies are of special interest. Among them, the most trending topics in 2019-2022 were biomedicine, energy, catalysis, and sensors.

What is observed are “mission-driven” nanomaterials (research on nanomaterials to solve specific problems, especially in different fields) and multifunctional hybrids of nanomaterials.[16]

Thin films, as well as 2D and pseudo-2D systems composed especially of nanomaterials, seem to be the next emerging trend. The usage of thin films can be justified not only by their specific properties but also by economic reasons, making them key to industry applications. Some hints behind this were delivered by Hughes et al., who identified topics such as membranes, coatings, solar cells, and sensors as vast branches of nanoscience applications. What is more important, the authors indicated explicitly advanced coatings as key further opportunities.[16]

The aim of this thesis is therefore to address the aforementioned issues raised in nanoscience and nanotechnology, and to develop knowledge and nanoengineering in the fields of thin films, 2D, and pseudo-2D systems.

First, the initial literature research revealed that this kind of system has never been summed up before; therefore, as the first part of this thesis, I am going to present selected aspects of the review article that I am a leading co-author of: “*Adaptive 2D and Pseudo-2D Systems: Molecular, Polymeric, and Colloidal Building Blocks for Tailored Complexity”*.[17] According to the best knowledge, it was the first literature review to summarise and categorise adaptive thin film systems developed worldwide.

These selected aspects are going to be an introduction to the experimental part of the work, where I am going to expand on the nanoengineering of advanced thin film systems. One of the best methods for examining interactions between molecules or nanoparticles, especially in two dimensions, is the Langmuir method. The old technique is recently stepping into its renaissance era.[18] Surprisingly, according to literature research, stimuli-responsive and adaptive Langmuir films are scarce examples of adaptive 2D and pseudo-2D systems, even though the Langmuir method perfectly answers the call, as emphasised by Mirkin et al., to develop an understanding and precise control of nanomaterials.

After exploring photoresponsive out-of-equilibrium Langmuir films of AuNPs and ZnO nanocrystals capped with azobenzene derivatives as part of my master's thesis, I moved towards other building blocks and stimuli to manipulate the systems. I focused on controlling with the electric field, which required designing and building a novel experimental setup to precisely examine and control thin films at the Langmuir trough (patent application P.450044).

Additionally, I focused on multi-responsive systems, with temperature change as the dominant stimulus. The latter is the topic of this thesis.

The up-to-date examples of colloidal thermoresponsive systems considered are nanoparticles capped with long thermoresponsive polymer chains, compared to the size of the nanoparticles. As a novel approach, I present the study on Langmuir films composed with relatively large nanoparticles (60-90 nm) capped with short thermoresponsive oligomers. I focused on the physicochemical aspects of the films.

Along with the physicochemical description of the systems, the study presents a few issues that are of interest in the field. First, the created system exhibited a decrease in surface pressure with increasing temperature, which is not typical for conventional thermodynamic systems. Second, the nanoparticles capped with the thermoresponsive polymer exhibited 2D facilitated aggregation below the lower critical solution temperature (LCST) and no explicit aggregation above the critical temperature – it is opposite to the well-known colloidal systems based on LCST-type polymers and derived nanomaterials. Finally, I present a surprising phenomenon: an increase in the spacing between compressed nanoparticles with increasing KCl concentration in the subphase.

The thesis is constructed as follows.

The literature review starts with a brief introduction to nanotechnology. Instead of the classical description and introduction to nanomaterials developed over the last few decades, which are well-covered in the literature reviews, I decided to briefly describe the current state of the art of nanotechnology from an economic and scientometric point of view, as well as perspectives and opportunities for further progress. By doing so, I aimed to answer whether nanotechnology delivered on its expectations, which is sometimes questioned within the scientific community. I find these aspects relevant to justify further investment of time and capital in nanoscience.

In the literature review, I present selected aspects of the literature on adaptive 2D and pseudo-2D systems, focusing on those most significant to the experimental parts of the thesis. Next, I present the key theory underlying the Langmuir method, which serves as the basis for the experimental work. At the end of the chapter, I briefly present the adaptive systems constructed and examined using the Langmuir method, as found in the literature study.

The experimental part of the work involves paraphrasing my two research articles, published in 2023 and 2025.[19,20] As the studies share materials and methods, these aspects are presented together. The two articles describe a chronological study; therefore, the results and discussion are presented as a subsequent story. Firstly, focusing on the pure-water-based system,[19] then describing the introduction of KCl to the subphase[20].

Finally, the thesis is summarised to highlight the work's main outlook and key takeaways.

Literature Review

This section (subsections 2 and 3 in particular) is partially based on the literature review article:

Zbonikowski, R.†; Mente, P.†; Bończak, B.†; Paczesny, J.* Adaptive 2D and Pseudo-2D Systems: Molecular, Polymeric, and Colloidal Building Blocks for Tailored Complexity. *Nanomaterials* **2023**, *13* (5), 855. https://doi.org/10.3390/nano13050855.

1. Nanotechnology

Although the term "nanotechnology" was first defined and introduced by Japanese scientist Norio Taniguchi in 1974, the history of this discipline actually began earlier.[21,22] Richard Feynman's talk to the American Physical Society in 1959 is often regarded as a symbolic beginning of nanotechnology. The American physicist emphasised the great potential of miniaturising machines, computers, and building structures atom by atom.[23] "*There is Plenty of Room at the Bottom*" – the title of the talk has become a motto of people developing the idea. The story of nanotechnology began much earlier, and there are examples of using nanomaterials in antiquity (e.g., ancient Roman dichroic glass),[24] in the Middle Ages (e.g., Damascus steel),[25] and the Renaissance period (Italian decorations in Umbria)[26]. Nonetheless, until the 20th century, those processes were not understood. The development of physics and chemistry, especially electron microscopy, brought a revolution in this matter.

The term "nano" originates from the Greek "*νᾶνος*" or the Latin "*nānus*" (also derived from Greek), both meaning "dwarf".[27–30] In 1960, the prefix "*nano-*" was adopted by the International System of Units (abbr. SI from French *Système International d'Unités*), meaning a factor of 10^{-9}.[31] Nowadays, the morpheme "*nano*" is used in various ways, conveying multiple meanings, especially in science and technology-related topics or in science fiction.[30] The National Nanotechnology Initiative (an American institution launched in 2000 to coordinate nanotechnological research between governmental agencies and departments such as NASA, NIST (National Institute of Standards and Technology) and U.S. Department of Defense)[32] presented nanotechnology as "the understanding and control of matter at the nanoscale, at dimensions between approximately 1 and 100 nanometres, where unique phenomena enable

novel applications."[33] A recommended by the European Commission definition of a nanomaterial was updated in 2022. Briefly, nanomaterial is a natural, incidental or manufactured material consisting of solid particles (on their own or as aggregates or agglomerates), and where at least 50% of particles is one of the following: a) at least one of the dimensions of a particle has a size between 1 nm and 100 nm, b) two of the dimensions of the particles are below 1 nm and one is over 100 nm, c) one of the dimensions of particle is below 1 nm and two others are over 100 nm.[34] According to this definition, materials like graphene sheets are also considered nanomaterials.

Nanomaterials are not just scaled-down versions of bulk materials, as they exhibit unique properties that are absent in their bulk counterparts.[35] Upon miniaturisation, the surface-to-volume ratio increases significantly, meaning that a larger fraction of atoms is exposed at the surface. Surface atoms are more chemically reactive, being relatively undercoordinated compared with bulk atoms. As a result, processes that are negligible at the macroscale may become crucial at the nanoscale.[36] Unique properties of nanomaterials arise as well from quantum effects, e.g. discretisation of energy levels, or quantum confinement.[37] Hence, the use of nanomaterials in engineering and the engineering of nanomaterials is not only beneficial from an economic perspective but also opens new possibilities to employ phenomena not available for conventional technologies.[38]

1.1. Did Nanotechnology Deliver on Its Expectations?

At the beginning of the 2000s, the rise of nanotechnology was perceived as the next huge technological revolution.[39] The vision of science-fictional nanobots, invisible to the naked eye, has become a common imagination of the future in pop culture, as seen in shows like *Doctor Who* or *Westworld*.[40,41] Where are those inventions, though?

True examination of the development of nanotechnology is problematic, however. First, nanotechnology is implemented in various branches of the economy. Among the examples are electronics, and especially the development of transistors,[42–44] quantum dot screens,[45,46] quantum computers,[47,48] photovoltaics,[49–51] functional coatings,[52,53] sensors,[54–57] chemical industry (e.g., catalysts),[58,59] and the medical industry[60–64]. As nanotechnology develops various products, it is challenging to define the boundaries of its expansion. Therefore, there is no consistency in the estimations of the global nanotechnology market size. For instance, Grand Review Research states that the market size was $3.69 billion in 2022 and is expected to rise with a CAGR (compound annual growth rate) of 33.1% until 2030, while Fortune Business

Insights reports $105.79 billion in 2025 with a CAGR of 15.7% until 2034.[65,66] Precedence Research estimated the global nanotechnology market size to be $6.59 billion in 2024, with a forecast of rapid growth to $115.41 billion (CAGR = 33.14%) within ten years.[67] A more conservative estimate was mentioned by Ulucan-Karnak et al. (CAGR for the years 2020-2030 is 11.7%). The authors combined the conclusions of two different reports.[68] An optimistic perspective on the development of the nanotechnology market is found in the implementation of AI-driven models that predict the behaviour and properties of nanomaterials, thereby accelerating research by reducing the need for physical experimentation.[67]

The development of nanotechnology is one of the key strategic policy points for the world's largest economies, the United States and China. The USA launched the National Nanotechnology Initiative, mentioned earlier, in 2000 to maintain its global leadership in the field.[69] The Chinese initiative Made in China 2025, implemented from 2015 to 2025, prioritised advanced new materials as one of the key fields of supremacy (alongside photovoltaics, electromobility, and artificial intelligence) in the future Chinese economy. As a result, China holds 43% of all granted patents in nanotechnology since 2000.[70] This and more were presented in 2025, as the report of the National Center for Nanoscience and Technology – a Chinese non-profit organisation co-founded by the Chinese Academy of Sciences and the Chinese Ministry of Education.[70] StatNano, the Internet portal regularly reporting statistics related to nanoscience, collected data related to the patents granted by the European Patent Office (EPO; Figure 1 a))[71] and granted by the United States Patent and Trademark Office (USPTO; Figure 1 b))[72]. The figure shows that the number of patents granted each year was rising, and seems to oscillate around a constant value in recent years. These data do not show the worldwide domination of China as they present only trends in American and European patent offices. They confirm, however, that the component originating in China has been significantly rising lately. A different conclusion is drawn from data collected by the OECD, which shows that the number of granted patents has been decreasing since the early 2000s.[73] However, the classification between these databases on what patents are related to nanotechnology may differ. The decrease in new nanotechnology patents may be caused by a decline in interest in the topic (which supports the thesis that nanotechnology has not delivered on its expectations) or by nanotechnology becoming mainstream in science and being incorporated into various branches of technology, with less recognition of nanotechnology itself.

Analysis of trends in the scientific literature is likely to provide additional insight into the current state of nanotechnology.

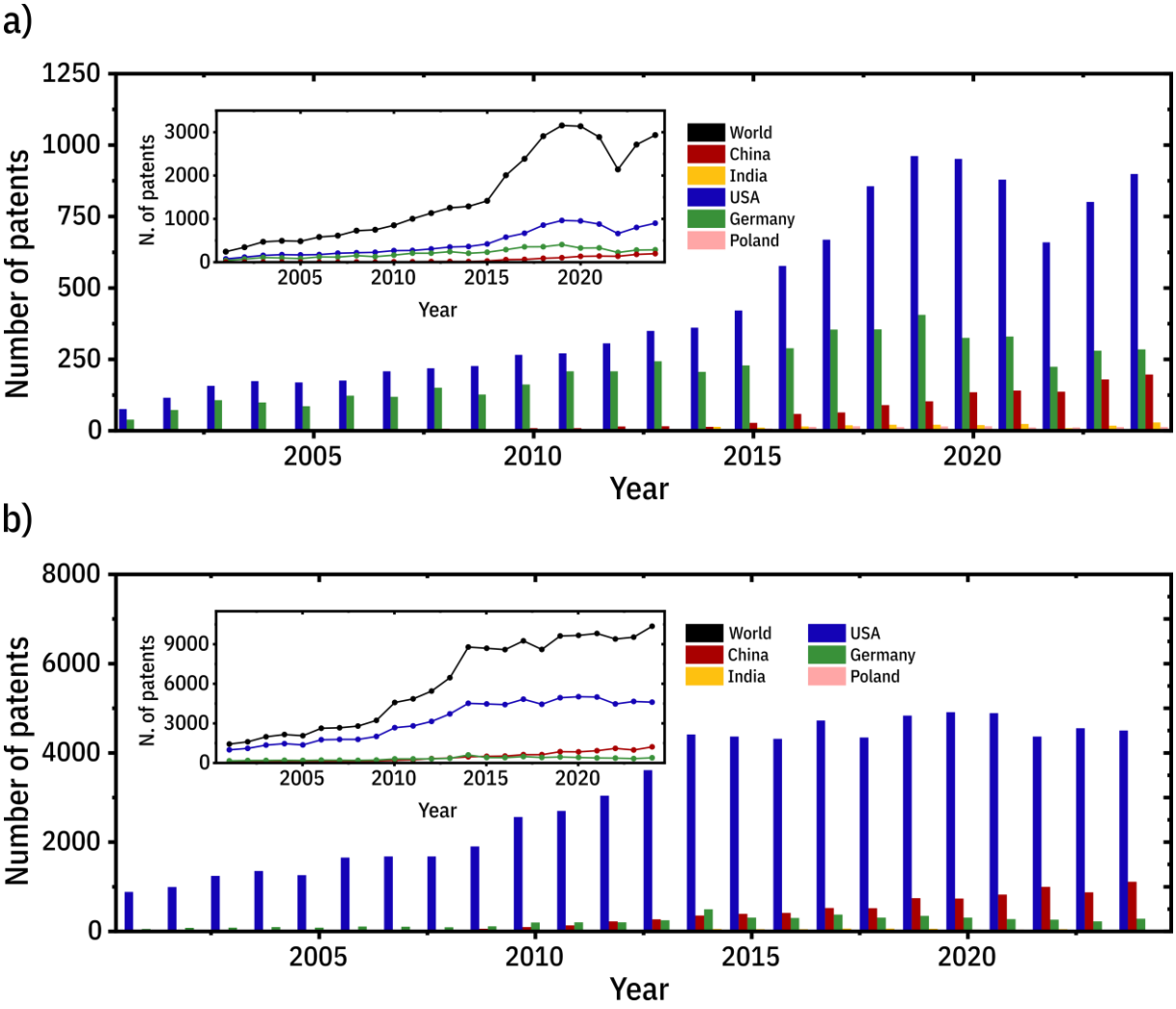

Figure 1. a) Number of nanotechnology-related patents granted every year by the European Patent Office to selected countries. Inset: Number of nanotechnology-related patents granted every year by the European Patent Office to selected countries compared with the total number of nanotechnology-related patents granted every year by the European Patent Office. Classification according to ISO/TS 18110:2015[b]. Own elaboration based on StatNano data.[71] **b)** Number of nanotechnology-related patents granted every year by the United States Patent and Trademark Office to selected countries. Inset: Number of nanotechnology-related patents granted every year by the United States Patent and Trademark Office to selected countries compared with the total number of nanotechnology-related patents granted every year by the United States Patent and Trademark Office. Classification according to ISO/TS 18110:2015. Own elaboration based on StatNano data.[72]

Nanotechnology publications have been rising in recent years. Figure 2 presents the number of nanotechnology-related scientific articles published around the world by the selected

[b] Patents that have at least one claim related to nanotechnology or have a classification code related to nanotechnology according to the International Patent Classification.

countries each year. The rapid increase is stimulated mostly by China, and the data indicate that the intense growth began even before the Made in China 2025 initiative was launched. Only 2022 was a year when the number of new publications decreased, likely a consequence of lockdowns during the first two years of the COVID-19 pandemic. Interestingly, the highest shares of nanotechnology publications in a country's total research output are observed in Middle Eastern countries. In 2024, 23.3% of research papers in Iraq were related to nanotechnology, 21.2% in Saudi Arabia, and 18.5% in Iran. By comparison, the nanotechnology shares were 8.9% globally, 13.3% in China, 16.5% in India, 4.4% in the USA, 6.1% in Germany, and 7.6% in Poland. Despite the increase in the total number of nanotechnology papers, the share in the leading countries remains relatively stable (in most cases), slightly decreasing (e.g., China) or increasing (e.g., Saudi Arabia). The latter instance of Saudi Arabia is most probably an aftermath of the National Science, Technology and Innovation Policy established in 2002, but ran exactly in the years of the intensive increase.[74] Counterintuitively, the share seems smaller in developed economies. For most of the presented countries, the peak of the share was around 2016. Nonetheless, these values are not heralding the end of nanotechnology. The data are presented in Figure 3.

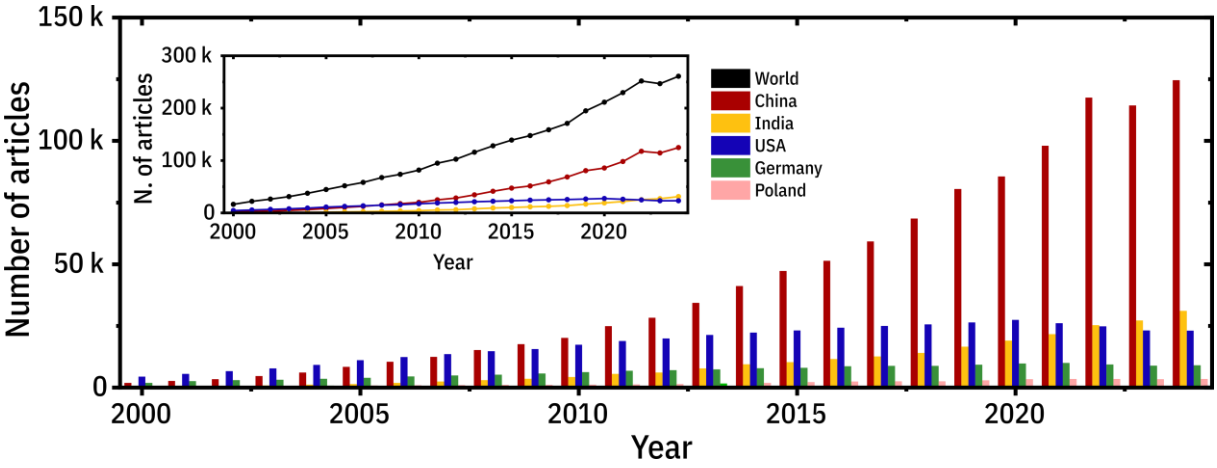

Figure 2. Number of nanotechnology-related articles published every year by the selected countries. Inset: Number of nanotechnology-related articles published every year by the selected countries compared with the total number of nanotechnology-related articles published every year. Own elaboration based on StatNano data.[75]

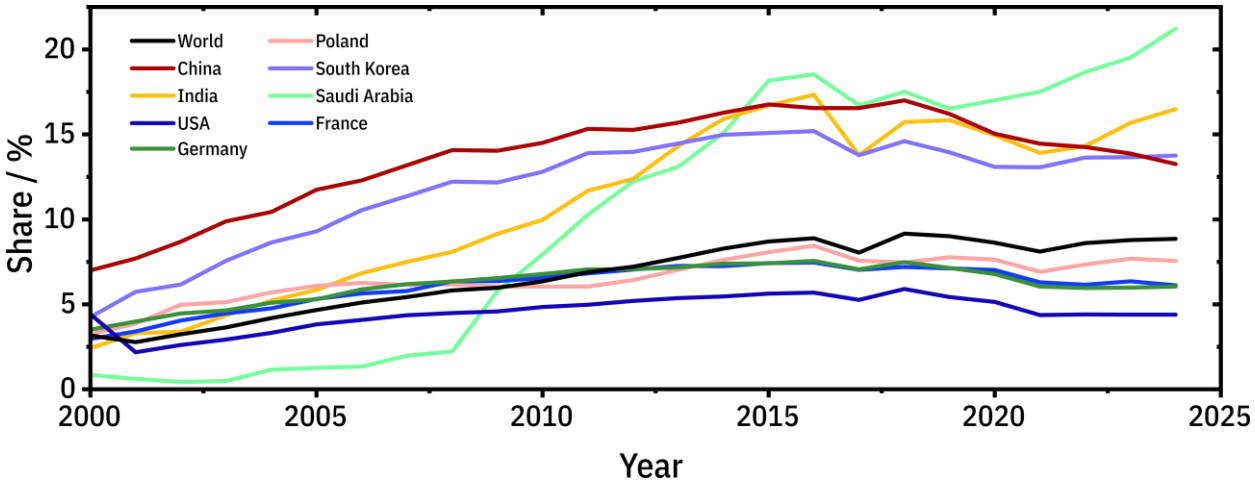

Figure 3. Share of nanotechnology-related articles published every year in total scientific articles published by the selected countries. The plot is presented as lines for clarity. Own elaboration based on StatNano data.[75]

An interesting literature analysis was published by Hughes et al. in 2025. Using NLP (natural language processing) and manual curation, the authors presented emerging topics in nanotechnology for the 2019-2022 period. Among the most emerging topics are triboelectric and piezoelectric nanogenerators, catalysis (especially CO and its storage), nanovaccines, and nanozymes. Among the trending materials are MXenes, covalent organic frameworks (COFs), nanovesicles, and natural-origin nanoparticles (e.g., lignin, biochar). The study reveals that topics related to complex nanomaterials and their applications are trending, whereas those related to basic nanoparticles (e.g., Ag, ZnO), nanocrystals, or carbon nanotubes are in stagnation. Large CAGRs in the number of publications, categorised by application, published in 2019-2022 were noted for applications such as solar desalination, bioinks, agriculture, water-based drilling, nanozymes, and vaccines. In terms of types of materials, the highest CAGRs were found for nanoplastics, MXenes, mesoporous materials, biochar, COFs, and $ZnIn_2S_4$. The authors also presented interesting statistics on the total number of nanoscience-related articles and patents based on the CAS Content Collection.[16]

Nowadays, the further development of nanotechnology can be accelerated by artificial intelligence and machine learning. In 2021, Tao et al. published an article in "*Nature Reviews Materials*" underlining the importance of using machine learning to improve the precision and efficiency of nanomaterials' synthesis.[76] The precision is crucial in applications in fields such as thermoelectrics, photovoltaics, pharmaceutics, or nanobiotechnology. The authors discussed the potential of certain machine learning approaches to aid in materials prediction. In the next

few years, some examples of the implementation of these ideas were presented; however, they were limited to only certain types of nanomaterials.[77–80] One of the main problems lies in collecting a proper database, as characterisation of nanomaterials is not standardised and depends on the application. However, the development of large language models (LLMs) appears to offer a new hope for solving this issue and enhancing the properties and synthesis predictions of theoretical nanomaterials.[81] This approach has a chance to fulfil the vision of the economist Norman Poire, who in 2000 expected nanotechnology to be the next industrial revolution, projecting the rapid adoption by economies starting from 2025. If we interpret the current development of artificial intelligence as the consequence of rapid adaptation of computerisation, then nanotechnology seems to be the next step, as Norman Poire postulated.[39] An interesting insight into applying artificial intelligence to nanoscience research was presented by Hughes et al. (Figure 4). A considerable increase in publications utilising AI has been noticed since 2015. Moreover, their dataset ends in 2023, just after the release of ChatGPT, which not only opened new possibilities for applying AI in science but also popularised machine learning. The authors compared the distribution of AI usage between four prominent fields of nanoscience related to energy (44%), nanosensors (28%), nanocatalysis (16%), and drug delivery systems (12%).[16]

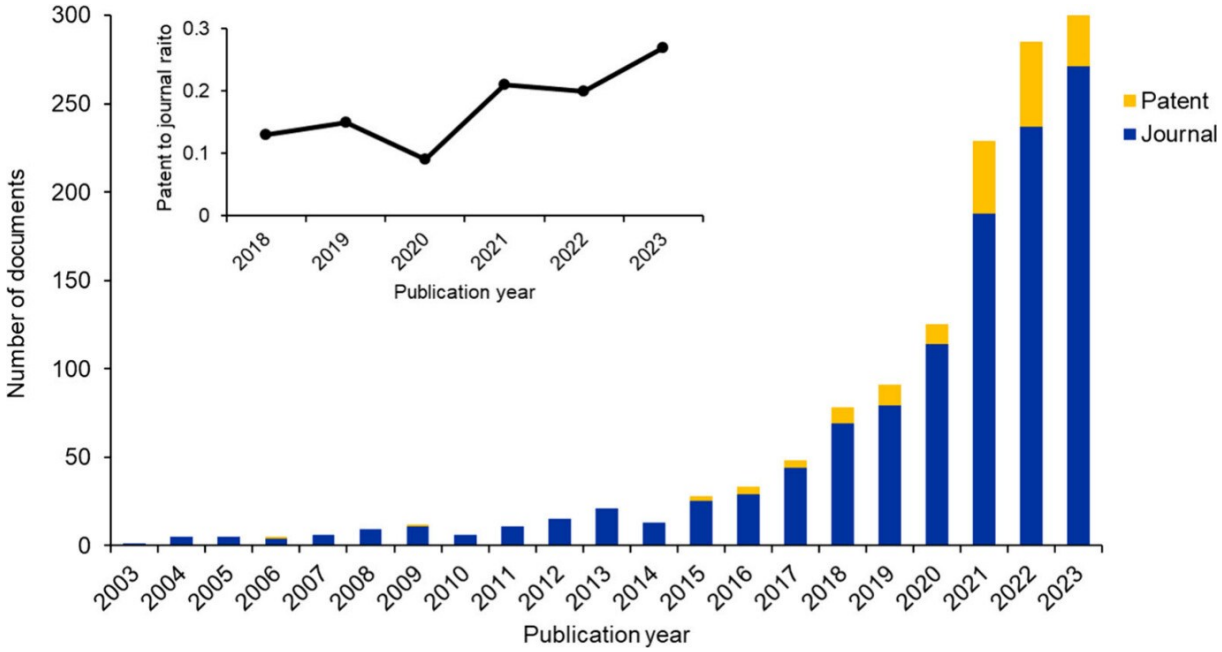

Figure 4. Number of journal publications and patents published every year from the CAS Content Collection, related to the use of artificial intelligence in nanoscience-related research in the 2003-2023 period. The inset presents the ratio of patents to journal publications from 2018 to 2023. Adapted from ref. [16] under CC-BY 4.0 licence.

As mentioned in the introduction, the current challenges in nanotechnology present 33 open questions/problems.[15] Questions 1-3 concern achieving the atomic and molecular precision necessary for the proper functioning of nanomaterials. Questions 4-5 focus on understanding the relationships between structure and function. Questions 6-8 show the necessity of building complex and hierarchical systems. In total, 11 questions still underscore that nanomaterials are not understood enough, both in terms of synthesis and predicting properties to build complex, functional applications. 7 questions indicate tools and techniques that would allow for boosting nanoscience. The last 15 questions highlight applications where nanotechnology can make significant contributions and explored the societal implications.

The vision of nanorobots (nanobots), known from various science-fiction films, is becoming a reality step by step. In 2016, J. Fraser Stoddart, Jean-Pierre Sauvage, and Bernard L. Feringa were awarded the Nobel Prize in chemistry "for the design and synthesis of molecular machines". They made significant contributions to the synthesis of catenanes, rotaxanes, and molecular rotary motors.[82–84] Since their work on molecular-level machines, huge progress has been made, especially in the development of stimuli-responsive nanoparticles and other micro- and nanosystems. The 161-page review, which cites over 1,700 articles, was recently published and summarises the principles and current state of the art of micro- and nanorobots.[85] The authors also presented a set of critical questions/problems to be of particular interest in the following decade. They emphasise that the expansion of advanced fundamental knowledge, as well as technical innovation, will lead to solutions for real-world challenges. Key open questions include further miniaturisation, compatibility of micro- and nanorobots with complex environments, principles and AI-assisted control of their collective behaviour, methods for reliable external control and real-time monitoring of large robot groups, enhancement of autonomy in life-like micro- and nanorobots, faithful mimicking of living microorganisms, development of medical application strategies, and scalable fabrication of precise micro- and nanorobots. Nonetheless, to overcome the main nanotechnological challenges, whether with or without AI's assistance, it is crucial to provide data on precisely defined nanoparticles. Understanding the interactions between the nanoparticles enables building increasingly complex systems. Not only for showing the new applications and solutions themselves, but also for providing high-value data for future applications of machine learning and artificial intelligence. Adaptive 2D and pseudo-2D systems are a field that perfectly aligns with the aforementioned prospects.

2. Adaptive 2D and Pseudo-2D Systems

2.1. Introduction

To begin, it is essential to define 2D and pseudo-2D systems. This problem is much trickier than it seems. Material science and nanotechnology usually consider 2D materials as free-standing monolayers of atoms, such as graphene or MoS_2; however, other definitions recognise 2D materials as materials with only one nanoscale dimension.[86–89] To avoid any misunderstandings, the term "pseudo-2D" expands the meaning to cover thin films or thin systems that operate in monolayers or even polylayers of molecules or particles, whose properties are the consequence of interactions also out of the plane. For instance, capillary forces at the liquid interface or interactions with a solid substrate on which a thin layer stands. The latter may be even required if the layer itself is not free-standing. Therefore, Langmuir films can be included in 2D and pseudo-2D systems. Langmuir films are thin films of molecules or particles at the gas-liquid interface (usually monolayers at the air-water interface), which are of considerable importance for functional materials due to the facile methods of examining and tailoring properties through mechanical compression.[90]

Two-dimensional and pseudo-2D systems, such as membranes and various examples of thin films and layers, exhibit a unique potential to enhance the development of materials and their applications, as well as expand knowledge in scientific disciplines including nanoscience and nanotechnology, physical chemistry, solid-state physics, and biotechnology. Reducing the number of dimensions to only two allows us to focus on different aspects of phenomena. It may simplify the mathematics and modelling or isolate specific interactions that are the subject of the study. Reducing the third dimension to a minimum provides a platform for innovation, primarily due to the unique properties not present in bulk materials.[91]

Modern industry places a strong emphasis on developing thin films.[91] Two-dimensional materials are essential for miniaturisation and play a vital role in many common devices, including batteries, solar panels, and displays. The high precision achievable in their physical and electrical properties can improve both efficiency and durability. Another advantage stems from the ratio of the exposed surface to the volume of the used material. This aspect is crucial, for instance, for catalysis and energy storage. Eventually, thin films are used as coatings on the surface. They provide protection (e.g., against corrosion) or functionalise the surface (e.g.,

antimicrobial coatings, hydrophobic coatings). Economically, they reduce the cost of the product by limiting the amount of essential components to the edges.[91]

2.2. Dynamic, Adaptive, or Stimuli-Responsive?

Some of the terms, such as stimuli-responsiveness, reversibility, switchability, energy dissipative system, dynamic system, and adaptive system, can be understood intuitively. However, what is intuitive to one reader may not be so to another, and this can lead to many misunderstandings. Hence, I would like to introduce these terms and explain their differences to clarify how certain phrases will be understood in this thesis.

Equilibrium self-assembly or static self-assembly is a self-assembly that is in a global or local thermodynamic equilibrium. Energy is not dissipated from the system. Formation of such self-assembly may require energy input; however, once formed, the self-assembly remains stable.[92] An example of such an assembly can be a gold nanoparticle stabilised with octanothiol as a ligand.

In 2002, the pioneers of dynamic self-assembly (DySA), Whitesides and Grzybowski, defined it as a process in which "*the interactions responsible for the formation of structures or patterns between components only occur if the system is dissipating energy*".[92] Therefore, a dynamic self-assembling system may be restricted to the system that transits between two states (1. equilibrium; 2. out-of-equilibrium, energy dissipative).[93] Diagram a) (Figure 5) shows the changes in the energy states. Dynamic systems can be characterised as systems that switch between I and II, or II and III states. In the first case, energy donation to the equilibrium state (II) excites it to a local energy minimum (I). This state (I) is not stable since the energy barrier required to return to the energy minimum (II) is lower than k_BT. Hence, the system will dissipate energy. The photoisomerisation of azobenzene is an example of such a process. After UV irradiation, the molecule is isomerised from the trans form to the cis form. The cis isomer requires activation energy to revert to the trans form. However, room temperature collisions with other molecules provide sufficient energy to overcome this barrier. Exactly this property of azobenzene was used by Klajn et al. to create a self-erasing ink.[94] The second transition (between II and III) describes a transition to an unstable state that may depend on the rate of energy delivery.

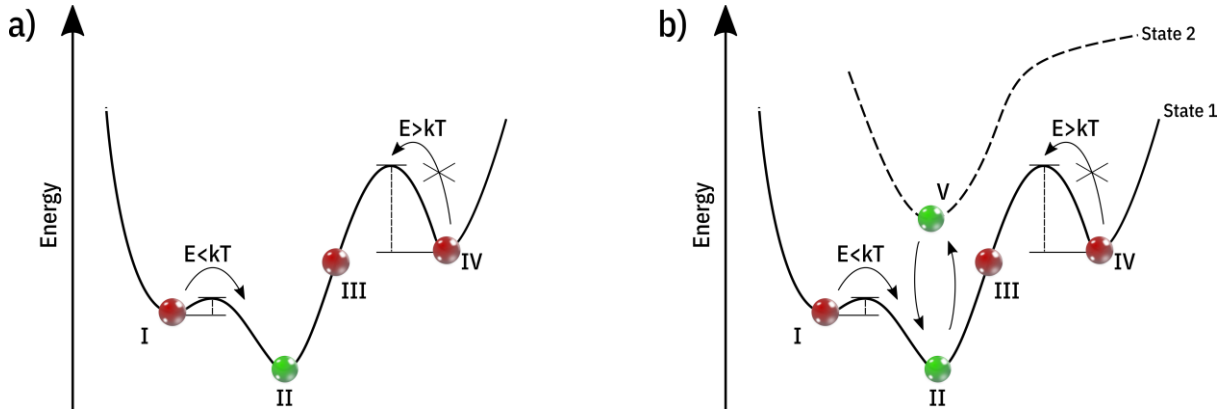

Figure 5. Schematic energy diagrams describing different states of stimuli-responsive systems. **a)** for one state, **b)** for two states. I. Metastable, energy-dissipative state, II. Equilibrium state, III. Out-of-equilibrium energy-dissipative state, IV. Kinetically trapped metastable state, local equilibrium, V. Second equilibrium state. Own graphic, published in ref. [17], CC-BY 4.0.

Stimuli-responsive systems react to external stimuli, such as light, temperature, pH, magnetic, and electric fields. They react to the presence of the stimuli or modulation of the stimuli. Therefore, a stimuli-responsive system is a general term encompassing both static and dynamic systems, which change irreversibly or reversibly between equilibrium and non-equilibrium states, or between two equilibrium states.

Finally, in this thesis, the term "adaptive systems" describes systems that (1) show a reaction to an external stimulus, (2) are reversible and can be switched between equilibrium states (Figure 5 b) II-V), equilibrium and non-equilibrium states (I-II, II-III), or between non-equilibrium states (I-III, between different positions of III). In brief, adaptivity is defined here as the ability of systems to reversibly adjust their state in response to external stimuli. The introduction of such a definition allows for avoiding nomenclature inaccuracies when describing, for example, temperature-dependent systems (thermodynamically switching between only equilibrium states) and energy-dissipating systems (e.g., the aforementioned azobenzene-based systems).[93] Such defined terms ("reversible", "stimuli-responsive", and "adaptive") are useful for distinguishing nuances in thermodynamics and for avoiding misleading or incorrect simplifications.

I have introduced these definitions in the review article on which this part of the thesis is based.[17] However, various authors defined adaptive materials differently. While the term "adaptive" is commonly used as a synonym for "responsive", some authors emphasise that adaptive materials self-regulate and change their response in time. Therefore, the difference

between responsive and adaptive materials lies in the form and complexity of the response, rather than in their reversibility. However, the changing response in time is not active (learning) but passive. For instance, Kaspar et al. distinguished four categories of matter that recognise the complexity of its intelligence. These are structural, responsive, adaptive, and intelligent. According to the authors, structural matter does not possess any functional elements. It still can be complex, but the matter does not change its properties – it is static. On the contrary, responsive matter changes its properties in response to an external stimulus. Adaptive matter has its own internal feedback that, beyond just responding to external stimuli, regulates the matter's properties. This can be realised by, for example, coupled chemical reactions. An example of such a system was presented by He et al. The authors presented a system based on a thermoresponsive hydrogel whose response modulates exothermic catalysis, introducing chemo-mechano-chemical self-regulation.[95] Intelligent matter interacts with the environment, learns from the responses, and is able to self-regulate.[96] Kang underlined that the term "adaptive" is broad and is interpreted differently in the literature. The author focuses on "dynamically adaptive materials", which he defines as stimuli-responsive materials whose responses to the environment vary in time.[97] Walther, in his "*Viewpoint: From Responsive to Adaptive and Interactive Materials and Materials Systems: A Roadmap*", discussed responsiveness, adaptiveness, and interactivity of materials. According to him, responsive materials are already reversible – they can switch from state A to state B reversibly (state B is stable only when the external stimulus is active or another stimulus is required to switch the system back). Adaptive materials are not only responsive materials in this definition, but their response changes in time. The response can even be quenched or can appear after repeating the external stimulus. Therefore, adaptiveness is related to the ability of learning and remember. Interactive materials operate with a feedback loop, being not only passively reactive to external stimuli from the environment but also responding to the environment to reach mutual adaptation.[98] Lehn described constitutional adaptive materials as those that dynamically change their constitution by assembly/disassembly, under certain conditions, leading to a change in the components of the material and connections between them, not only their state. In other words, the elements of the system compete under certain conditions to be constituents of the material, and changing the conditions influences the competition, leading to different constitutions.[99]

The articles authored by Walther and Kaspar et al. were published in late 2019 and in the middle of 2021, respectively. Since that time, these articles have been cited multiple times, and currently, their definitions of adaptive materials are slowly becoming a common standard.

The article I co-authored was published in early 2023, which means that it was written when these definitions were still gaining recognition. Nonetheless, similar definitions of adaptive materials to mine were common in other highly cited review papers from that period.[100,101]

Despite the emerging trend, in this work, I will remain consistent with the definition of adaptive materials used in the publication this thesis is based on, defining them as stimuli-responsive materials, capable of reversible switching between equilibrium and equilibrium states, equilibrium and non-equilibrium states, or between non-equilibrium states.

3. Design Principles of Adaptive 2D and Pseudo-2D Systems

Designing a complex system in terms of its adaptivity requires basing it on components that react to external stimuli. These components can be further arranged into networks that not only react but also process the signal or perform the desired work. A comprehensive review on building blocks that can be used in such systems was presented by Zhang et al.[102] The authors showed a plethora of examples, distinguishing them by mechanisms, such as a) change in molecular structure (trans-cis transition, ring opening-closing, extension-coiling of polymers, etc.), b) bond formation and/or cleavage (electrostatic interaction, host-guest interaction, covalent bond, etc.), and c) response to external fields (magnetic field, electric field). These mechanisms are then composed into functional entities. Among the practical functions of materials described by Zhang et al.,[102] are targeting (recognising specific environment),[103,104] gating (regulation of transport through the material),[105–107] rupturing,[108] capturing and releasing,[109,110] shape change,[111–113] pattern formation,[19,114,115] motion,[116–118] and communication[119,120]. Then, regulatory functions are self-regulation,[121,122] self-oscillation,[123–125] rectification (selective transport in a specific direction),[126–128] amplification,[129–132] self-organisation,[133–136] and self-replication[137,138]. Eventually, analytical processing functions include memory/data storage,[139–142] logic gates,[143–145] and computing[143,146–148].

Analogously to living organisms, building complex systems that adapt to external stimuli and react in a specific, desired manner involves constructing a network of these components. Merindol and Walther described such a perspective and approach in their review.[149] According to them, any out-of-equilibrium system requires three elements: fuel, catalyst, and feedback control. In this context, fuel serves as an energy supply, a catalyst is an operational unit that drives the function, and feedback regulates the interactions.

While three-dimensional systems are prevalent in scientific literature,[13,150–152] two-dimensional ones (including pseudo-two-dimensional) remain relatively unexplored. This type of system, as described in the introduction, has specific advantages and unique features for applications, particularly in thin films, membranes, and coatings.

3.1. Classification of 2D Systems Based on a Type of Building Blocks

A review of the literature identifies three principal categories of building blocks and, thus, corresponding systems among adaptive 2D and pseudo-2D systems. These categories are molecular, polymeric, and colloidal systems. Each of them can be characterised by a different set of building blocks and phenomena driving the systems, and consequently, different principles of operation. The systems are often combined into complex systems, and the boundaries between them are rather arbitrary. Nonetheless, principles of every component prevail. Moreover, every subsequent category brings more possibilities for forming hierarchical structures, particularly through their conjugation. Consequently, this enables a path to attack the challenges set by Mirkin et al.[15]

3.1.1. Molecular Systems

Biological systems rely on complex molecules and networks of equilibria involving them.[153] Molecules are used for processing information and performing actions of a living organism. Food, being a supply, delivers material to directly or as precursors/substrates for proteins, lipids, and carbohydrates that are building blocks for cells, then tissues, and organs.[93,154]

Adaptive systems require an analogical approach, with one specific shift in the importance of responsiveness to external stimuli. Within a molecule, this postulate can be realised by a response such as a change in electronic distribution, energy levels, spin states, conformation, or breaking/creating bonds. These causes lead to changes in, for instance, dipole moment, hydrophilicity, thermal stability, and solubility.[155] Light-sensitive molecules such as spiropyrans,[156] azobenzene,[157] and their derivatives are common examples of molecular building blocks that allow for light-induced changes in structure (isomerisation, cyclisation) and properties (magnetic moment, change in light absorption). Light is not the only stimulus that is used in adaptive systems. Tetrathiafulvalene (and its derivatives) is a molecule that can be reversibly switched into a radical cation due to chemical/electrochemical activation.[158] In the context of Langmuir-Blodgett films, which historically started with fatty acid, self-

assembled fatty acids respond to multiple stimuli such as pH, temperature, and CO_2.[159] Molecules can themselves be more complex systems, such as molecular machines. For example, stimuli-responsive rotaxanes and molecular engines that transform supplied energy into movement.[84,160,161]

3.1.2. Polymeric Systems

Life is also based on polymers, such as proteins and nucleic acids. Similarly, synthetic polymeric materials have played a vital role in the advancement of societies.[162] Early polymers were valued mainly for their inherent chemical structure or interactions between chains, which could be adjusted by mixing different polymers, small molecules, or through copolymerization. A polymer's backbone affects its flexibility, phase transition temperatures, and polarity, while side groups influence glass transition temperature, polarity, and hydrophilicity. These features impact intermolecular interactions and, consequently, solubility. Side groups can also be modified by post-polymerisation to enhance solubility, enable functionalisation, or allow cross-linking.[163]

Block copolymers exhibit markedly different physicochemical properties, often displaying spontaneous chain twisting and segregation into domains with similar characteristics.[164] This is especially evident when blocks have contrasting polarities, such as hydrophobic and hydrophilic segments.[165,166] Advances in copolymer design, including random and ordered block arrangements, have introduced new material properties, such as enhanced mechanical strength, amphiphilicity, reduced glass transition temperatures, and shape memory.[167]

Polymerisation gives monomers new properties – for example, thiophene is electrically inert, but its polymerised form becomes semiconducting.[168] Advanced polymerisation techniques such as nitroxide-mediated polymerisation (NMP),[169] atom transfer radical polymerisation (ATRP),[170] reversible addition–fragmentation chain-transfer polymerisation (RAFT),[171] and coupling reactions[172] have enabled the design of complex architectures, including vertically grafted polymer chains on 2D substrates.[173] These materials exhibit unique features such as thermoresponsiveness, particle detection, and pH sensitivity.[174–176]

A promising direction involves controlled two-dimensional polymerisation at phase interfaces (e.g., liquid-liquid, metal-gas), offering potential alternatives to graphene. Usually, the selected polymerisable monomers are trapped at the interface.[177–180]

Since the 1990s, polymers have been widely investigated for use in smart surface applications.[181] Approximately twenty years ago, Koberstein proposed core guidelines for designing such materials.[182] This involves assessing whether surface energy is affected by the polymer backbone or its functional groups, ensuring an adequate density of functional groups, and allowing the material to reorganise in response to environmental stimuli. Such adaptability is crucial for creating responsive and dynamic surfaces.

Conventional methods for surface patterning, such as lithography, nanoimprinting, or adjusting material composition, often result in static, unchanging designs.[183–186] In contrast, surfaces that rely on constant energy input can exhibit dynamic and adaptive behaviour. A well-known example is the wrinkling effect in polymer films,[187] which can be tailored to respond to various stimuli such as light,[188] heat,[189] pH, or the presence of specific substances like water,[190] by incorporating suitable responsive units or additives.[187]

The most common examples of polymeric building blocks are polymers exhibiting lower critical solution temperature (LCST) and upper critical solution temperature (UCST). LCST-type polymers are soluble due to the hydrogen bonding formed with solvent molecules (usually water). Above the lower critical solution temperature, the enhanced thermal motion is too high to maintain stable hydrogen bonding; inter- or intramolecular polymer-polymer interaction is favoured. Among the most popular examples of LCST-type polymers are poly(N-isopropylacrylamide) (PNIPAM; LCST=32 °C), poly(ethylene glycol) (PEG; LCST=85 °C) and poly(methyl vinyl ether) (PMVE, LCST=35-36 °C).[174] UCST-type polymers exhibit a miscibility gap below the upper critical temperature. In this case polymer-polymer interactions (e.g. Coulomb interactions) and solvent-solvent interactions are dominant. As the thermal energy becomes sufficient to overcome these interactions upon reaching the upper critical solution temperature, the polymer dissolves.[191] A typical example of UCST-type polymers is poly(N-acryloylglycinamide) (PNAGA, UCST=13 °C-22 °C)[c]. Polymers can exhibit both LCST and UCST.[191] Thermodynamically, the miscibility of polymer solutions can be described by the Flory-Huggins theory.[192,193]

3.1.3. Colloidal Systems

Another large category of building blocks and systems in general is those based on colloids. Nanoparticles are promising platforms that enable the construction of complex systems,

[c] The UCST of PNAGA is highly dependent on concentration, molecular weight and technically on heating or cooling rates during the measurements.[191]

carrying functional groups and advanced mechanisms. The nanoscale size is not only suitable for miniaturisation but also fosters the integration of quantum-physics-based solutions. Some of the inspirations also come from living organisms, where micro- and macromolecules are involved in complex chemical networks operating far from equilibrium.[194] Nanoscale biomolecules, such as proteins, perform various functions that are crucial for the proper operation of a living system. A typical example of an impressive complex protein structure and functionality is kinases that "walk" along microtubules, enabling cargo inside a cell.[195]

Two-dimensional systems based on functional colloids can benefit from the facile possibilities of tailoring their properties. Due to the structure of the nanoparticles, the output of the system based on them benefits from the interplay between organic and inorganic components, leading to the creation of functional nanodevices.

In the most conventional nanoparticles, the central building block unit of colloidal adaptive 2D systems, three essential constitutional parts can be distinguished. These are the core, the shell, and the capping layer; however, the structure of a nanoparticle can be simpler, e.g., by not being composed of one of these constituents. Stimuli-responsiveness, adaptivity, or more advanced features can be obtained by altering these components.

The properties of the core depend primarily on the material from which it is made and/or its size. For example, quantum dots (QDs) are semiconductor nanoparticles capable of absorbing incident photons and emitting light at a wavelength typically longer (lower energy) than that of the incident photons.[196,197] When the dimensions of QDs are comparable to the Bohr radius of the exciton, the motion of charge carriers is spatially confined, leading to the discrete electronic energy levels. As a result, the optical and electronic properties of QDs strongly depend on their size. This phenomenon is known as quantum confinement. This confinement can be intuitively understood in terms of standing matter waves that fit within the nanoparticle, resulting in discrete allowed energy levels. A specific category of QD-related nanomaterials is upconverting nanoparticles.[198–201] By doping the core (e.g., a host lattice such as $NaYF_4$)[49] with lanthanide ions, multiple long-lived intermediate energy levels become available. This enables the sequential absorption of two or more low-energy photons, ultimately resulting in the emission of higher-energy (shorter-wavelength) light upon radiative relaxation.

The core may be magnetic (e.g., Fe_3O_4 or Co_3O_4), enabling remote manipulation by the external magnetic field.[202,203] Bulk ferromagnetic and ferrimagnetic materials exhibit a magnetisation hysteresis loop, which arises from the presence and reorientation of magnetic

domains within the material. Below a specific critical particle size, magnetic domains are no longer formed. Then, a nanoparticle becomes a single-domain magnet.[204]

In such single-domain nanoparticles, magnetisation results from the reorientation of the particle's magnetic moment. Assemblies of sufficiently large single-domain nanoparticles may still exhibit magnetic hysteresis. However, when the particle size becomes small enough that thermal energy (k_BT) overcomes the magnetic anisotropy energy barrier, the nanoparticles exhibit superparamagnetic behaviour, characterised by negligible remanence and an almost vanishing hysteresis loop.[205] For instance, spherical Fe_3O_4NPs are superparamagnetic below the diameter of 20 nm and are multi-domain above the diameter of 76 nm.[206]

Many significant features of nanoparticles originate from processes and phenomena that occur at the surface (e.g., catalysis,[207,208] surface plasmon resonance[209,210]) or are related to the surface morphology[211]. These properties may originate from the core of the nanoparticle; nevertheless, it is not always feasible or optimal. Among many reasons, the core can be unstable in the target environment, may exhibit one function but not possess the desired surface properties, may be economically unjustified, or other properties (e.g., density) may need to be tuned. To overcome these problems, the core can be surrounded by one or more additional layers. Such a created architecture is called a core-shell nanoparticle.[212] The remarkable diversity of such structures is difficult to capture concisely in this literature introduction. A comprehensive review describing different shapes of core-shell structures, classes of core-shell nanoparticles, approaches to synthesis and characterisation was provided by Ghosh Chaudhuri and Paria.[213]

Plenty of modifications can be applied to the capping layer that sensitise the outcome nanoparticle to external stimuli. Initially, the capping layer (a layer of ligands attached to the surface) was used to stop the synthesis at the nanoscale size by decreasing the surface energy and preventing colloids from aggregating. However, as the capping layer usually consists of organic molecules anchored to the surface, it enables a wide range of possibilities for modification and functionalisation by applying ligands specific to the application or stimuli-responsive ligands. The latter are of particular interest in this study.

The true beauty of nanoengineering lies in combining the core, the shell, and the capping layer into a complex chain mechanism. For example, attaching an electron-accepting group to a QD can allow for the separation of the charge and the formation of a nanocapacitor.[214,215] Consider a quantum dot with a fullerene derivative that enables the transfer of the photoexcited

electron to the fullerene. Photoexcitation depends on the core structure (energy gap). When such a nanoparticle is irradiated, the negative charge is localised on the ligands, while the core remains positive.[214,215] An example of a conjugated fullerene derivative attached to AuNPs behaving as an "electron sponge" was shown by Bończak et al.[216]

Another interesting extension of the nanoarchitecture is the so-called "Janus" nanoparticles, named after a Roman god with two faces.[217,218] These nanoparticles typically have two distinct domains (multidomain Janus-like particles are also reported in the literature). Thanks to that, nanoparticles exhibit anisotropy in their properties, even when they have shape isotropy. Different domains can also exhibit distinct functions. These specific features of these nanomaterials enable new possibilities in self-assembly, colloidal surfactants (and Pickering emulsions), and micromotors or microswimmers.[218,219]

A typical example of remotely modulating interactions between nanoparticles is the isomerisation of azobenzene induced by UV irradiation. As a result of the isomerisation, the Debye moment of azobenzene changes from 0 D (trans isomer) to around 3 D (cis isomer).[220] That change, when localised in the ligand layer, regulates aggregation-disaggregation of nanoparticles in polar and non-polar solvents.[115,221,222] However, the switch is limited by the minimal space required for isomerisation. That can be adjusted by the length of the ligand that azobenzene is attached to and the curvature of the surface, spacing between single ligands (increased by increasing the size of the anchoring group or by side chains of the ligand; self-assembled during the synthesis process), or by capping the nanoparticle with mixed ligands of different lengths. In the latter case, the azobenzene is attached to the end of the underrepresented longer ligands; therefore, neighbouring ligands do not interfere with the isomerisation.[223,224] Photoswitching of azobenzene may also be used as gates regulating the access to catalytic sites[225] or to release transported cargo[226]. Other interesting mechanisms that consume light use, e.g., Förster resonance energy transfer[227] or transform light into heat[228,229].

Construction of colloidal adaptive systems benefits from all the aforementioned properties of nanoparticles.[151,152,230,231] A thorough understanding of the interactions between particles and their responses to external stimuli is a crucial principle for tailoring complexity in particle-based nanotechnology.

3.2. Adaptive Colloidal Langmuir Films

The review article "*Adaptive 2D and Pseudo-2D Systems: Molecular, Polymeric, and Colloidal Building Blocks for Tailored Complexity"* categorises adaptive systems by the stimulus they respond to. The stimuli were voltage, light, temperature, changes in chemical environment, and other systems, collecting interesting examples of systems that did not fit into the other groups. Each category contains systems predominantly based on molecular, polymeric, or colloidal building blocks.

Adaptive colloidal Langmuir films have not been widely explored yet.[232] Nonetheless, some representative examples of adaptive colloidal Langmuir films and other interfacial colloidal systems will be presented below as particular realisations of adaptive 2D and pseudo-2D systems. These studies establish the conceptual and experimental framework required to contextualise the results of this thesis within the current state of the art and are worth recalling in this text in particular.

Vialetto et al. demonstrated the reversible UV-light-induced crystallisation of anionic polystyrene microparticles (5.1 μm in diameter) at the air-water interface. The particles were mixed with a photoactive surfactant, an azobenzene derivative called AzoTAB. After UV irradiation, the surfactant changed its form to cis and desorbed from the interface. The desorption led to the formation of a 2D close-packed structure of microparticles. This colloidal crystallisation-like process took 30 s, followed by relaxation for 30 min with no further UV-light irradiation, due to the resorption of the surfactant.[233] A similar approach was used to oppose the "coffee ring" effect. 500-nm polystyrene particles mixed with an azobenzene derivative surfactant were drop-cast onto a solid substrate. UV irradiation caused desorption of surfactant molecules from the interface. As a consequence, water evaporation did not imply aggregation of particles on the edges of the droplet.[234] The use of additives in adsorption and the organisation of colloid particles at fluid interfaces was elaborated in a recent review.[235] A photo-induced assembly. Bończak and Fiałkowski presented reversible adsorption and desorption of gold nanoparticles capped with a ligand containing a photoresponsive donor-acceptor Stenhouse adduct, switching between hydrophilic and hydrophobic properties. Green light irradiation organised nanoparticles at the water-oil interface, which could desorb due to thermal relaxation.[236]

Another intriguing study was presented by Sashuk et al. showing an interfacial (gas-liquid) dynamic self-assembly system. The authors investigated positively charged amphiphilic gold nanoparticles spread at the air-water interface and demonstrated a surface-tension-gradient-driven mechanism. Surface tension gradient was modified by adding THF, or by removing solvent vapour from the proximity of the interface. The authors showed that the phenomenon is capillary-based.[237]

An interesting example of an interfacial colloid system was constructed by Montelongo et al. In principle, this system also focused on an adsorption-desorption switch that was triggered by adjusting the voltage bias at the phase boundary between the water and organic phases. Additionally, the system allowed for the control of distances between nanoparticles (AuNPs capped with dodecanoic acid).[238] The distance determined the reflectivity of the formed layer; therefore, the system was in fact an electrotunable nanoplasmonic mirror.[238]

Most instances of adaptive interfacial colloidal systems focus on temperature as the external stimulus. This is due to the popularity of thermoresponsive polymers (characterised by a lower critical solution temperature or an upper critical solution temperature), which change their conformation and solubility at these temperatures.[174] By attaching such polymers to the surface of nanoparticles, so-called "hairy" nanoparticles are formed. These types of polymers were extensively investigated using the Langmuir method and an air-water system, and will be discussed thoroughly later, in the context of the experimental results.[239–245] Switching between the above and below the critical temperature, the area occupied by nanoparticles changed, e.g., inducing plasmonic effects. These examples presented relatively small nanoparticles compared to the length of the polymers (the length of the chains was at least comparable to the diameter of the particle). Therefore, the behaviour of the nanoparticles was mainly determined by the conformation of the polymer chains at the interface, which could adapt, for example, a "pancake" or "brush" conformation. No experiments were performed for nanoparticles with large radii (60-100 nm), capped with polymers of much shorter lengths. These nanoparticles do not adopt a typical "pancake" or "brush" conformation, but rather form Janus-like structures, due to the impossibility of hydrating chains that were attached above the interfacial contact line. In "pancake" conformation, the polymer chains anchored above the water level can bend and be immersed. Short polymer chains also raise a question about whether crosslinking between the particles is possible or how the interactions between nanoparticles will change. This thesis fulfils this gap.

3.3. Interfacial Phenomena and Interactions between Particles at Interfaces

Bresme and Oettel, and later Guzmán et al., provided articles that in detail summarised most of the principles of interfacial phenomena of particles.[232,246]

The thermodynamic stability of a particle at an interface is determined by the reduction in interfacial free energy. The trapping energy (ΔE) for a spherical particle can be described as follows:

$$\Delta E = -\pi R^2 \gamma_{1,2} (1 \pm \cos(\theta))^2$$

where R is the radius of a particle, $\gamma_{1,2}$ is the surface tension at fluid-fluid interface, θ is the contact angle of a particle; the sign of the term $(1 \pm \cos(\theta))$ depends on the position at the interface (immersion). Micron-sized particles are considered to adsorb irreversibly to the interface, due to the high trapping energy, usually in the range between 10^6 k_BT and 10^7 k_BT. However, the particles smaller than 10 nm in diameter have the trapping energy of several k_BT, typically.[232,247,248] The position of a particle at the interface depends then on the contact angle. And can be described with Young's equation:

$$\cos\theta_0 = \frac{\gamma_{p,1} - \gamma_{p,2}}{\gamma_{1,2}}$$

$\gamma_{x,y}$ describes surface tension at the interface between the particle (p), and fluid phases (1 and 2). However, the abovementioned equation is not precise. With the decreasing size of a particle, a line tension τ becomes more significant:[246]

$$\cos\theta = \cos\theta_0 \left(1 - \frac{\tau}{R\gamma_{1,2}\sin\theta}\right)^{-1}$$

Changes in interactions between nanoparticles are key factors of self-assembly. Bresme and Oettel, as well as Guzmán et al., distinguished the following interactions as crucial.[232,246,249]

Electrostatics and Dipolar Repulsion

If the particle is trapped at the fluid-fluid interface, it is immersed partially in two phases. In the water phase, especially not ultrapure water, the particles are surrounded by the ion clouds (electric double layer), screening the charge of the particle (including the surface

charge). This creates an asymmetry when the charge of the particle is not screened (or differently screened) in the second phase. This results in the dipole moment and depends on the immersion and screening (ionic strength). Therefore, between particles at the interface, an interplay between screened Coulombic repulsion and dipolar interactions emerges, regulating the self-organisation of the material.

Van der Waals and Short-Range Repulsive Interactions

Van der Waals forces are short-range attractive forces. However, similarly to the electrostatic interactions at the interface, the strength of the forces also depends on the immersion of particles due to the different dielectric properties of the upper and lower phases. Therefore, simple equations describing van der Waals interactions are not sufficient, and amended ones are required to accurately describe them. When nanoparticles are very close to each other, short-range repulsion occurs, originating from the steric hindrances, due to the overlapping of capping layers.

Capillary Forces

Particles of size approximately larger than 10 μm gravitationally deplete the interface. For smaller ones, depletion is negligible, and the contact angle of a particle determines its immersion. The deformations of the interface create capillary forces that originate from the wetting of the particle surface and its roughness. As a result, various kinds of capillary forces can appear and influence an interfacial system. The phenomena of capillary forces at particle-laden interfaces were thoroughly investigated and described by Kralchevsky and his coworkers.[250–254]

Fluctuation Forces

Thermal fluctuations of the medium cause interactions between particles. The effect is analogous to the quantum Casimir effect. These forces are typically of the order of k_BT, so they can matter more for nanoparticles than for micron-sized particles, and they depend on the contact line.

Solvation Forces

At very small distances between particles, effects related to the solvent and its interaction with the particle (e.g., hydration, so-called hydrophobic interactions) can introduce additional interactions that are not captured by simple DLVO-type models.[255–257]

4. Langmuir Trough and Interfacial Phenomena

4.1. A Brief History of Langmuir Films

Thin films of oil on water were reported in ancient Babylonia, Japan and Greece (Aristotle). However, Benjamin Franklin is credited with being one of the first to investigate the problem of spreading oil on water scientifically. He spread a teaspoon of oil onto Clapham Pond in London in 1760 to demonstrate its calming effect on the water's surface. Lord Rayleigh revisited the problem and estimated the thickness of the oil on water film (1.6 nm) in 1889.[18]

Two years later, Agnes Pockels showed that the film on the surface of water can be controlled using barriers.[258] Her work was so advanced that it essentially became what we now call a Langmuir trough and Langmuir film. Irving Langmuir, while investigating oil films at General Electric, built upon the ideas presented by Agnes Pockels. He replaced oils with pure substances in his experiments and presented a theory of monolayer.[259] He also published a precise drawing of a Langmuir balance, which allowed for the measurement of surface tension (Figure 6), and demonstrated that the film can be transferred onto a solid substrate. Katherine Blodgett then developed that idea in 1934-1935.[260,261] She transferred films from the water surface by vertically immersing a solid substrate. Films transferred with this technique are called Langmuir-Blodgett films.[18] Analogously, Langmuir-Schaefer films refer to the technique developed by Vincent J. Schaefer, who, working with Langmuir, developed a method for transferring Langmuir films onto a horizontally oriented substrate in 1938.[262] Then, after a break caused by the Second World War, further development of the Langmuir trough came in the 1960s.[18] The Langmuir-Blodgett method reached its peak in the 1990s as an unfulfilled promise for an approach to molecular electronics; it then returned to the topic of thin-film nanoarchitectonics.[18] In contrast, Langmuir films continued to be actively developed. Nowadays, with the introduction of powerful characterisation techniques (e.g., Brewster angle microscopy, electron microscopy, atomic force microscopy), Langmuir and Langmuir-Blodgett films provide a powerful platform for investigating biological membranes, smart thin films, and even photovoltaic systems.[18] The above-mentioned history was described in detail by Oliveira et al..[18]

4.2. Nanoarchitectonics in Langmuir Films

Nanoarchitectonics is a term introduced by Masakazu Aono in 2000 (the laureate of the Feynman Prize in Nanotechnology in 2010), and later popularised especially by Katsuhiko Ariga and coworkers, the Japanese scientist specialising in supramolecular chemistry, surface science, and functional materials (especially Langmuir and Langmuir-Blodgett films, layer-by-layer assembly, and self-assembling materials). Nanoarchitectonics is a concept that involves forming functional materials dynamically by precisely harmonising various factors, including molecular and atomic control, self-organisation, and organisation in external fields. Therefore, such an approach is crucial in dynamically functioning systems – adaptive systems.[263] Katsuhiko Ariga described it as follows:[264]

"Nanoarchitectonics is a way to integrate existing scientific fields rather than create a totally new scientific field. It integrates the knowledge gained from nanotechnology with research fields related to the creation of materials, such as organic chemistry, inorganic chemistry, polymer chemistry, supramolecular chemistry, coordination chemistry, various other material sciences, fabrication at the nano- and microlevel, and biology. In nanoarchitectonics, the goal is to architect high-performance functional materials using nanounits of atoms, molecules, and nanomaterials."

The author emphasises that biological systems, being full of high-performance functional materials systems, mainly operate in 3D; however, key functional components – membranes – are in fact two-dimensional structures that regulate hierarchically built compartmentalised living organisms. Hence, the nanoarchitectonics of two-dimensional systems seems to be the best strategy to create highly functioning materials systems. The most promising platforms to architect these systems are Langmuir, Langmuir-Blodgett, and layer-by-layer methods.[264–269]

4.3. Historical and Modern Construction of a Langmuir Trough

The historical origins of precise control over the surface in interfacial experiments date back to Agnes Pockels, who was able to, for example, measure how the area per molecule contamination of the surface influenced the surface pressure.[258,270–272] Irving Langmuir developed her idea, and in 1917, he presented his setup (Figure 6).[259] He poured water into the enamelled tray (T) (approx. 60 cm x 15 cm) and trapped oil film between paper strips A and B.

Paper strip B's length is shorter than the width of the trough and can be moved freely. Above the trough, there was a support with a balance placed on it, standing on a knife edge K. This part was connected with a paper strip B via glass rods placed in two small holes of the paper strip B. Paper strip A was moved forward the oil film until pushing the paper B. To prevent the oil film from leaking to the area behind paper B, two air jets (F, F') were applied. When the edge of the strip B is directly under J, the oil film acts on the strip with a force equal to (considering the lever arm ratio) the weight hanging on the pan P. Paper strip C was used at the beginning of the experiment to remove contamination from the experimental area. Adding extra weights to the pan and recording the subsequent distances between A and B at equilibrium in (paper strip B under J) allows plotting an isotherm of compression (relation between force and distance or area).

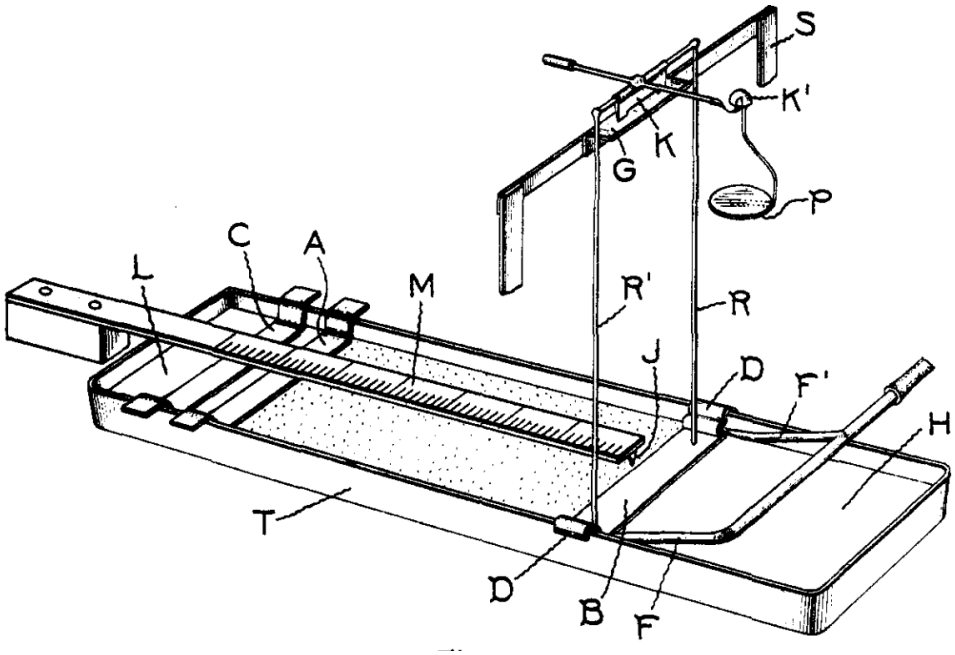

Figure 6. A setup used by Irving Langmuir. A, B, C – paper strips; D, D' – pieces of sheet metal; F, F' – tubes with air jets; G – glass plate; H – water surface; J – measurement point indicator; K, K' – knife edges; L – space where contamination is accumulated; M – metre stick; P – pan; R, R' – glass rods; S – support; T – enamelled tray of approx. 60 cm x 15 cm; Adapted with permission from ref.[259] Copyright 1917 American Chemical Society.

Modern examples of the Langmuir trough differ little in principle. As a common example, I will describe the general setup (Figure 7) used in this study to perform on-water experiments. However, the system is not limited to this particular solvent, and even mercury[273] or organic solvents[274] are used. A hydrophobic, e.g., Teflon, trough (1) is filled with deionised water (2) (R = 18.2 MΩ·cm). Usually, in the centre of the trough, there is a Wilhelmy plate or

a paper sensor (4) hanging on the balance (3). Instead of paper strips, hydrophobic, motorised barriers (5) are used.

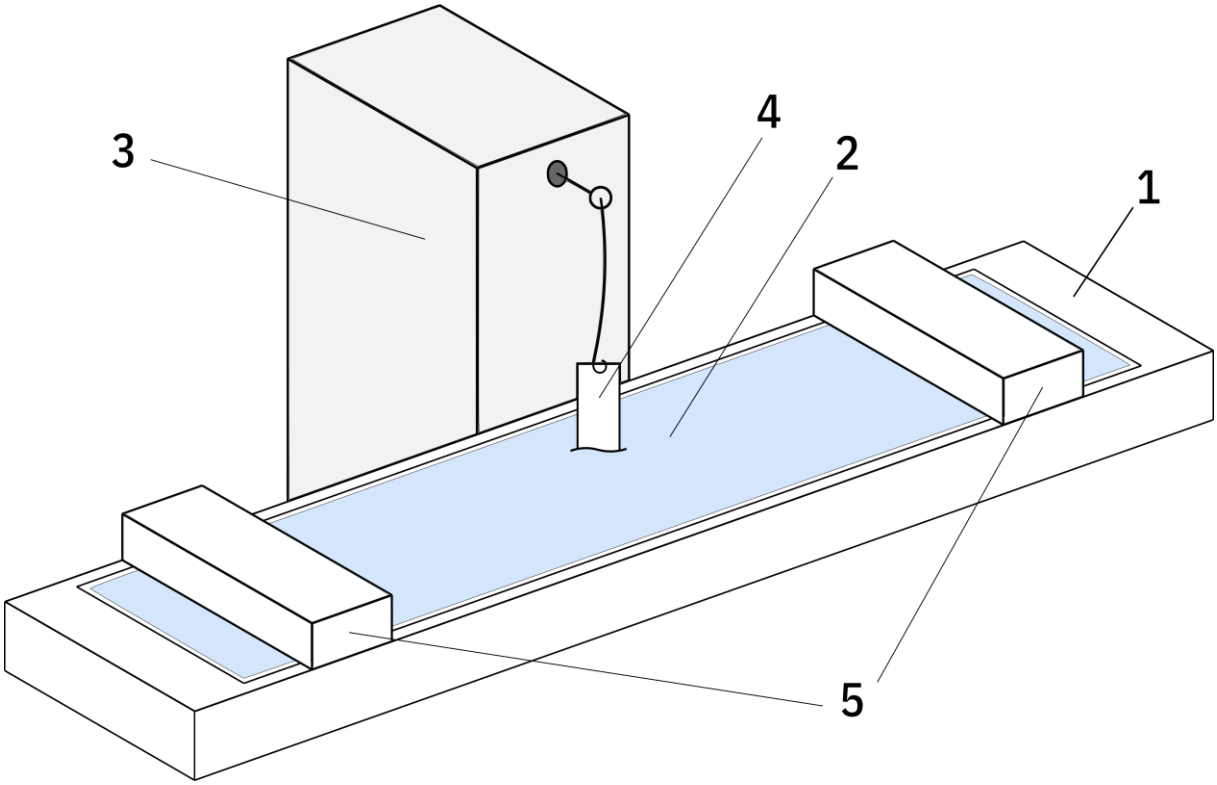

Figure 7. Representation of a modern Langmuir trough. 1. a Teflon trough, 2. deionised water, 3. balance, 4. sensor of the surface pressure (Wilhelmy plate or piece of paper), 5. motorised barriers. Own graphic, the modified one was previously used in the patent application P.450044

4.3.1. Langmuir, Langmuir-Blodgett, Langmuir-Schaefer Method of Monolayer Formation

In this section, I am going to briefly present the most common methods of forming monolayers using the Langmuir trough.

Langmuir Method

This method relates to what Langmuir presented in his initial works, i.e., they refer to deposition of a material (e.g., molecules, nanoparticles, proteins, polymer molecules) on a gas-liquid interface.[259] A classical, benchmark experiment, also one of the oldest registered ones, is the deposition of fatty acids at the surface of water. The Langmuir trough is cleaned, rinsed, and dried. Next, ultra-pure water is poured into the trough to the level that allows for the observation of a convex meniscus above the trough's edges. The barriers are moved towards the centre of

the trough, compressing the area between them. This process is initially carried out to concentrate the contamination of the water surface and aspirate it. The compression is controlled by reading the surface pressure and repeated until the rise in pressure due to the concentration of contaminants does not interfere with the experimental results (the rise in pressure during full compression is no higher than $0.1 - 0.2\ mN \cdot m^{-1}$). The term "full compression" is arbitrary and usually refers to the movement of the barriers from their maximally expanded positions to the smallest possible distance between the barriers, allowing for the measurement of surface pressure with the sensor (4). When the experimental area of the water surface is clean, the barriers are expanded. A solution of the analysed material is deposited onto the water surface. For that use, the material is dissolved in a solvent that preferably does not mix with water, is fast-evaporating, and is able to reside on the water surface (due to the density difference or surface tension). For fatty acids such as stearic acid or palmitic acid, chloroform is a common choice. Deposition of the solution of a known concentration is performed with a precise syringe (e.g., Hamilton syringe or an automatic dispenser). After the deposition, the system is left to fully evaporate the solvent and for the system to reach equilibrium. Next, the barriers compress the thin film of the material in a programmed manner, registering the relation between surface pressure and area.

Langmuir-Blodgett Method

This method was developed by Katherine Blodgett in 1934.[260] It enables the transfer of the Langmuir film (a thin film compressed at the Langmuir trough) onto a solid substrate. In principle, the substrate is immersed, usually vertically, in the trough and pulled up with the precise control of the surface pressure (Figure 8). Depending on the hydrophilicity of the material and the substrate, the substrate can be initially immersed in water (before the sample is deposited) or dipped into an already prepared film. The films transferred onto the substrate are called Langmuir-Blodgett films. The substrate can be covered with the Langmuir film several times. Consider the situation where an initially immersed hydrophilic substrate was pulled up and covered with a monolayer of a fatty acid (Figure 8. a)). The hydrophilic part of the molecule, the COOH group (marked as a grey circle), is in contact with the hydrophilic surface of the substrate. Such an arrangement allows for the transfer of the film. Subsequent immersion of the same substrate results in the substrate being covered with a reversed layer (hydrophobic outside). Subsequent pulling covers the plate with the third layer, making the surface hydrophobic again (as after the first pulling out).

Langmuir-Schaefer Method

This method, developed by Schaefer, is an alternative approach to transferring a film from the water surface (or from another liquid) onto a solid substrate.[262] The substrate is placed parallel to the surface, above it, and slowly descends to the surface (Figure 8. b)). While it touches the surface, the reversed film is stamped on the substrate. Again, the process is driven by the hydrophilicity of the deposited material and the substrate.

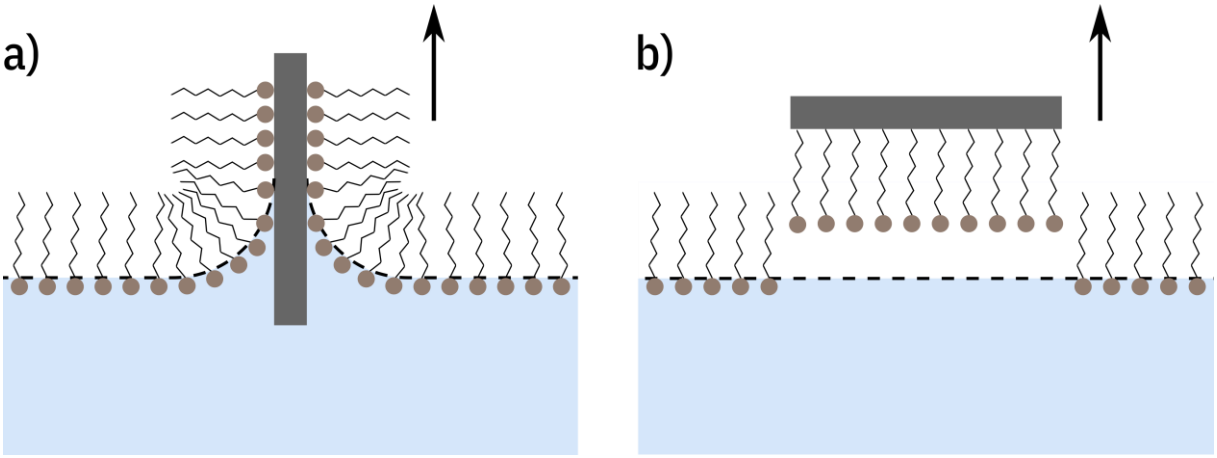

Figure 8. a) Scheme of a Langmuir-Blodgett method with a film of fatty acid and a hydrophilic substrate. **b)** Scheme of a Langmuir-Schaefer method with a film of fatty acid and a hydrophobic substrate.

Transferring onto Solid Substrates

Transferring the Langmuir films with the aforementioned methods is sometimes used as an indirect method for analysing the structure of the film in situ at the subphase surface. However, this is not always true, especially because of the stresses generated at the meniscus (Langmuir-Blodgett method), leading to breaking the film.[275] The film may also be distorted by the interactions between molecules (or particles) of the thin film with the substrate.[276] Other factors that are significant in monolayer transfer are the amphiphile structure of the molecules, subphase composition (including pH and ionic strength), dipping rate, and surface pressure at which the film was deposited.[18] Discrepancies after the transfer may also occur due to the evaporation of subphase residues, e.g. coffee-ring effect.[277]

4.4. Theory of Langmuir Monolayers

4.4.1. Surface Pressure

Surface pressure (Π) is defined as the difference between the surface tension of a subphase in a fluid/liquid system (γ_0) and the surface tension of a subphase with a Langmuir layer at the interface (γ).[278]

$$\Pi = \gamma_0 - \gamma$$

Surface tension can be measured with a Wilhelmy plate (or paper) and calculated as follows:

$$\gamma = \frac{F}{l \cos\theta}$$

where F is a force of the surface pulling the plate down (discounting the mass of the plate and buoyancy), l is the perimeter of the plate that is immersed in the subphase (contact line), and is a contact between the subphase and the plate, usually assumed to be 0 due to complete wetting (e.g., for filter papers).[278]

4.4.2. Surface Rheology

In a classical compression-decompression experiment at the Langmuir trough, the Π–A isotherms are registered. By slowing the compression and decompression processes, the isotherms can be considered to represent equilibrium, especially at low surface pressure, where the compression rate is slower than the relaxation of the examined layer. Physical states and phase transition of the layer are classified due to the surface compressional modulus (ε_s), which can be interpreted as 2D elasticity and is defined as:[278]

$$\varepsilon_s = -A\left(\frac{\delta\Pi}{\delta A}\right)_T$$

where A represents the area and Π stands for the surface pressure.

Various scientists approached dividing the phases of the monolayer.[18,279–281] One of the classifications of them is presented in Table 1.

While the surface compressional modulus considers static (equilibrium) conditions, the surface dilatational elasticity modulus (E) is a dynamic approach. The latter is measured using

the oscillating barrier method. The barriers of the Langmuir trough oscillate with specific frequencies, changing the experimental area by a certain percent.

$$E(i\omega) = E_d(\omega) + iE_v(\omega)$$

E_d is interfacial dilatational elasticity moduli, E_v is the surface dilatational viscosity moduli, $\omega = \frac{2\pi}{f}$, f is the frequency. Alternatively, E can be described as $E = \frac{d\Pi}{dA/A}$.

Therefore,

$$E_d = |E| \cos\theta$$

$$E_v = |E| \sin\theta$$

θ is a phase angle describing the delay between area deformation and the response in the surface pressure. The higher E_d, the more elastic is the response of the film. The deformation energy is accumulated and returned rapidly. High E_v means viscous response, in which energy is dissipated during deformation.[282–284]

Table 1. Two-dimensional states of Langmuir Monolayers according to Oliveira et al.[18]

ε_s / mN m^{-1}	State
~0 mN m^{-1}	gaseous phase, collapse or first-order transition
0-25 mN m^{-1}	low-density liquid phase
25-50 mN m^{-1}	liquid-expanded phase
100-250 mN m^{-1}	liquid-condensed phase
>500 mN m^{-1}	solid

4.4.3. Surface Potential

Oliveira and coworkers provided comprehensive discussions on surface potential measurements of Langmuir films.[18,285] Surface potential is a useful measurement complementary to surface pressure-area isotherms. In contrast to the latter, it can provide information on a monolayer already at early stages of compression, when surface pressure is close to 0. The air-water interface possesses an intrinsic electrical potential because of the orientation of water molecules (oxygen atoms are oriented to the air and hydrogen atoms toward the water subphase).[18,285] A Langmuir film spread at the interface modifies this potential. The

difference depends on the orientation of the molecules trapped at the interface; therefore, measurements of surface potential can provide insight into the structure of mono- and polylayers, the ionisation state of interfacial molecules and the orientation of molecular dipoles. In this study, surface potential, defined as the difference between the potential with and without a Langmuir film, was measured using a Kelvin probe. This method uses a vibrating capacitor. The vibrating electrode (Kelvin probe) is placed above the surface of the interface, and the reference electrode is immersed in the subphase. The oscillation of the probe changes the capacitance of the system, which enables the determination of the potential difference between the clean and film-covered interface. Then, the difference in potential between the situation with the Langmuir film at the interface and without it depends on the dipolar organisation of the interface and, for ionised monolayers, also on the electrical double-layer contribution.[18,285] As amphiphilic compounds are typically analysed with the Langmuir method, the charge distribution occurs due to the polarisation within the molecule.[285] This relation can be presented as:

$$\Delta V = \frac{1}{A\varepsilon_0}\left(\frac{\mu_1}{\varepsilon_1} + \frac{\mu_2}{\varepsilon_2} + \frac{\mu_3}{\varepsilon_3}\right)$$

where ΔV is surface potential, μ_i are normal components of the dipole moment originating from reorientation of water molecules, hydrophilic headgroups, and hydrophobic tail groups, respectively. A is area per molecule, ε_0 stands for vacuum permittivity and ε_i are effective relative dielectric constants of the respective regions the dipoles are related to.[18,285]

The equation, especially useful for nanoparticles, can be simplified to

$$\Delta V = \frac{\mu \cos\theta}{A\varepsilon_0\varepsilon_r}$$

where ΔV is surface potential, $\mu \cos\theta$ is dipole moment perpendicular to the interface, A is area per molecule and ε_r stands for effective relative permittivity of the monolayer.[18]

Surface potential isotherms often remain close to zero at large molecular areas and increase only after a critical area is reached. This area is associated with the structuring of the monolayer.[285]

Surface potential measurements are very sensitive to contamination of the water subphase. Impurities may lead to irreproducible values of ΔV at large areas.[285]

4.4.4. Brewster Angle Microscopy

In 1991, two pioneering studies emerged, demonstrating the potential of using Brewster Angle Microscopy to observe Langmuir monolayers in situ.[286,287] P-polarised light is not reflected from the subphase if the incident beam is shed under the Brewster angle (α); however, it is propagated through the subphase. Therefore, if light is shed at the Langmuir film, it can still pass through it and the subphase (depending on the layer's properties), but is also reflected to the detector, as the presence of the Langmuir film changes the effective optical properties of the system. A scheme of the phenomenon is presented below (Figure 9).[288,289]

Brewster angle depends on the refractive indices of the media of light propagation:

$$\tan \alpha = \frac{n_2}{n_1}$$

where n_2 is the refractive index of the subphase and n_1 is the refractive index of the upper phase (usually air). Brewster angle for the air-water system is around 53°.[288,289]

Similar to surface potential measurements, Brewster angle microscopy complements surface pressure measurements and can be applied simultaneously. Significantly, it is a label-free and non-invasive technique. BAM allows us to notice the morphology of the film when the surface pressure is close to zero. This technique is especially useful for registering early-forming aggregates – particularly for colloidal Langmuir films.

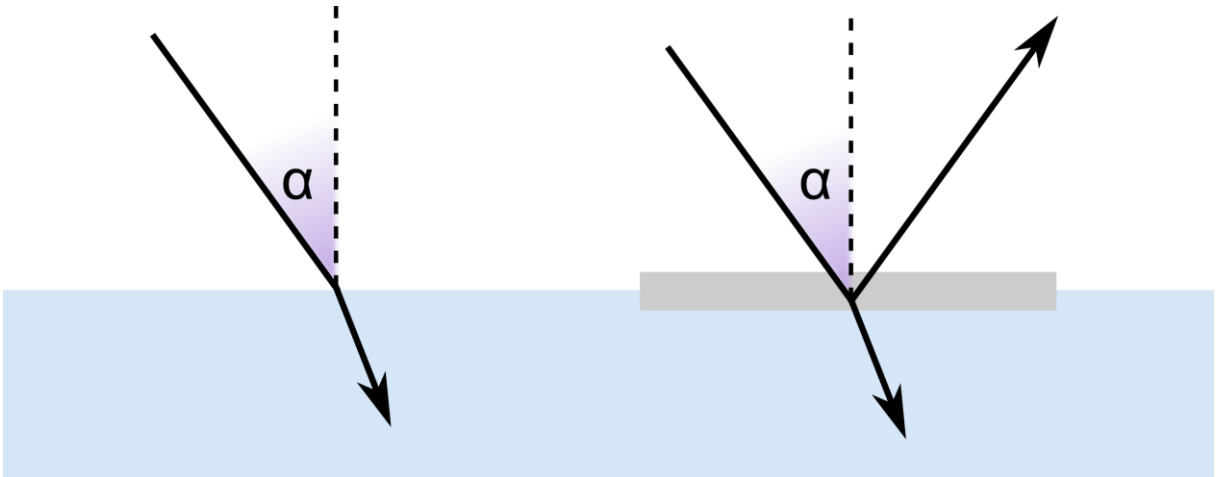

Figure 9. Principles of Brewster Angle Microscopy. Propagation of p-polarised light shed at the subphase at Brewster angle (left) and shed at the Langmuir film at Brewster angle of the subphase.

4.4.5. Other Methods

Although the 1990s are often described as the peak of Langmuir monolayer research, the measurement methods related to the topic are continually evolving. Because these methods were not used in this thesis, I am going to briefly mention some of them.

Infrared Reflection-Absorption Spectroscopy (IRRAS)

IRRAS is an in situ technique used to study Langmuir monolayers. It is based on the detection of reflected from the film infrared radiation providing information on functional groups, their orientation and conformation of the examined molecules (including lipids, peptides and proteins).[290]

Synchrotron-Based X-ray Methods

Using advanced methods, such as grazing incidence X-ray diffraction (GIXD), provides an insight into the two-dimensional lattice structure and ordering of the molecules within the film. X-ray reflectivity (XRR) and grazing-incidence X-ray off-specular scattering (GIXOS) are used to investigate the electron density profile normal to the interface. They provide information on the thickness of the film.[291]

Neutron Reflectivity

One of the promising methods in Langmuir monolayers' investigation is neutron reflectivity. It is similar in principle to XRR, delivering insight into the depth profile of the film normal to the interface. Using neutrons instead of X-rays allows for differentiating specific parts of the film by isotopic substitution. Thanks to that operation, specific components of the film can be hidden or enhanced in the results.[292]

The Aim of the Study

Nature has long served as a blueprint for scientific advancement, inspiring researchers to develop systems that mimic its utility, complexity, and responsiveness. However, nowadays, science moves beyond simple imitation, creating dynamic, adaptive systems capable of responding to external stimuli. The development of these systems is the next step toward revolutionising nanotechnology and its applications through precise design and control. The development of nanoarchitectonics, in my opinion, leads toward advanced nanotechnology that will be applied in medicine and industry. The aim of the study is to add a step in the direction of nanorobotics, nanomachines, and revolutionary smart materials – a vision so far mostly presented in the science-fiction literature and media. My contribution to this objective is to develop a deeper understanding of the controllable interactions between specially designed building blocks. Without knowing the principles governing these interactions, the rational design of more complex structures remains highly challenging.

Adaptive colloidal systems are one of the means to achieve that goal through the collective behaviour of stimuli-responsive nanoparticles. The Langmuir method, however, is a promising platform for investigating the interactions between nanoparticles, their self-assembly, and physicochemistry at the interface – nanoarchitectonics in its pure form. In this work, I aimed to demonstrate that the Langmuir method is a useful and practical tool for developing complex, adaptive systems.

In the thesis, I focus on thermoresponsive colloidal Langmuir films, which have received limited attention in the literature. Most of the examples present relatively small nanoparticles coated with comparable-sized thermoresponsive polymers. That approach exposes the thermal response in the occupied area at the interface, therefore highlighting changes in self-organisation. A specific goal of this study is to develop knowledge of the nanoarchitectonics of a system composed of nanoparticles close to the upper limit of dimensional definition, driven by short thermoresponsive polymers attached to their surfaces. This was aimed to be realised through an understanding of the formed adaptive Langmuir films and a description of the observed phenomena. The detailed context behind the specific goal is discussed in the next section.

Briefly, to realise the vision and goals of the study, a two-dimensional (2D) adaptive system composed of PNIPAM-functionalized Fe_xO_y@SiO_2NPs, termed PSiFeNPs, was designed to precisely respond to temperature changes and reorganise at the air-water interface. I have also observed the magnetic susceptibility of the formed films, but the results were poorly reproducible and are not presented in this thesis.

Previous works have explored PNIPAM-coated nanoparticles in 3D systems for drug delivery or thermal responsiveness.[293,294] Less is known about their behaviour at interfaces, especially in adaptive thin films. Therefore, to bridge that gap, I aimed to characterise the stimuli-responsive properties of PSiFe nanoparticles confined within Langmuir and Langmuir-Blodgett films.

Experimental

This chapter is based on the following publications:

Zbonikowski, R.; Iwan, M.; Paczesny, J.* Stimuli-Responsive Langmuir Films Composed of Nanoparticles Decorated with Poly(N-Isopropyl Acrylamide) (PNIPAM) at the Air/Water Interface. *ACS Omega* **2023**, *8* (26), 23706–23719. https://doi.org/10.1021/acsomega.3c01862.

Zbonikowski, R.*; Aryanfar, A.; Iwan, M.; Presselt, M.; Paczesny, J.* Langmuir Nanoarchitectonics of Thermoresponsive Adaptive System of PNIPAM-Decorated Nanoparticles Induced by the Ionic Strength of the Subphase. *The Journal of Physical Chemistry C* **2025**. https://doi.org/10.1021/acs.jpcc.5c02555.

1. The Design of the Nanoparticles

The literature on the topic presents few examples of PNIPAM-covered nanoparticles with well-defined structures and behaviour at the fluid-liquid interface. The project aimed to go beyond the general exploration of 2D adaptive systems and related phenomena. Phenomena that are difficult to describe due to the problematic methodology of investigating nanoobjects' behaviour at the water surface.

Nanoparticles were to be controlled by multiple external stimuli – this potential feature could enable increasing the complexity of the adaptive system step by step. Therefore, the magnetic core of Fe_xO_y was incorporated into a composite nanoparticle and isolated with a silica layer, creating a core-shell structure. Nanoparticles of Fe_3O_4 within a size lower than approximately 20 nm are superparamagnetic, and the critical size for them to form a multi-magnetic-domain structure is estimated to be 76 nm for a cubic shape and 128 nm for a spherical shape.[206] Therefore, designing the nanoparticle to be composed of 15 nm magnetic core, and the silica shell of ca. 37.5 nm thickness for the first study (first batch) or ca. 25 nm thickness for the second study (second batch), potentially allowed to observe differences in magnetic behaviour of PSiFeNPs compared to superparamagnetic NPs, as PSiFeNPs remained single domain particles with a much bigger size. That larger size theoretically increases the energy required to disorganise the magnetic superstructures of aggregated/ordered nanoparticles, and, for superparamagnetic nanoparticles, is smaller than k_BT. At the same time, the magnetic field required to organise particles ought to be stronger. The shell was composed

of silica for two more reasons: first, silica is relatively non-reactive and stable; second, ligands attached to the silica are bonded covalently and, in consequence, are not labile. I have explored the possibility of manipulating the PSiFeNPs layers using external magnetic fields. The studied films showed magnetic-field susceptibility, but the observed alterations were poorly reproducible. Thus, these results are not included in this thesis.

As the surface of nanoparticles is crucial to their physicochemical properties, considerable attention has been paid to precisely preparing and investigating the thermoresponsive surface coverage. PNIPAM is a well-known thermoresponsive polymer with the LCST of 32 °C. In a water solution (suspension), below this temperature, amide groups on the polymer's side chains are solvated by water molecules, forming hydrogen bonds. When the temperature rises above 32 °C, k_BT in the system is high enough to break the hydrogen bonds between water and the polymer. As a consequence, hydrogen bonds between amide groups are favoured (inter- or intramolecular interactions).[174] Macroscopically, the polymer becomes hydrophobic, with a wetting angle of around 30-50° below the LCST and 80-90° above it.[295] At the PNIPAM-grafted surface, the values were around 50° below the LCST and around 90° above the LCST.[296] For long polymeric chains of PNIPAM, this transition is usually described as a coil-to-globule transition, and, in the concentrated solutions, is related to reversible gelation of the mixture.

Most examples investigating nanoparticles coated with thermoresponsive polymers considered either random polymer coverage or polymer grafting. In both cases, the nanoparticles were relatively small compared to the capping layer, to observe potentially large changes in the desired properties. In this work, nanoparticles with diameters of around 90 and 65 nm are controlled by short oligomers of a PNIPAM derivative anchored to the surface.

Tucker and Stevens demonstrated that the thermal transition behaviour of isolated PNIPAM oligomers depends on their chain length. They examined oligomers composed of 18 and 30 monomers (denoted as 18 N and 30 N).[297] Short chains, particularly those with 18 N or fewer, remain in an extended conformation below the LCST and only adopt a partially folded structure upon heating above the LCST. In contrast, longer chains, such as those with at least 30 N, are capable of forming coiled structures below the LCST and transition into a globular form when the temperature exceeds the LCST. Notably, the tacticity of the polymer does not significantly influence the LCST of oligomers, although it does affect that of longer PNIPAM chains.[297]

Shan et al. further observed that the LCST of PNIPAM oligomers is altered when they are grafted onto nanoparticle surfaces.[298] Intermolecular (interligand) interactions between nanoparticles are present at high concentration, and the attachment of PNIPAM to the surface of a nanoparticle reduces the LCST, compared to that of isolated oligomers. For grafted chains shorter than 18 N, the LCST decreases significantly with decreasing molecular weight. In contrast, longer oligomers and polymers (free or surface-bound) typically exhibit LCSTs near 30-32 °C. Interestingly, free oligomers show the opposite trend: the LCST increases as molecular weight decreases, sometimes exceeding 60 °C.

Based on these findings, the design of the studied PSiFe particles was aimed at capturing the coil-to-globule-like transition of PNIPAM in response to temperature changes. Oligomers were selected to be longer than 18 N to allow folding above the LCST, but as short as possible to ensure a "closed" conformation above the LCST. PNIPAM triethoxysilane derivative with an average molar mass of 2750 $g \cdot mol^{-1}$ and a polydispersity index (M_w/M_n) below 1.8 was used as the derivative was available commercially (Sigma Aldrich). This corresponded to chain lengths of approximately 20-29 N, with an expected length of around 24 N. To ensure the transition of the PNIPAM, further experiments were conducted at 20 °C and 40 °C, positioning the LCST approximately in the middle, with an offset of around 10 °C on either side. Attachment of PNIPAM to the surface of nanoparticles was to facilitate the polymer transition.[298]

Jones et al. showed that the presence of free PNIPAM chains in a suspension is crucial for nanoparticles of a similar structure (AuNPs capped with PNIPAM copolymer) to aggregate. The size of the nanoparticles and the length of the chains have an impact, but it is not considerable. Hence, the method of nanoparticle purification (e.g., centrifugation parameters) becomes much more significant for direct measurements of interactions between nanoparticles.[299]

A comparable PNIPAM chain length grafted onto gold nanoparticles has previously been investigated; however, those studies involved significantly smaller core diameters, typically only a few nanometres.[240,298] It was demonstrated that PNIPAM layers could not overlap effectively when attached to such small gold cores.[240] Two key distinctions exist between those earlier systems and the one investigated in the present study. Firstly, in this system, the ligands were firmly anchored to the oxide layer. The typical bond energy of a Si-O bond is approximately 100 $kcal \cdot mol^{-1}$, and each PNIPAM ligand is capable of forming up to

three such bonds with the surface.[300] This contrasts with the Au-S bond, commonly reported to have bond energies ranging from 20 to 60 kcal·mol^{-1},[301] which permits ligand mobility and rearrangement on the nanoparticle surface.[302]

Not many studies have shown similarly constructed systems of thermoresponsive so-called “hairy” nanoparticels. Stefaniu et al. presented a cycle of articles describing Langmuir films and Gibbs films (adsorbed from the subphase) of magnetic nanoparticles (6.4 nm Fe_3O_4 core) capped with thermoresponsive polymers (4.8 nm and 4.9 nm layers). The authors showed that nanoparticles were trapped at the interface and could be compressed till the critical pressure (ca. 25 mN·m^{-1}).[303] Above this pressure, nanoparticles were expelled from the interface and could readsorb to a free surface.[303] The authors found the maximum particle coverage and the maximum surface pressure.[244] They investigated possible conformations of nanoparticles depending on the temperature.[242,243] Then, the adsorption to the DPPC layer (1,2-dipalmitoyl-sn-glycero-3-phosphocholine; cell membrane model) was examined.[241]

Another cycle of articles was published by Shan et al.. The authors synthesised 4.2 nm gold nanoparticles capped with PNIPAM (3000 g·mol^{-1}) and PS (3200 g·mol^{-1}) and investigated them at the Langmuir trough. They observed an unexpected blue shift in the SPR maximum with increasing surface pressure. Based on this, the authors concluded that the nanoparticles' conformation had to change with compression.[240] This hypothesis was further tested with 3.4 nm AuNPs capped with PNIPAM (13680 g·mol^{-1}) via contrast-matched neutron reflectivity. “Pancake” and “brush” conformations were observed due to the compression, as well as contraction and expansion of the structures with the temperature. The latter resulted in a decrease in the interparticle distance by overcoming the polymer's LCST.[239] Shan et al. took a glimpse of the different lengths of NIPAM oligomers attached to nanoparticles (2.0-4.1 nm) in water suspensions. The LCST of nanoparticles decreased with shorter oligomers. Larger cores also had a decreasing effect on the LCST.[298]

An interesting example of SiO_2 (ca. 200 nm capped with an 8.2 nm layer of PNIPAM) was presented by Liu et al.. The study, however, did not consider Langmuir films. The authors showed a membrane made out of the nanoparticles (1.5 mm thickness, 10 mm in diameter) and compared properties at 20 °C and 40 °C. At lower temperatures, the membrane was liquid-like, and at higher temperatures, it became solid. In the latter case, the membrane was capable of stopping a steel bead (4 mm diameter, 0.26 g) at velocities up to 328 cm·s^{-1}.[304]

2. Materials and Methods

The nanoparticles used in this study were prepared with the help of Dr Michalina Iwan. The description of the synthesis is based on a protocol developed by her and published in the ref.[19]

A scheme summarising materials and methods is attached at the end of the section as Figure 10.

2.1. Synthesis of PSiFeNPs

Among the syntheses, two batches of different particles could be distinguished, differing in the thickness of the silica layer. Experiments using pure water as the subphase (*ACS Omega*) were conducted with batch I (approx. 90 nm in diameter particles), while experiments using KCl solution (*J. Phys. Chem. C*) were performed with batch II (approx. 65 nm in diameter particles).

2.2. Synthesis of Fe_xO_y@SiO_2NPs

In a plastic vial, 30 ml of 99.8% ethanol (23.348 g), 3.0 ml of distilled water (2.999 g), and 1.5 ml of a 23% aqueous ammonia solution (1.487 g) were combined. The mixture was stirred at room temperature, and 1 ml of Fe_xO_y Siliquan nanoparticles (15 nm in diameter, Warsaw, Poland) was added. After 15 min of stirring, 150 µl of tetraethyl orthosilicate (TEOS) was introduced, and the vial was sealed. The reaction mixture was stirred continuously at room temperature for 24 h. The final nanoparticle dispersion had a concentration of 1.89 $mg \cdot ml^{-1}$.

2.3. Functionalisation of Fe_xO_y@SiO_2NPs (Synthesis of PSiFeNPs)

Thriethoxysilane derivative of PNIPAM oligomer (M_n = 2750 $g \cdot mol^{-1}$, and the polydispersity index (M_w/M_n))[d] was purchased from Sigma Aldrich. 8.40 mg of the PNIPAM derivative was dissolved in ethanol (99.8%, 3 ml). The solution was poured into a glass vial containing the previously prepared Fe_xO_y@SiO_2NPs at 28 °C (30 ml). The mixture was stirred for 72 h at 28 °C.

2.4. Purification of PSiFeNPs

30 ml of hexane and 18 ml of 99.8% ethanol were added to the PSiFeNPs post-reaction mixture, resulting in a homogeneous solution/suspension. The mixture was centrifuged at 9000 rpm for

[d] M_n stands for number-average molecular weight and M_w stands for weight-average molecular weight

45 minutes. After removing the supernatant, 10 ml of ethanol was added to the remaining orange precipitate. The mixture was sonicated for 5 min and centrifuged for 30 min at 9000 rpm after the addition of 20 ml of hexane. The supernatant was removed after every centrifugation. This procedure was repeated 4 times. At the end, 9.9 ml of distilled water was added to obtain a 5 $mg \cdot ml^{-1}$ suspension of PSiFeNPs. Such a prepared solution was further sonicated for 30 min and left in the open air for 30 min to allow hexane residues to evaporate before sealing.

2.5. Characterisation of Nanoparticles

Key parameters and the characterisation of the PSiFe nanoparticles will be presented and discussed in the following sections. The detailed characterisation of nanoparticles at different synthesis steps was provided in the Supporting Information of publications in *ACS Omega* and *Journal of Physical Chemistry C*.[19,20] The characterisation has been attached as Appendix 1.

2.6. Sample Preparation

The purified water suspension of PSiFe nanoparticles (5 $mg \cdot ml^{-1}$) was stored in a fridge. To prepare a sample for Langmuir experiments, the suspension was diluted with THF in a volumetric flask to obtain a final solution at 1 $mg \cdot ml^{-1}$. The mixture was sonicated for a few minutes and stored at room temperature. Just before the sample was deposited at the air/water interface, the mixture was sonicated again for at least 2 minutes.

2.7. Langmuir Systems

Experiments described in this work were performed with two different experimental setups. That allowed us to confirm experiments in analogous, very similar conditions, as observations were in accord. Furthermore, certain experiments could benefit from different setups to produce higher-quality results. Both setups were placed in Plexiglas boxes:

1. NIMA setup consisted of a 375 cm^2 trough, Teflon barriers, surface pressure sensor (filter paper Wilhelmy plate), multimeter KEITHLEY 196 system DMM with a temperature sensor (Pt100), passive antivibration table. If necessary, the setup was extended with MiniBAM, dipper or Kelvin electrode.
2. KSV NIMA setup consisted of an 835 cm^2 trough, Delrin barriers, surface pressure sensor (filter paper Wilhelmy plate), default temperature sensor provided by KSV NIMA, pneumatic antivibration table STANDA (for experiments performed at ultrapure water,

published in *ACS Omeg*a, used passively). If necessary, the system was extended with a KSV NIMA Kelvin electrode, a dipper, or a KSV NIMA MicroBAM.

For long-term experiments in which water evaporation could influence the experiment, the saturated level of water/KCl solution was maintained by gently pouring an additional amount of subphase behind the barrier.

2.8. Preparation of the Langmuir Trough

Langmuir troughs were cleaned before experiments with chloroform, ethanol and ultrapure water (Type 1, 18.2 MΩ·cm at 25 °C), then left to dry. If necessary, the trough was cleaned with dishwashing liquid or aqua regia, and rinsed thoroughly with ultrapure water. After pouring ultrapure water or a KCl solution as the subphase, with the barriers in an“open” position (maximal distance between the barriers), the barriers were “closed”, and the interface was cleaned using a Teflon sucking nozzle. The procedure was repeated until the surface pressure measured with a balance equipped with a filter-paper sensor did not differ by more than 0.1 $mN \cdot m^{-1}$ between the “open” and “closed” positions of the barriers. To maintain the desired temperature, a NESLAB RTE 7 thermostat was used.

2.9. Deposition of PSiFeNPs at the Air-Water Interface

After cleaning the interface, the subphase was heated to 40 °C (±2 °C). The deposition took place with the barriers in the “open” position. A previously cleaned glass rod was partially immersed in the subphase, approximately in the middle of the trough. The desired amount of the sample (sonicated suspension of PSiFeNPs, 1 $mg \cdot ml^{-1}$) was added dropwise with a Hamilton syringe onto the glass rod, just above the subphase surface. Thanks to this approach, the sample gently flew down onto the interface. The glass rod was then carefully removed from the system, and the prepared trough was left for 10-20 min to let the solvent evaporate. If the experiment was performed at 20 °C, the thermostat was set to the corresponding temperature. The spreading assisted with a glass rod was inspired by Pathirana et al., to increase the efficiency of the deposition of the sample suspended in a water/THF mixture that mixes with water.[305] The elevated temperature was used to maintain PNIPAM in a more hydrophobic state (above the LCST) to prevent desorption from the interface during the process.

2.10. Preparation of KCl Solutions

KCl solutions used as subphases were prepared in volumetric flasks with pure water (ultra-pure water, class I) as the solvent.

2.11. Langmuir Experiments

2.11.1. Compression-Decompression Cycles

The desired amount of the PSiFeNPs sample (between 500 µl and 1500 µl) was deposited on the subphase (ultrapure water, 0.001 M KCl solution, 0.01 M KCl solution or 0.1 M KCl solution).

2.11.2. Stability Experiments

These experiments were conducted using the NIMA setup. A Kelvin electrode was used for experiments with pure water as a subphase. 500 µl of the sample was deposited on the interface according to the method described above. After approx. 10-20 min, a cycle of compression and decompression was conducted with a barrier speed of 10 $mm \cdot min^{-1}$. In stability experiments, portions of 250 µl of the sample were added consecutively, allowing experiments to be performed with 500 µl, 750 µl, and 1000 µl. Surface potential was measured simultaneously. It proved impossible to measure surface potential for all the KCl-solution subphases due to measurement perturbations, most likely caused by the high ion concentration.

2.11.3. Stimuli-Responsive Langmuir Isotherms

The experiments were conducted with the NIMA setup. The PSiFeNPs sample (500 µl) was deposited on the pure water interface at 40 °C and left to equilibrate for 10-20 min. Compression and decompression were performed with a speed of 10 $mm \cdot min^{-1}$. The second cycle was carried out at 20 °C. Then, the third one at 40 °C and the final one at 20 °C again. The time left for the temperature change and the film's disaggregation was 2 h between the 1^{st} and 2^{nd} cycles, 18 h between the 2^{nd} and 3^{rd} cycles, and 2 h between the 3^{rd} and 4^{th} cycles. The water level was checked before every cycle and corrected if needed by gently pouring pure water into the trough, but behind the barrier. This experiment was performed by Prof. Jan Paczesny.

2.11.4. Elasticity and Viscosity

Surface compressional moduli were calculated based on the derivatives of the compressional isotherms. The oscillatory barrier method was used to investigate interfacial dilatational elastic and viscous moduli. 500 µl of the PSiFeNPs sample was deposited on the pure water surface, and after equilibration, compressed to a surface pressure of approximately 6.5 $mN \cdot m^{-1}$ at a rate of 10 $mm \cdot min^{-1}$. Then the system was equilibrated for 1 h, and the barriers began oscillating with the specific frequencies within the range of 0.015 to 0.209 Hz. During the experiment, 10 cycles of the area amplitude of 2.5 cm^2 were measured for each frequency, which corresponded to the area changes of around 5 to 10%. The experiments were conducted using the NIMA setup.

2.12. Relaxation Experiments

1500 µl of the PSiFeNPs sample was deposited on the pure water interface at 40 °C, and the sample was left for 20 min to allow solvent evaporation. Then, the experiment was performed in two paths. In the first path, the system was left to further equilibrate for an additional 20 min. The film was compressed to around 11 $mN \cdot m^{-1}$ with a rate of 10 $mm \cdot min^{-1}$. The surface pressure was measured in relation to just after the barriers were stopped while reaching the target pressure. The second path was analogical; however, after the 20 min for solvent evaporation, the system was cooled to 20 °C and left to equilibrate. This procedure took 2 h. The experiments were performed using the KSV NIMA setup.

2.13. Transfer of the Samples onto Solid Substrates

The Langmuir trough setups were prepared as described before. Then, a silicon wafer (used as a solid substrate) was hung in a dipper and immersed vertically at the centre of the trough in the subphase. The procedure for cleaning the interface was repeated. The film was compressed to the target pressure (10 $mm \cdot min^{-1}$) and then pulled out at the rate of 13 $mm \cdot min^{-1}$.

2.14. Preparation of Solid Substrates

One-sided-polished silicon wafers were cleaned with 30% nitric acid, then rinsed thoroughly with distilled water, ethanol, and acetone, hung unimmersed in a dipper, and left to dry before immersion.

2.15. Other Instrumentation

Dynamic light scattering (DLS) and zeta-potential measurements were performed with Zetasizer Nano ZS (Malvern Instruments Ltd.; He-Ne laser 633 nm, max. 4 mW, backscattered light at 175° and forward-scattered light at 12.8°)

Scanning electron microscopy (SEM) was conducted using FEI Nova NanoSEM 450.

Profilometry was performed with Dektak XT (Bruker Corporation) using a stylus of 2.5 μm radius.

A Hettich Universal 320 centrifuge was used for the synthetic procedures.

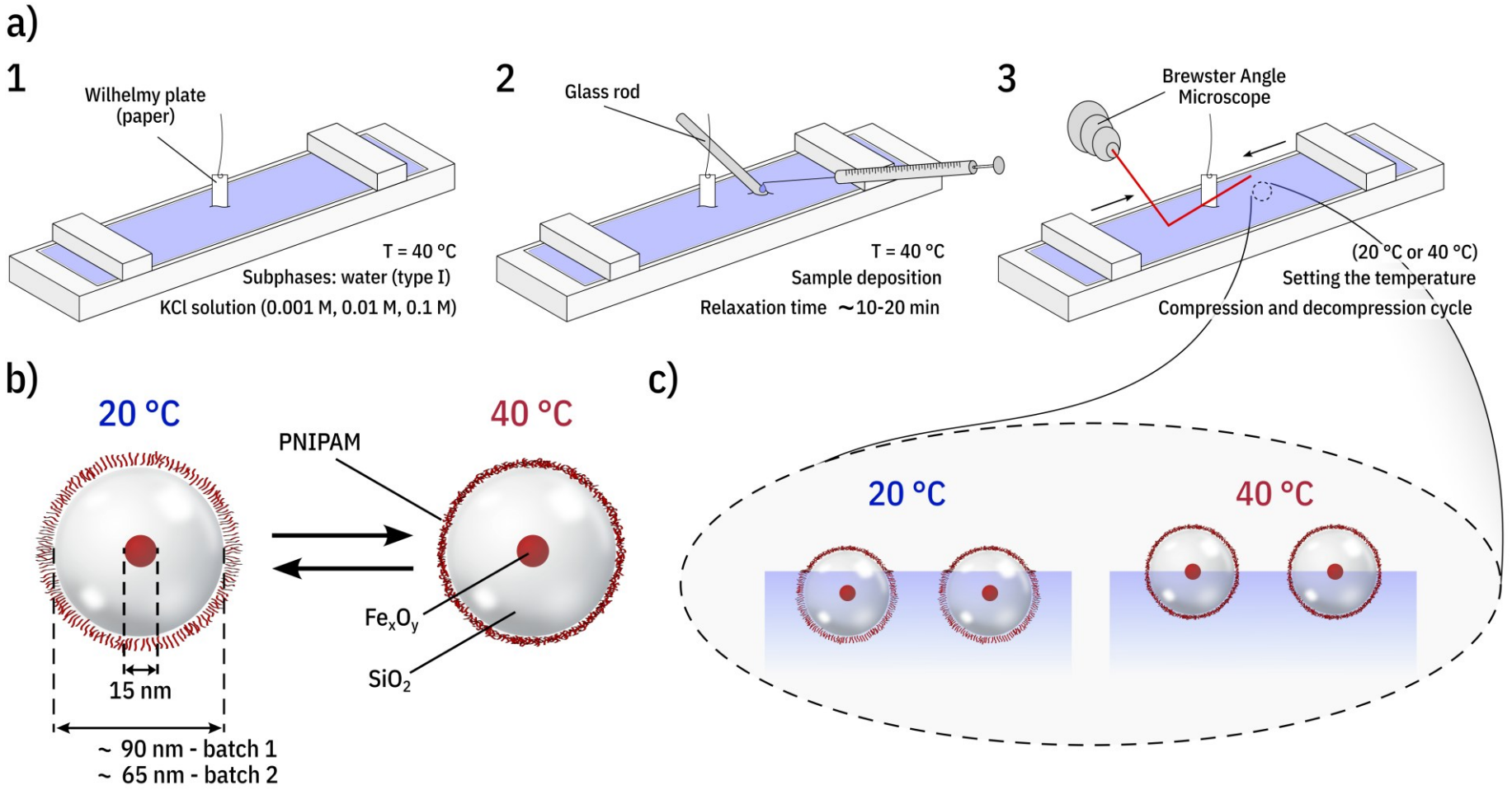

Figure 10. a) Scheme of the regular Langmuir experiments. **1.** The subphase (ultrapure water or KCl solution) was poured into the trough and heated to 40 °C. **2.** PSiFeNPs sample (1 mg·ml^{-1} in THF/water = 4:1, v/v) was deposited at the interface using a Hamilton-type syringe and a glass rod as a support. **3.** Compression and decompression cycles were performed at the desired temperature of the subphase, with the Brewster angle microscopy performed simultaneously. Surface potential was measured with an analogical system. The Kelvin electrode was not included in the scheme due to the picture's clarity. **b)** Scheme of PSiFeNPs. **c)** Schematic representation of the immersion and conformation of PSiFeNPs at the interface. The author's own figure; a modified version was previously published in ref.[20] (CC-BY 4.0).

3. Results and Discussion – Pure-Water-Based System

To facilitate further analysis and the interpretation of the nanoparticles' conformation, the subsequent terms related to the PNIPAM capping layer were defined as follows: 1) **extended/open** – these terms describe hydrated, short, not bent chains; below LCST or in a nonaqueous environment. 2) **closed** – bent, short polymer chains or short chains, interconnected or intraconnected with hydrogen bonds at the surface of the nanoparticles. 3) **HT** – depending on the context, high or higher temperature, refers to the temperature of 40−42 °C; in other words, a high temperature regime, being far above the LCST of PNIPAM. 4) **LT** – depending on the context, low or lower temperature, refers to the temperature of 18−20 °C; in other words, a low temperature regime, far below the LCST of PNIPAM.

3.1. Langmuir Films of PSiFeNPs at Pure Water

Nanoparticles were gently deposited at the air-water interface. Using the glass rod and a mixture of solvents (water/THF) in the sample allowed the deposition of water-suspendable nanoparticles at the interface, as described in Materials and Methods. The triple cycles of compression and decompression were recorded to assess the reversibility and repeatability of the isotherms at 40 °C and 20 °C. The isotherms (Figure 11) were poorly reproducible in consecutive cycles at the LT; however, they were reproducible at the HT. Lower reproducibility cycle to cycle at LT was most likely due to nanoparticle aggregation. This issue will be further investigated in the following chapters. For further evaluation, only the first isotherms (unless otherwise stated) were analysed to allow meaningful comparison between experiments.

The entrapment of the nanoparticles at the interface is theoretically justified. The trapping energy of a particle at the interface can be expressed as follows:[306,307]

$$E = -\frac{\pi R^2}{\gamma_{1,2}}(\gamma_{1,2} - (\gamma_{P1} - \gamma_{P2}))^2$$

At the air-water interface and for spherical nanoparticles it can be expressed as:

$$E = -\pi R^2 \gamma_{1,2}(1 \pm \cos\theta)^2$$

where the minus sign in the brackets indicates desorption into the water, and the plus sign indicates removal of the particle into the air.[308]

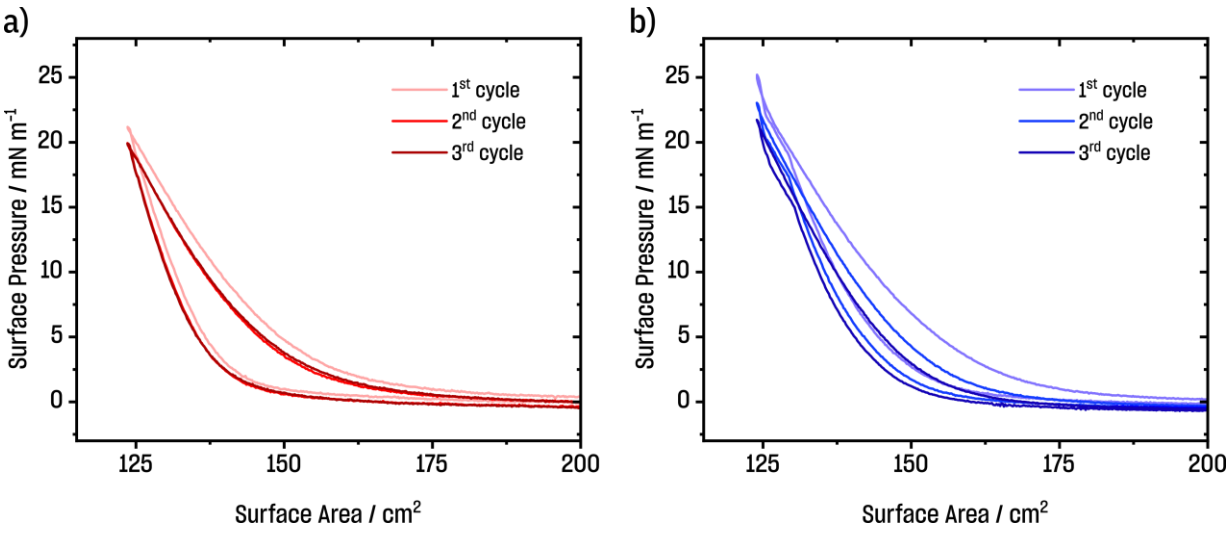

Figure 11. Reversibility and reproducibility of the PSiFeNPs Langmuir films' compressional isotherms. Three subsequent compression-decompression cycles of PSiFeNPs Langmuir films at the **HT** (left) and the **LT** (right). Experiments were carried out with 500 µl of the sample at the air-water interface. The author's own figure, previously published in ref.[19] (CC-BY 4.0).

The trapping energy depends on the radius of a particle (R), the surface tension of the air-water interface ($\gamma_{1,2}$), and the contact angle of the particle (θ). γ_{P1} and γ_{P2} stand for the surface tensions of a solid particle and a fluid phase (in this case, water and air). For the numerical calculation, the parameters were used as follows: $\gamma_{1,2;\,20\,°C} = 72.75 \text{mN·m}^{-1}$, $\gamma_{1,2;\,40\,°C} = 69.60 \text{ mN·m}^{-1}$, and $R = 45$ nm.[309]

Table 2 shows the energy ranges needed to remove a PSiFe nanoparticle (batch I) from the interface. The exact value depends on the contact angle.

According to this, to remove a 90-nm particle from the interface into the water, the contact angles were calculated to be $\theta = 4.41°$ for 20 °C and $\theta = 4.53°$ for 40 °C. On the other hand, the contact angle of PNIPAM microgel varies between 30-50° below LCST to 80-90° above LCST.[295] The trapping energy for $\theta = 30°$ at T = 20 °C is approximately 2000 k_BT, and for $\theta = 80°$ and T = 40 °C, the trapping energy is approximately 73000 k_BT. Therefore, despite their hydrophilicity caused by the PNIPAM capping layer, PSiFeNPs should be stable at the interface.

Table 2. Comparison of k_BT and energies required to remove a PSiFe nanoparticle (batch I) from the interface at 20 °C and 40 °C.

	20 °C	**40 °C**
k_BT	$4.047 \cdot 10^{-21}$ J	$4.324 \cdot 10^{-21}$ J
Range of energies required to remove a nanoparticle from the interface	0-$1.851 \cdot 10^{-15}$ J	0-$1.771 \cdot 10^{-15}$ J

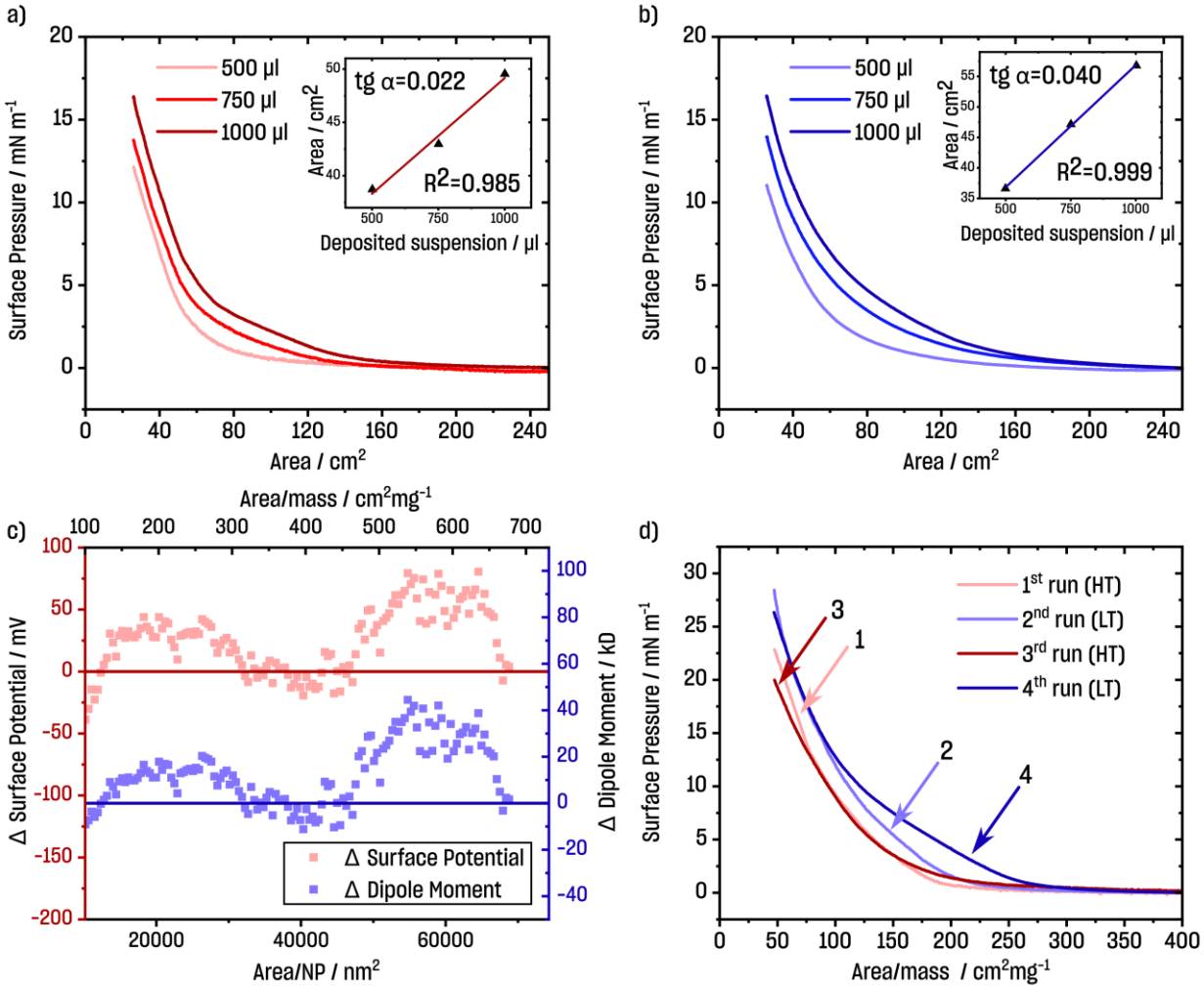

Figure 12. Properties of the PSiFeNPs system. **a)** Subsequent compressions of the PSiFe nanoparticles film after depositing consecutive portions of the sample at the HT. The inset presents the linear dependence between the deposited volume of the sample and area at surface pressure of 7.5 $mN \cdot m^{-1}$; **b)** Subsequent compressions of the PSiFe nanoparticles film after depositing consecutive portions of the sample at the LT. The inset presents the linear dependence between the deposited volume of the sample and area at surface pressure of 7.5 $mN \cdot m^{-1}$; **c)** The differences (LT minus HT) in surface potential and consequently in dipole moment according to the Helmholtz equation; **d)** Switchability experiment. The compression isotherms of consecutive compression-decompression cycles. Decompression isotherms were omitted from the figure for clarity. The author's own figure, previously published in ref.[19] (CC-BY 4.0).

Next, the reliability of the deposition process was confirmed through stability experiments in which Langmuir films containing different amounts of nanoparticles (subsequently added between cycles) were compressed. The isotherms were shown in Figure 12 a) at the HT and Figure 12 b) at the LT. With increasing sample size (amount of PSiFeNPs) at the interface, the isotherms shifted to the right at both temperature regimes. Linearity of the shifts was calculated and plotted (tangents) for the areas where the surface pressure reached 7.5 $mN \cdot m^{-1}$. The normalised isotherms (area per mass; $cm^2 \cdot mg^{-1}$) revealed only small deviations (Appendix 2. Figure A2.1. a) and b)). The origin of this observation comes from the local imperfections of spreading of the nanoparticles upon the additions of PSiFeNPs, as seen by the Brewster angle microscopy (Figure 15). Despite the linear shift, the proportionality coefficient was below 1, indicating that some fraction of the nanoparticles was lost during the experiment or preaggregated during the subsequent depositions.

The possibility of desorption of the nanoparticles could not be excluded, as the *b* parameter ($y = ax+b$) of linear regressions for the surface pressures of 0.5 $mN \cdot m^{-1}$, 1.0 $mN \cdot m^{-1}$, 2.5 $mN \cdot m^{-1}$, and 5.0 $mN \cdot m^{-1}$ was not equal to 0, even if the trapping energy was much larger than k_BT. However, the linear relation implies that if desorption were the cause of the observed phenomenon, the same fraction of nanoparticles would sink at every deposition (which would result in $b = 0$). Against this explanation was high trapping energy. Nanoparticles might preaggregate before deposition or at the interface. The first case was analogous to the sinking of a certain fraction of nanoparticles at every deposition. The latter should result in increasing deviation from linearity with the subsequent additions of the sample, but could be linear within the tested sample amounts, as the number of nanoparticles was far from filling the whole initial area of the trough. In such a case, the first deposition spreads less-aggregated particles, and the subsequent deposition causes local aggregation near the glass rod. Another explanation concerns the deposition process itself. Using a glass rod, even if it was a more subtle method of deposition than direct dropwise deposition, could not slow the flow of the PSiFeNPs sample enough to prevent preaggregation. Alternatively, some of the nanoparticles could remain on the glass rod. But the last one would yield a negative *b*, whereas *b* was positive.

The repeatability (experiment to experiment) and scalability of colloidal Langmuir films are known to be much more problematic than those of amphiphilic molecules. Nonetheless, the linearity presented with the protocol above is sufficient to compare and conclude on the

colloidal PSiFeNPs system Langmuir and Langmuir-Blodgett experiments, with the repeatable control of the number of PSiFeNPs deposited at the interface.

Further addition of even 1.5 ml of the sample did not result in a typical, sudden collapse; therefore, continuous collapse was suspected, as present in other nanoparticle Langmuir systems.[310,311] This suspicion was confirmed by SEM pictures (Appendix 3). The study was focused on the low surface pressure; however, avoiding uncontrolled collapse was favourable for designing an adaptive (stimuli-responsive and reversible) system.

Comparing different experiments at the HT and the LT (ceteris paribus) revealed shifts toward higher surface area with decreasing temperature below the LCST (also surface area per nanoparticle; Figure 12 and Appendix 2). This is unusual, as in the case of non-thermoresponsive particles or molecules, the thermal expansion occurs, being the dominant factor. A typical thermal expansion of a model molecule (stearic acid) was shown in Appendix 4. The shape of the isotherm shifts to the right as temperature increases.

Reversibility and repeatability are formidable for advanced systems to operate.[230] The system presented in this study exhibited reversible switching between two states as a function of temperature. Figure 12 d) presents the experiment of alternative switching of the temperature and performing a compression-decompression cycle with relaxation between the cycles (more details in the Materials and Methods section). What can be observed, the isotherms are reproducible, especially in the HT regime. The LT regime shows some discrepancies below 10 $mN \cdot m^{-1}$. That could have been caused by the differences in relaxation (disaggregation processes). In this experiment, the decrease in surface pressure due to the switch in temperature from 20 to 40 °C is profound and clearly visible.

Surface potential isotherms (Figure 13), registered simultaneously with the surface pressure isotherms, reveal new insights into the investigation. The LT isotherm showed a gradual growth of the surface potential upon compression with considerable hysteresis during decompression. Higher surface potential values during decompression suggest that the nanoparticles aggregated and the film decomposed slowly as the available area increased. On the contrary, at the HT, hysteresis was almost absent; however, opening the barriers and spreading the film left the surface potential above 0. The steep rise in surface potential at the maximal compression at the HT might have resulted from interference between the Kelvin electrode and the barrier holder; however, this phenomenon was not observed at the LT. Therefore, this observation was most likely due to differences in the film's properties. A rise in

surface potential is usually observed before a rise in surface pressure, as the concentration of nanoparticles at the interface and between the electrodes increases, but they are still not close enough to interact. This was also observed in the PSiFeNPs experiments.

Furthermore, based on the surface potential, the difference of a dipole moment perpendicular to the surface was calculated and plotted (Figure 12 c)). The dielectric permittivity was estimated as it changed linearly with the linear compression rate from 1 to 3.9, being a value of ε for SiO_2. The difference in the dipole moment (LT minus HT) was positive throughout most of the compression, reaching approximately zero at 40000 nm^2 per nanoparticle, as well as at the minimal and the maximal compression.

There are not many reports on the impact of temperature on surface potential. Nakahara et al. showed the decrease of the surface potential as well as a shift toward smaller surface areas for Surfactant TA, and mixtures of dipalmitoylphosphatidylcholine, egg-phosphatidylglycerol, amphiphilic α-helical peptide (Hel 13-5) and palmitic acid.[312] Higher temperature fosters disordering of the Langmuir film due to increased movement of the molecules at the interface.

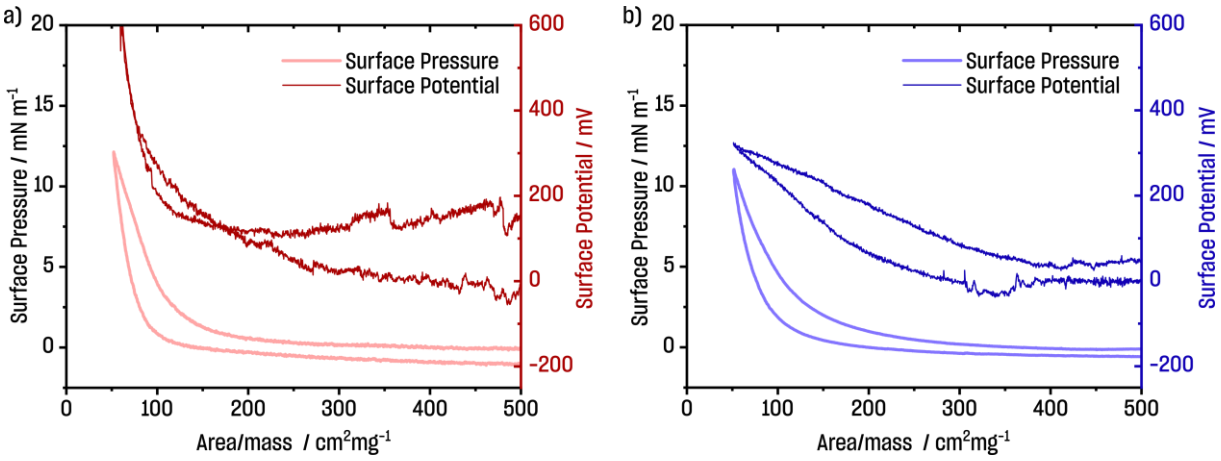

Figure 13. Surface potential isotherms and corresponding surface pressure isotherms **a)** at the HT and **b)** at the LT. The author's own figure, previously published in ref.[19] (CC-BY 4.0).

3.2. Surface Compressional Modulus

The surface compressional modulus expresses the change in surface pressure relative to the change in area. Its value being in a certain range can be interpreted as an indicator of a two-dimensional phase, as described in Section 4 in Literature Review. Experimental isotherms and calculated surface compressional modulus (cf. section 4.4.2 in Literature Review) are presented in Figure 14 a). The surface compressional modulus for LT was higher than that for HT upon

compression. The values in both cases did not exceed 30 $mN \cdot m^{-1}$. That means that within the experimental range, the adaptive system of PSiFeNPs operates in the low-density liquid phase. That was in line with the previously mentioned observation of constant collapse. As individual nanoparticles could buckle out of the plane upon compression, this could explain why the surface compressional modulus remains in that low range of values (0-30 $mN \cdot m^{-1}$).

3.3. Surface Rheology

To shed light on the interactions between PSiFeNPs at the interface, the 2D-rheological experiments have been performed. In Langmuir experiments, compression-decompression isotherms, one usually aims to perform the experiments as close as possible to the equilibrium. When the velocity of the barriers $|v| \rightarrow 0$, or the registered isotherm shows the exact equilibrium values of the surface pressure (or surface potential) at any area. Nevertheless, the investigation of the dynamic out-of-equilibrium phenomena may bring new insights. Therefore, the visco-elastic properties were measured using the oscillating barriers method (as described in Materials and Methods). Briefly, the film was compressed to approximately 6.5 $mN \cdot m^{-1}$ and relaxed. Then it was compressed again to the target pressure adjusted, so that the surface pressure response to 5-10% changes in area varied with the movement frequency. The results were calculated according to the equations in Section 4.4.2. of the Literature Review and depicted in Figure 14 b). The experiment revealed that, regardless of the temperature regime, the elastic properties were dominant for all frequencies. On the other hand, viscous properties were negligible as the surface dilatational viscosity modulus was close to 0. That means the PSiFeNPs film responded immediately to the mechanical compression, similar to a layer of ping-pong balls rearranging under compression.

Figure 14 c) and d) show the related Lissajous diagrams prepared analogously as in the literature.[313] The small positive hysteresis was noticed at LT. This observation indicates that the nanoparticles did not accumulate during the oscillations, suggesting slightly more viscous properties than at the HT. No hysteresis was observed at the HT, which can be interpreted as fully elastic properties. Additional Lissajous diagrams for 0.05 Hz, where the hysteresis difference was more pronounced, were presented in Appendix 5. The appendix contains an additional discussion on rheology, including linearity of the experiments.

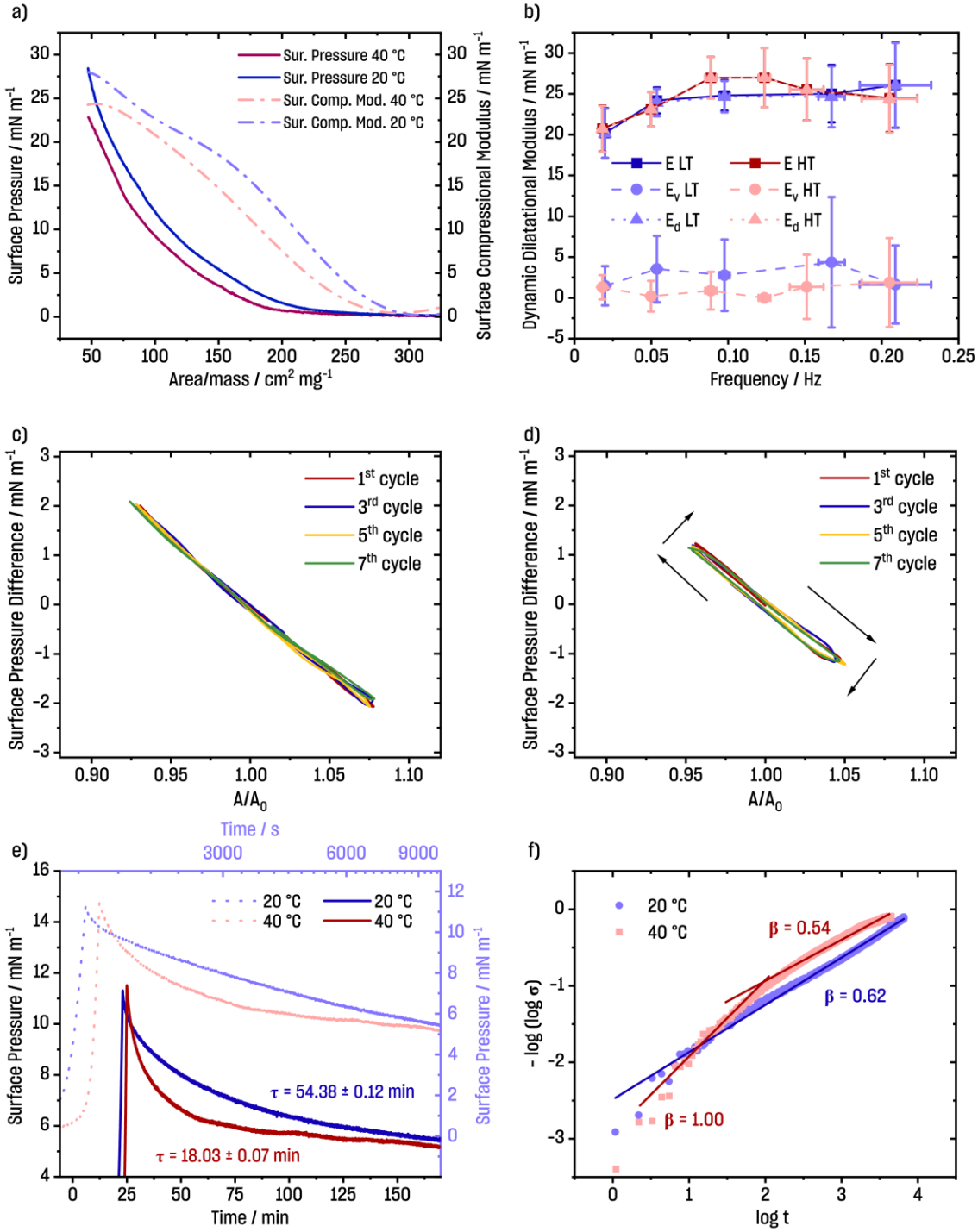

Figure 14. Surface rheology of PSiFeNPs films. **a)** surface compressional moduli of PSiFeNPs films at 20 °C and 40 °C, and corresponding compression isotherms; **b)** surface dilatational elasticity moduli of PSiFeNPs films at 20 °C and 40 °C (E – complex surface elasticity, E_v – surface dilatational viscosity, E_d – surface dilatational elasticity); **c)** Lissajous diagram for the PSiFeNPs film at the HT (oscillation experiments with a frequency of 0.10 Hz); **d)** Lissajous diagram for the PSiFeNPs film at the LT (oscillation experiments with a frequency of 0.10 Hz); **e)** relaxation experiments in linear scale (vivid colours) and logarithmic scale (pale colours); the films were compressed to 11 mN·m^{-1} and left to relax; the 40 °C relaxation was corrected by subtracting the evaporation drift; **f)** analysis of Kohlrausch-Williams-Watts function, and estimation of β parameters related to interactions within the film. The author's own figure, previously published in ref.[19] (CC-BY 4.0).

3.4. Relaxation Experiments

An additional way to analyse interactions between nanoparticles within the analysed film is to investigate the kinetics of relaxation. Briefly, in these experiments, films were compressed to the target pressure and, once the programmed value was reached, barriers were stopped, and the surface pressure was recorded over time (see Materials and Methods). The comparison of the two temperature regimes is presented in Figure 14 e). In contrast to the rheological experiments described above, the difference between 20 °C and 40 °C was much more visible.

Next, the results were further analysed according to the method derived for polymeric films and described by Hilles et al.[314] The relaxation was fitted with the function:

$$y = y_0 + Ae^{-\frac{x-x_0}{t}}$$

resulting in a relaxation time t equal to approx. 54 min and 18 min for the LT and the HT, respectively. Interestingly, plotting the relaxation curves on a logarithmic timescale indicated that the process was different. In contrast with the HT regime, relaxation was almost linear on a logarithmic scale at the LT. These characteristics of the curve indicate that stronger attractive interactions occur between nanoparticles at the LT. The shape of the curve at the HT suggested a more liquid-like phase. That supported the hypothesis that, by exceeding the LCST of PNIPAM, the conformation of the whole nanoparticle may change, and the closing of PNIPAM at the HT most likely occurred only with oligomers attached to the same nanoparticles (no interparticulate hydrogen bonds). Open conformation fostered interactions with other particles, including aggregate formation, as observed with BAM.

In the further analysis, the relaxation results were investigated using the Kohlrausch-Williams-Watts function,[314] the method used to study interactions in polymeric films:

$$\sigma(t) = \sigma_0 e^{-\left(\frac{t}{\tau}\right)^{\beta}}$$

σ_0 stands for the amplitude of the relaxation, t is the relaxation time, β is a parameter describing interactions, τ is time needed to reach the equilibrium. Furthermore, $\sigma_0 = \Pi_{t0} - \Pi_{\infty}$, where Π_{t0} is the surface pressure at the beginning of the relaxation and Π_{∞} stands for the surface pressure at the equilibrium. Therefore:

$$\ln\frac{\sigma}{\sigma_0} = -\left(\frac{t}{\tau}\right)^{\beta}$$

$$\ln\frac{\sigma_0}{\sigma} = \left(\frac{t}{\tau}\right)^{\beta}$$

$$\log\left(\ln\frac{\sigma_0}{\sigma}\right) = \beta\,(\log t - \log\tau)$$

$$\log\left(\frac{1}{\log e}\cdot\log\frac{\sigma_0}{\sigma}\right) = \beta\,(\log t - \log\tau)$$

$$\log\left(\frac{1}{\log e}\right) + \log\left(\log\frac{\sigma_0}{\sigma}\right) = \beta\,(\log t - \log\tau)$$

Since $\log\left(\frac{1}{\log e}\right)$ *and* $\log\tau$ *are constants, the derivation (tangent) of this relationship is an equivalent of the derivation (tangent) of* $\log\left(\log\frac{\sigma_0}{\sigma}\right) \sim \beta\log t$

Figure 14. f) shows $\log\left(\log\frac{\sigma_0}{\sigma}\right)$ plotted versus $\log t$. The β parameter mentioned by Hilles et al.[314] is equal to 1 if there is no coupling in the system. Values around 0.5 are interpreted as "*high cooperative motions*". Such a strong cooperative motion (β = 0.62) was observed at 20 °C. The tangent of the plotted relation was almost constant throughout the whole analysed time. On the contrary, the tangent was changing with time at 40 °C, suggesting no coupling in the first minutes of the relaxation and strong cooperativity (β = 0.54) at almost, and after τ. While the interpretation of the values of β parameters in the initial minutes of relaxation is consistent with the other rheological experiments, the theory is derived for polymers. PSiFeNPs are capped with a thin layer of PNIPAM, thanks to which they sometimes exhibit properties more similar to soft matter (e.g., shifts in compression isotherms) and sometimes behave like solid spheres (e.g., dynamic dilatational modulus). Further conclusions should be restricted due to the limitations of the theory applied to the studied system.

3.5. Brewster Angle Microscopy

Simultaneously with registering the $\Pi - A$ isotherms, the air-liquid interface was monitored in vivo with a Brewster angle microscope. The results from different stages of compression-decompression cycles are presented in Figure 15. Changing the temperature between the two analysed regimes revealed distinguished morphologies of the films. The film was barely visible during the compression at 40 °C (Figure 15 a) and c)). Only small and single bright dots were noticed and they became less visible upon decompression (Figure 15 d)), disappearing eventually. On the contrary, the single and small aggregates were observed just after cooling

down the film before the compression (Figure 15 b)). At only 0.2 $mN \cdot m^{-1}$ the BAM pictures showed a dense, bright film (Figure 15 e)). At the decompression, the fractal, dendrimer-like aggregates were noticed (Figure 15 f)) or a consecutively disintegrating network (Figure 15 g)).

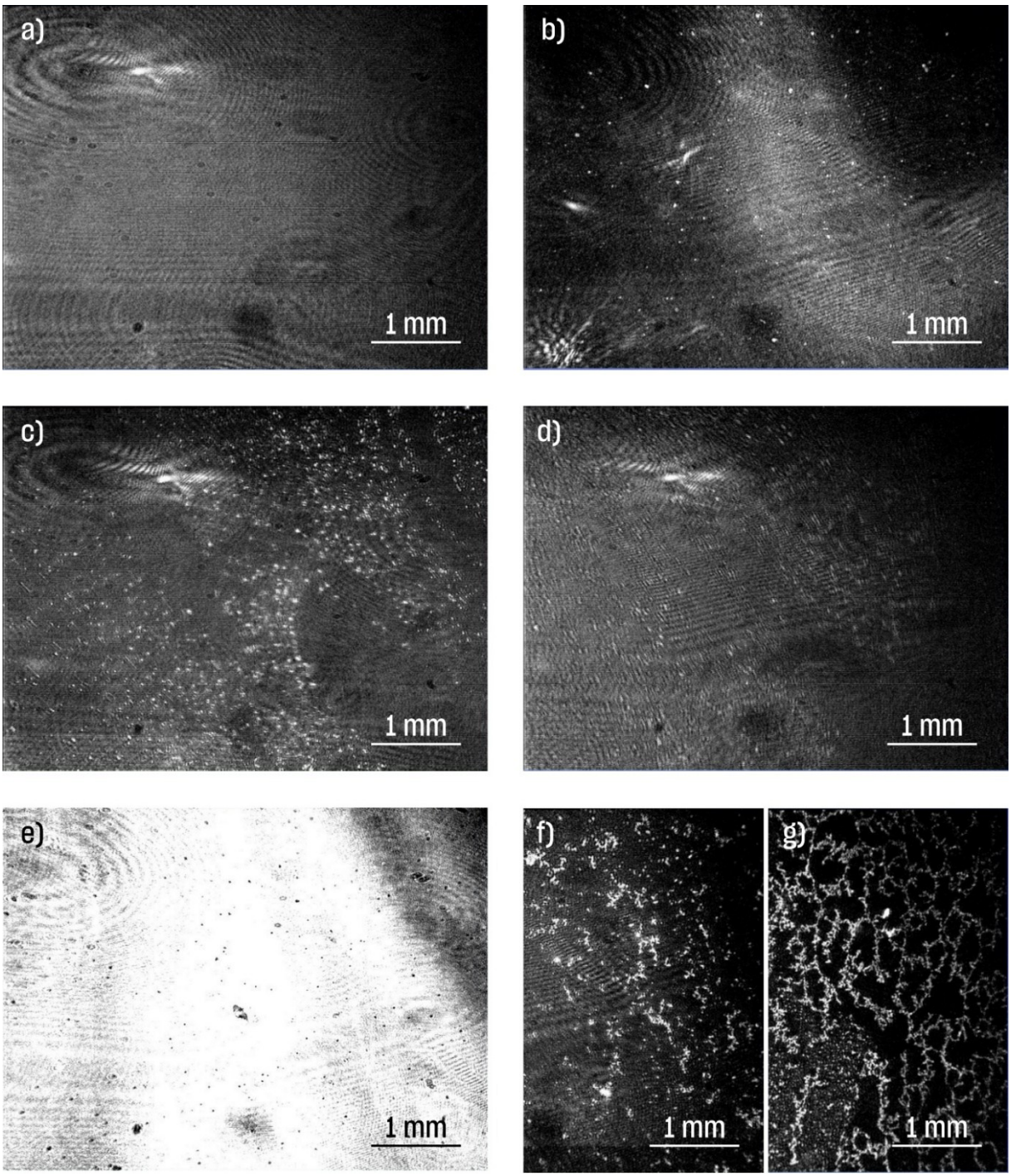

Figure 15. Brewster angle microscopy of PSiFeNPs Langmuir films. The pictures were taken **a)** after deposition and relaxation at the HT, **b)** after the deposition at the HT and cooling down to LT, **c)** upon the compression at the HT (122 cm^2, 0.3 $mN \cdot m^{-1}$), **d)** during the consecutive decompression at the HT (126 cm^2, 0.2 $mN \cdot m^{-1}$), **e)** upon the compression at the LT (132 cm^2, 1.9 $mN \cdot m^{-1}$, and **f)** upon the decompression at LT (142 cm^2, 0.2 $mN \cdot m^{-1}$), with **g)** a visible dendrimer-like network (LT). The author's own figure, previously published in ref.[19] (CC-BY 4.0).

3.6. Scanning Electron Microscopy of Langmuir-Blodgett films

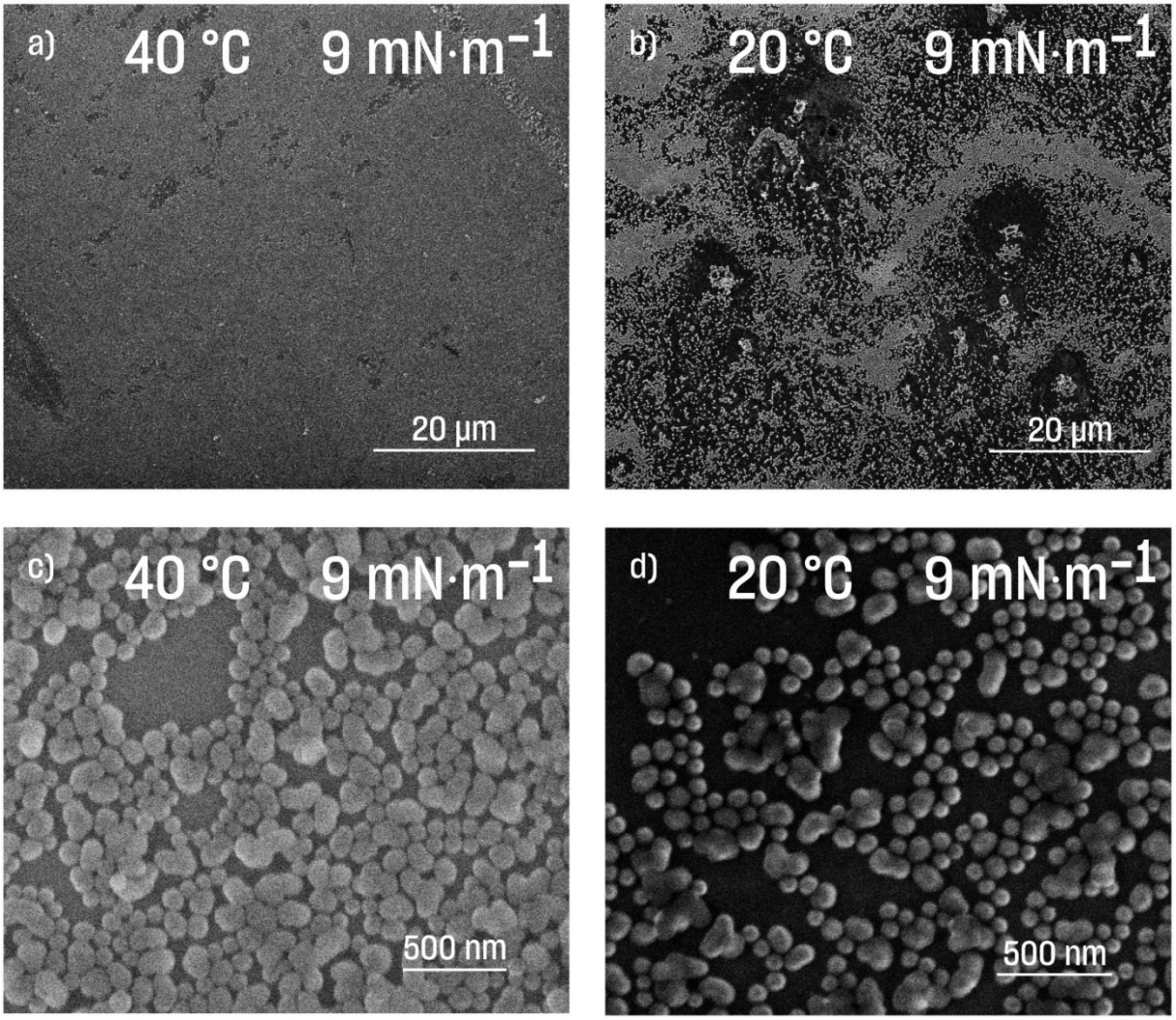

Figure 16. Scanning electron microscopy pictures of PSiFeNPs films transferred at 9 mN·m^{-1} at 40 °C (**a** and **c**) and 20 °C (**b** and **d**). The author's own figure, previously published in ref.[19] (CC-BY 4.0).

The films were transferred onto the polished silicon wafers for further investigation of the morphology using the Langmuir-Blodgett technique. The transfers were done at 9 mN·m^{-1}. The nanoparticles at the HT were densely packed and uniformly distributed (Figure 16 a)) and c)).

The neighbouring particles were near each other. On the other hand, the same surface pressure at the LT was reached when nanoparticles were still separated, organised in small 2D clusters, with huge voids between them (Figure 16 b) and d)). Individual particles were also a bit further from each other, even within the clusters, than at the HT. The distribution of the

distances between PSiFe nanoparticles is shown in Figure 21 and will be further discussed in comparison with the KCl-solution experiments.

Additional SEM pictures, the pictures of films transferred at 5 $mN \cdot m^{-1}$ and 25 $mN \cdot m^{-1}$ were presented in Appendix 3 with a description. High compression resulted in local multilayering of the films (3D aggregates) without apparent collapse, characteristic of amphiphilic molecules.

Typically, ordering, such as crystallisation, results from decreasing the temperature. However, this system intriguingly operates in the opposite way.

3.7. PSiFeNPs at the Pure Water Surface – Discussion

Shan et al. described three regions that can be distinguished in compression isotherms of 4.2 nm AuNPs capped with PNIPAM mixed with polystyrene (PS), of around 28 and 24 monomers, respectively.[240] These regions were correlated with the conformational change of the thermoresponsive polymer as a result of the compression and temperature's influence. A similar shape was observed in the case of PSiFeNPs compression. However, there are certain problems with establishing an analogy between these two observations. First, Shan et al. provided surface plasmon resonance (SPR) measurements only at the temperature of 30 °C and lower,[240] which may not be enough to observe fully closed nanoparticles above the LCST. Furthermore, PSiFeNPs compression isotherms showed these three regions both at the HT and the LT (Figure 12 a) and b)). Therefore, these three regions are more probably related to the behaviour of the whole nanoparticles. Especially, that PSiFeNPs' cores are relatively huge compared to the capping layer (90 nm of core's diameter vs 5-6 nm-layer of PNIPAM), contrary to the Shan et al. work, where the capping layer is larger than the diameter of the nanoparticle. What is more, experiments suggest that below the LCST, the interactions between PSiFe nanoparticles add complexity to the system, but at the HT, the nanoparticles should behave more like solid spheres.

3.7.1. Conformation and Immersion of PSiFeNPs

Figure 17 I presents the conformations of nanoparticles capped with LCST-type polymer chains (PNIPAM), in the case where the diameter of the particle is comparable to or smaller than the thickness of the polymer layer.[239,240,242] The possible conformations, such as "Janus", "brush", "jellyfish", "pancake", and "closed", are the representations of how PNIPAM chains can be

oriented depending on the nanoparticles' properties, temperature and rate of mechanical compression of the film. However, PSiFeNPs are much larger than the PNIPAM shell. Therefore, other factors must be considered to explain the nanoparticles' interfacial behaviour.

The immersion of nanoparticles becomes more important for the interfacial phenomena of PSiFeNPs. Above the water surface, PNIPAM should be in “closed” conformation both at the LT and the HT because of the lack of water. A case presented in Figure 17 I b)-d), where the chains above water could still be immersed and hydrated in case of PSiFeNPs, is possible only for the ligands located in the proximity of the interface. Therefore, the possible cases of conformations and immersions of PSiFeNPs below LCST were symbolically presented in Figure 17 II. The scenario of mostly non-immersed nanoparticles was excluded, as in such cases the nanoparticles could interact only in the “closed” state, regardless of temperature. The shifts of Langmuir isotherms and the differences in area per nanoparticle suggested that the conformation change mattered. Alternatively, changes could be explained by partial desorption from the interface into water with rising temperature, but this was unlikely because PNIPAM above the LCST is significantly less hydrophilic.

Therefore, the remaining immersion scenarios were taken into consideration. Further analysis restricted the nanoparticle shape to spherical and neglected gravity-induced interface deflection.[246,254] Such an assumption was justified, since for particles smaller than approximately 5 μm, immersion is determined by wetting properties.[246,254,315,316] With a negligible meniscus, the floatation capillary force should not be noticed in the system; hydrophilic particles should be more immersed than hydrophobic ones. The system can still be driven by capillary forces arising from wettability itself if the nanoparticles are trapped in a thin film of another liquid at the interface. Otherwise, no interface deformation should occur, nor should immersion capillary force be present, as in the PSiFeNPs system. [253,254]

Since the change of the area occupied by a nanoparticle in the PSiFeNPs system should originate in the conformation’s change, the registered area should change by around 8% to 23%. The lower limit was calculated regarding the results of Tucker and Stevens, a theoretical study showing that free PNIPAM chains of this length should bend above LCST.[297] As mentioned earlier, Schan et al. showed that surface attachment facilitates bending.[298] That strengthened the assumption. The upper limit assumes the disappearance of the PNIPAM layer – change of the area if the PSiFeNPs consisted only of the core-shell part. Both limits assume 100% deposition efficiency. These numbers can still differ, as the surface pressure changes can occur due to long-

range interactions and because Tucker and Stevens' calculations considered free-standing molecules, not densely-packed, one-sided anchored ligands. Nonetheless, experimental results showed changes around 10-20% in different runs (Figure A2.1 c)). The fact that a single oligomer in the capping layer was surrounded by other oligomers could facilitate the adoption of the "closed" conformation above the LCST.[298]

The next important aspect to address regarding the mechanical phenomena of nanoparticles at the interface is interdigitation of ligands. Surface compressional moduli of the PSiFeNPs film were slightly higher at the LT than at the HT (Figure 14 a)). The interfacial dilatational elastic modulus and the interfacial dilatational viscous modulus showed that elastic properties were dominant (Figure 14 b)). If interdigitation occurs, the viscoelastic properties should be more profound as interdigitation fosters aggregation and slows disaggregation of nanoparticles. The relaxation experiments distinguished the film. The relaxation time was shorter at the HT. That indicated that there are fewer interparticle interactions in this temperature regime. Furthermore, investigation with the Kohlrausch-Williams-Watts function showed strong cooperative motions at 20 °C ($\beta = 0.62$). On the other hand, the linearity was not registered at 40 °C, showing $\beta = 1$ in the first seconds of the relaxation. This suggests no cooperative motion; therefore, there are no strong interactions between nanoparticles at this stage. That was noticed, but after this initial, crucial period.

Taking all of the above into consideration, some conclusions can be drawn. By exceeding the LCST of PNIPAM, hydrogen bonds are no longer created between polymer and water molecules. Therefore, intramolecular, intermolecular, or internanoparticulate (intramolecular – within the same PNIPAM chain, intermolecular – between PNIPAM chains at the same nanoparticle, internanoparticulate – between PNIPAM chains anchored to different nanoparticles) hydrogen bonds can be formed. Intramolecular hydrogen bonds were improbable for 24 N chains or limited. Internanoparticulate hydrogen bonds, if formed, would lead to nanoparticle aggregate formation. Nevertheless, the indifference of interfacial dilatational elastic modulus and interfacial dilatational viscous modulus to the temperature shows that no strong bonding of such a type appeared. Hence, intermolecular bonds are the most likely. A similar conclusion has been reported in the literature for particles of smaller diameter.[298]

Figure 17 I presents how PSiFeNPs can conform in at the LT, before (a)) and upon compression (b), c)) . As interdigitation was excluded due to the surface rheology, the c) case does not happen. It is reckoned to be caused by the steric hindrances. These were caused by the

relatively large radius of the nanoparticles and side chains in the PNIPAM structure. Alternatively, the PNIPAM ligands were too long, hence not rigid enough, contrary to what was expected based on Tucker and Stevens' study.[297]

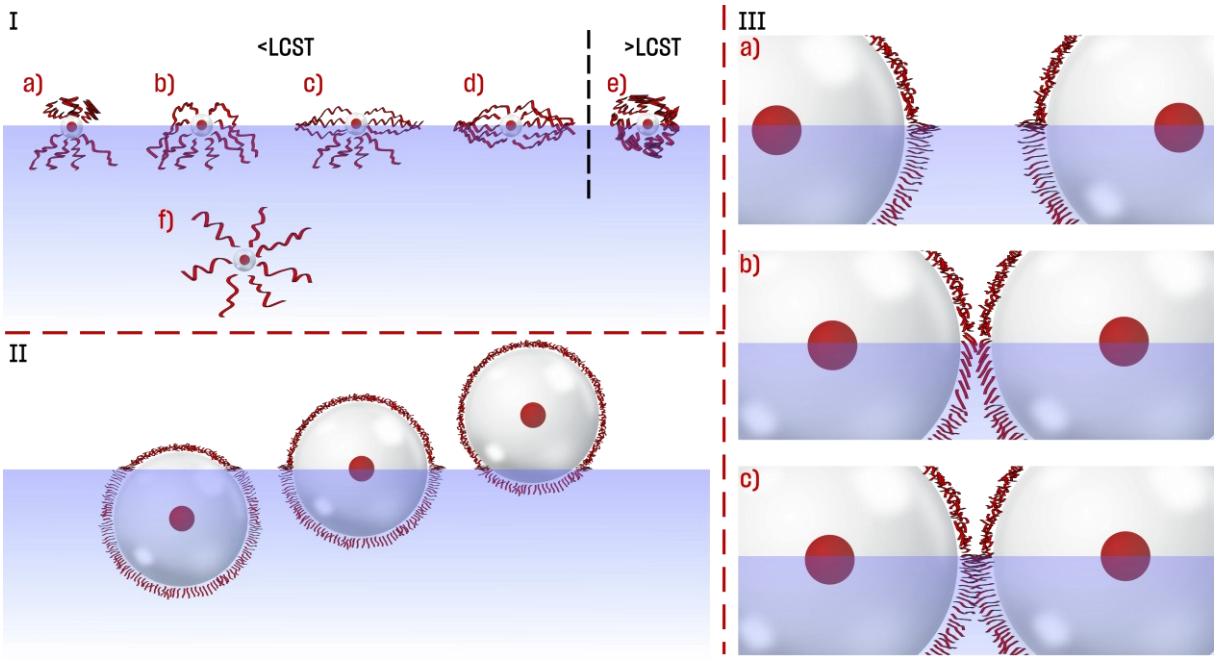

Figure 17. I. Possible conformations of nanoparticles capped with thermoresponsive polymers proposed in the literature. Nanoparticles could adapt as follows: **a)** a "Janus-like" conformation, **b)** a "brush" conformation, **c)** a "jellyfish" conformation, **d)** a "pancake" conformation, **e)** a "closed" conformation, and **f)** a "fully open", anisotropic conformation. Structures **a)**, **b)**, and **c)** are possible above a threshold (critical) surface pressure, and **d)** below the threshold surface pressure, only below the LCST. The conformation **e)** is present above the LCST. **f)** "Fully open" conformation could be present for nanoparticles desorbed from the interface. **II.** Possible immersion of PSiFe nanoparticles below LCST. **III.** Possible conformational adjustments of PSiFe nanoparticles at the air/water interface: **a)** at low surface pressure, **b)** at high surface pressure without interdigitation of the polymer chains, **c)** at high surface pressure with the interdigitation of the polymer chains. The capillary effect (if present) is neglected. The author's own figure, previously published in ref.[19] (CC-BY 4.0).

More evidence supporting the explanation of the conformation was provided by surface potential measurements. Subtracted values (LT minus HT), shown in Figure 12 c), were positive throughout most of the compression (compression of liquid-like state at surface area <400 $cm^2 \cdot mg^{-1}$, especially). In general, nanoparticles that have a surface charge in an aqueous medium (PSiFeNPs are negative) can exhibit an effective interfacial dipole moment when the immersed part is dissociated, charged, and screened. The anisotropy in the z-direction is expected to be smaller if a particle is less immersed. That could happen at the HT. Then, an additional effect comes from the conformation. At the HT, the whole particle is covered with

"closed" PNIPAM, while at the LT, PNIPAM is hydrated and "open". This is consistent with the bulk measurements of ζ-potential ($|\zeta_{20\,°C}|>|\zeta_{40\,°C}|$) and supports the conclusions of surface potential analysis.

A similar conclusion can be found in Shan et al.'s work.[240] AuNPs showed a blue shift of the SPR band as a result of compression. AuNPs, being of a small diameter, adapted the "pancake" conformation at the LT. In this conformation, the bottom part of the nanoparticle is exposed to water molecules, while PNIPAM aligned with the interface spaced the particles from each other. Upon compression, the PNIPAM chains were deflecting, covering the gold surface and decreasing the distance between the cores. This explained the blue shift.

This, however, should not be that important in the case of PSiFeNPs, because ligands are much shorter compared to the diameter of the particles; therefore, most of them should constantly cover the particle. According to Bresme and Oettel,[246] the charged particles at the interface are screened at the immersed side of the nanoparticles much more than at the part exposed to air . This can induce long-range repulsion between the nanoparticles as the dielectric constant of air is low. The anisotropy induces the electrical dipoles. In such a case, immersion could be crucial. A more immersed particle would show a smaller electrical dipole moment. However, in the PSiFeNPs case, water is needed to dissociate Si-OH, and this is the origin of the charge at the surface. Hydrophilicity is higher at the LT; therefore, immersion should be higher there, and in consequence, the dipole moment as well. This is the opposite of the case discussed by Bresme and Oettel, because here the repulsion does not arise from unscreened charges above the interface.

Taking a closer look at the experimental data (Figure 12 c) and Figure 13), one may find that upon compression, the dipole moment is higher at the LT till the compression reaches approximately 100 $cm^2 \cdot mg^{-1}$. At this point, the slope of the *Π–A* isotherm becomes steeper (the surface pressure rises more rapidly with further compression). The dielectric permittivity of PNIPAM decreases with temperature and drops more significantly above the LCST.[317] According to the equations presented in the Literature Review (section 4.4.3), the surface potential at HT increases when the relative dielectric permittivity decreases. That explains why the difference between surface potentials (LT-HT) and between dipole moments (LT-HT) became negative when the film was compressed below the area of 100 $cm^2 \cdot mg^{-1}$ (Figure 12 c)).

3.7.2. Aggregation of PSiFeNPs

Looking closely at BAM images, one can observe that PSiFeNPs were most prone to aggregation at the LT. Figure 15 g) shows fractal-like structures. Different morphologies of the films transferred at different temperatures were also revealed by SEM (Figure 16). The compared films were transferred at the same surface pressure, which means that the film at the HT was more compressed (smaller area per nanoparticle). Nonetheless, under these conditions, due to changes in the PNIPAM form and interactions between nanoparticles, the film prepared at 40 °C was uniform and well-ordered, with an area of at least 4000 μm^2. The films transferred at 20 °C were much more distorted, with locally higher concentrations of nanoparticles and local voids (Figures 16 b) and d)). Despite the fact that the voids were present, the distance between the nanoparticles lying next to each other was larger at LT. Figure 21 shows the distributions of the distance between the edges of nanoparticles (the data were collected with a threshold of 40 nm to count only nanoparticles "touching" each other). This is another piece of evidence for changes in PNIPAM conformation, while the presence of fractal-like structures and voids, rather than a well-structured layer of NPs, suggests a change in interparticulate interactions.

Reynaert et al. considered sulphonated polystyrene microparticles (3.1 ± 0.2 μm in diameter) at the decane-water interface.[318] NaCl dissolved in water caused fractal aggregation of the microparticles, which occurred faster with increasing salt concentration. According to the authors, it was caused by diminishing the electrostatic repulsion. PSiFeNPs aggregated at the LT; therefore, the long-range repulsion could be weaker at this temperature, or the short-range attraction was weaker at the HT. Section 4 in this chapter investigates the behaviour of the nanoparticles in at similar conditions to Reynaert et al. – at a KCl solution used as subphase.

In general, a similar aggregation was observed in systems driven by the other forces. Kumar et al. described altering the fractal dimension (Hausdorff dimension) through the interplay among van der Waals attraction, electrostatic repulsion, and an osmotic pressure gradient.[319] Flores-Tandy et al. indicated long-range attractive capillary forces as the key factor of aggregation of ellipsoidal nanoparticles at the interface.[320] Large diversity of the factors and the similar results is not surprising, as fractal aggregation is well-known and usually is described by two models: DLA (diffusion-limited aggregation)[321] and DLCA (diffusion-limited cluster aggregation)[322]. Both are based on random Brownian motions. In DLA, particles, when approaching each other at the critical distance, are attracted and aggregate. In DLCA, clusters

of already aggregated particles behave analogously; however, the model is extended, including the rotation of the clusters.[323] These models are further extended by, for example, considering the minimal time of the contact between the nanoparticles that is needed to aggregate. Such an approach, called reaction-limited cluster aggregation (RLCA), simulates that a reaction occurs on the molecular level between two nanoparticles.[323] Therefore, the model can assume that the probability of establishing a connection (aggregation) between two particles at the collision is not equal to 1. It is because the particle has to overcome a certain activation energy, related to, for instance, electrostatic repulsion. While basic DLA and DLCA do not analyse the type of the interaction, more sophisticated ones try. Polimeno et al. showed extensions to DLCA and indicated van der Waals interactions, DLVO theory and hydrodynamic interactions as potential further fields of study.[324] These were explored, for instance, by Antonsson et al..[325]

Types of interactions that may occur between nanoparticles, as well as other important phenomena in the analysis of nanoparticles at the interfaces, were thoroughly covered in the article by Bresme and Oettel.[246] The authors discussed six main interactions driving the assemblies at fluid interfaces. Among them are electrostatic interactions, van der Waals and short-range repulsive interactions, capillary forces, fluctuation forces, and solvation forces. Henceforth, the changes in conformation of PNIPAM on the nanoparticles due to the temperature change the attraction-repulsion equilibrium in the system, leading to patterns originating from diffusion-limited cluster aggregation at LT or almost no such patterns at HT.

3.8. Summary – Pure-Water System

This work, as reported in *ACS Omega* (Zbonikowski et al. 2023), showed that the interfacial assembly of 90-nm nanoparticles can be driven by relatively short thermoresponsive polymers – chains built from ca. 24 monomer units. Langmuir films composed of PSiFeNPs formed a switchable system in which the surface pressure dropped with the temperature rise. This implicated a switch in the types of aggregation that were observed. While the drop of the surface pressure is quite unusual for physical systems, the increased aggregation of PNIPAM-capped nanoparticles in an aqueous system below LCST is atypical for this kind of thermoresponsive polymers. Upon compression at different temperature regimes, PSiFeNPs formed distorted (LT) or ordered (HT) packing at the same surface pressure, bringing an illusion of reaching highly ordered crystals at higher temperatures. Surface rheology experiments, supported by SEM, BAM, and other complementary analyses, confirmed that exceeding the LCST of PNIPAM modified the system's behaviour. The distances between nanoparticles decreased (according to

the expected “closing” of PNIPAM). That could also be an effect of the interaction equilibrium change due to the temperature. Neither interdigitation nor inter-nanoparticulate bonding was present in the system. This is the opposite observation to a switchable membrane reported by Liu et al. about a year earlier, also composed of SiO_2 particles coated with PNIPAM (approx. 200-nm particles with a hydrodynamic diameter of around 400 nm below LCST and around 300 nm above).[19,304]

PSiFe nanoparticles were examined in an external magnetic field; however, the impact of the magnetic field on the films was not discussed. . The theoretical background of magnetism of PSiFeNPs was introduced in Section 2 of the Experimental Chapter. Nanoparticles reacted visibly to the neodymium magnet after sedimentation (a few months of storage). A proof of concept experiment at the Langmuir trough with a neodymium magnet was described in the Supporting Information of ref.[19], However, the results were too irreproducible to draw conclusions from them and are not presented in this thesis.

Additional interfacial phenomena arising from the temperature gradient were noted in the article this chapter is based on. Dr Konrad Giżyński, by performing COMSOL simulations, showed that the largest temperature gradient observed in the Langmuir trough heated from the bottom was 0.1 K between the bottom of the trough and the subphase surface. Therefore, the impact of convection on the phenomena in the system was negligible.[19] Since I did not participate in this part, I did not include it in the thesis.

To thoroughly investigate the principles of the PSiFeNPs system, focusing on changes in interactions, KCl solution was used as the subphase, thereby increasing electrostatic screening. This procedure should minimise long-range repulsion.

4. Results and Discussions – KCl-Solution-Based System

To better understand the study in this section, it is important to note that the experiments presented here, as a follow-up study, have some small but significant nuances. PSiFeNPs synthesised for this part (the second batch) differed slightly from those previously presented. Analogous Fe_xO_y core (15 nm) was surrounded by 25 nm of silica. The core-shell structure was capped with PNIPAM (the same length of the silane derivative). The total diameter of the PSiFeNPs was approximately 65 nm. In the ultrapure water experiment, the difference was observed only in the silica shell; therefore, the nanoparticles reached a total diameter of around 90 nm. Most of the comparisons are done between these two batches, except for the results presented in Table 3 and Appendix 6, which correspond to the second batch only.

4.1. PSiFeNPs in Suspensions (ζ-potential, Electrophoretic Mobility and Hydrodynamic Diameters)

PSiFeNPs (1 $mg \cdot ml^{-1}$) were suspended in ultrapure water and three differently concentrated KCl water solutions. The measured values of ζ-potential, electrophoretic mobility, conductivity and hydrodynamic diameters, depending on the temperature, are presented in Table 3.

Table 3. ζ-potential, electrophoretic mobility, conductivity and hydrodynamic diameters of PSiFeNPs.

	ζ-potential / mV	El. Mobility / $\mu m \cdot cm \cdot V^{-1} \cdot s^{-1}$	Conductivity / $mS \cdot cm^{-1}$	Hydrodynamic diameter / nm
20 °C, water	-44.8 ± 7.9	-3.18 ± 0.66	0.097 ± 0.001	68 ± 21
40 °C, water	-41.4 ± 6.5	-4.15 ± 0.60	0.128 ± 0.001	74 ± 24
20 °C, 0.001 M KCl	-48.2 ± 7.2	-3.42 ± 0.51	0.214 ± 0.002	67 ± 21
40 °C, 0.001 M KCl	-41.6 ± 8.9	-4.17 ± 0.71	0.277 ± 0.002	73 ± 24
20 °C, 0.01 M KCl	-46.0 ± 8.3	-3.26 ± 0.54	1.51 ± 0.091	68 ± 20
40 °C, 0.01 M KCl	-38.3 ± 7.5	-3.84 ± 0.63	1.88 ± 0.085	72 ± 23
20 °C, 0.1 M KCl	-20.2 ± 1.5	-1.43 ± 0.10	12.8 ± 0.446	66 ± 21
40 °C, 0.1 M KCl	-18.6 ± 2.0	-1.86 ± 0.20	15.3 ± 0.485	103 ± 57

± symbol marks standard deviations

The presence of ions and, consequently, the ionic strength influences the behaviour of PNIPAM. The solubility of the macromolecules, originally proteins, is described by the Hofmeister series. Depending on the ion, the macromolecule undergoes a "salting-in" or "salting-out" effect. Analogically, the thermoresponsive polymers, whose thermoresponsive behaviour is driven by the competition of hydrogen bondings, are influenced by the presence of K^+ and Cl^-. According to Freitag et al,[326]. Increasing the concentration of KCl facilitates "closing" of PNIPAM. The LCST temperature drops linearly with rising KCl concentration for the oligomer of molecular mass 2300-2700 $g \cdot mol^{-1}$, similar to the one used in this thesis). However, at a KCl concentration of 0.1 M the LCST does not drop below 30 °C. A similar change of the LCST (around 1 °C) was reported for PNIPAM-capped silica nanoparticles.[327] Therefore, the salting effects are not significant enough to affect the results in this thesis, especially when the experimental temperature regimes were 20 °C (LT) and 40 °C (HT).

Electrophoretic mobilities were registered for the two temperature regimes. The absolute values are decreasing with the rising concentration of KCl, and are higher for the higher temperature. The latter property may be related to the PNIPAM conformation at the nanoparticle's surface, but at the same time, electrophoretic mobility rises with the temperature as it depends on viscosity, dielectric permittivity, ζ-potential and the electric double layer.[328,329]

Electrophoretic mobilities in similar systems were studied by Humphreys et al.[327] They showed that the values changed from -0.3 $\mu m \cdot cm \cdot V^{-1} \cdot s^{-1}$ at 20 °C to -2.7 $\mu m \cdot cm \cdot V^{-1} \cdot s^{-1}$ at 40 °C in water. The electrophoretic mobilities decreased in absolute values in measurements conducted in 0.1 M KCl, reaching -0.1 $\mu m \cdot cm \cdot V^{-1} \cdot s^{-1}$ swollen (open) and -0.3 $\mu m \cdot cm \cdot V^{-1} \cdot s^{-1}$ in collapsed (closed) stated of the polymer. These results confirmed trends observed in the PSiFeNPs measurements at increasing KCl concentration. Humphreys et al. observed that adding salt at 40 °C caused the aggregation of the particles even before the full PNIPAM transition occurred. Similarly, for PSiFeNPs, the abnormal increase of hydrodynamic diameter was observed at 40 °C in 0.1 M KCl, indicating the aggregation, and it was confirmed by DLS measurements (distributions by intensity and volume, Appendix 6).

This analysis was done in bulk; however, some conclusions will be further used to discuss the interfacial behaviour of PSiFeNPs at subphases containing KCl.

4.2. Langmuir Films

PSiFeNPs were deposited at the interface analogically as for ultrapure water experiments. However, a certain KCl solution was poured into the trough instead of ultrapure water. This change resulted in a considerable shift of compression isotherms (Figure 18). Increasing the concentration of KCl shifted the isotherms to higher surface area values. The effect was more significant at the LT. The relative shift was also increasing with the compression itself. Nominal surface areas at certain surface pressures were presented in Table 4. Low concentrations of KCl (0.001 M and 0.01 M) showed very similar shifts (Figure 18 a) and b)). All of these observations were unexpected, as the addition of salt to the subphase was believed to screen electrostatic interactions and facilitate nanoparticle aggregation.[330,331]

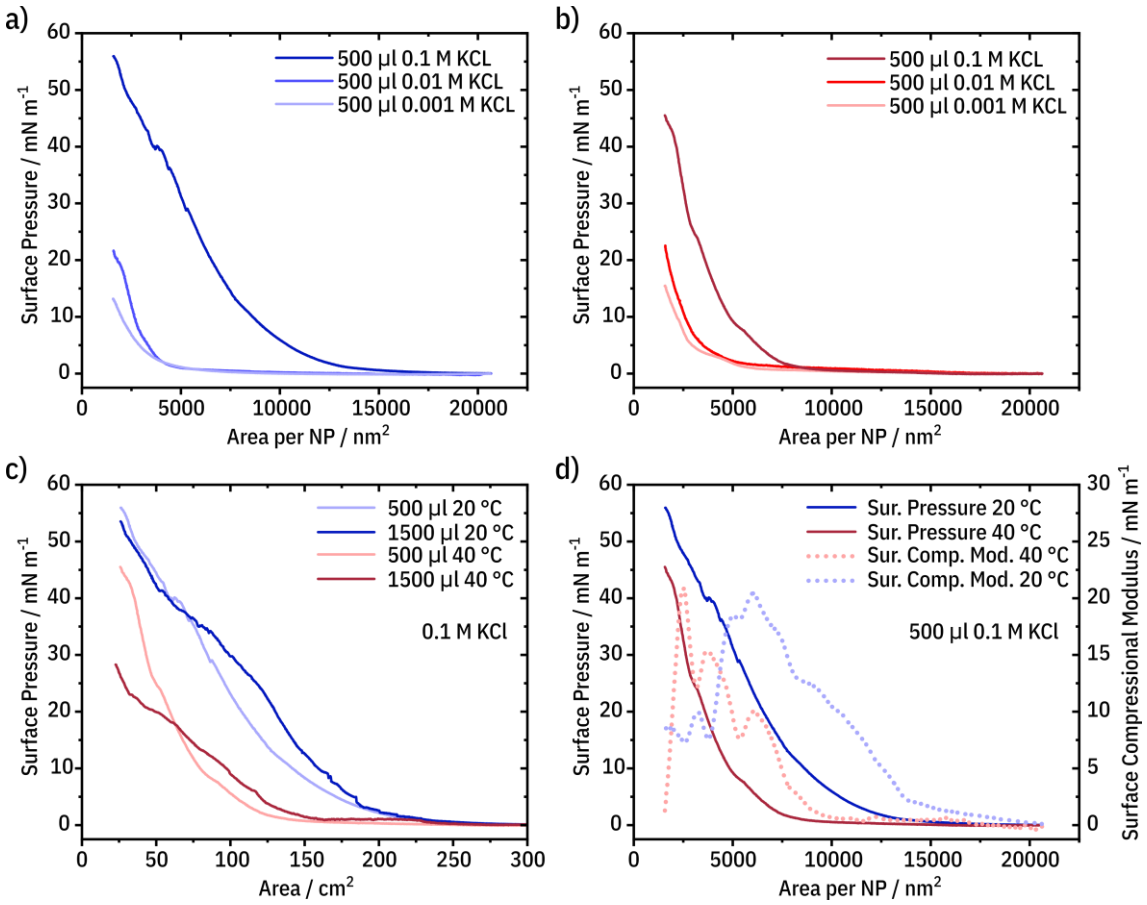

Figure 18. a) Compression isotherms of 500 µl of the PSiFeNPs sample (1 mg·ml^{-1}) deposited on different solutions of KCl at **LT** (20 °C). The higher the concentration of KCl, the more the isotherms were shifted towards higher values of surface area. **b)** Compression isotherms of 500 µl of PSiFeNPs sample (1 mg·ml^{-1}) deposited on different solutions of KCl at **HT** (40 °C). Similarly, the isotherms were shifted towards higher values of surface area with rising KCl concentration similarly as at LT. **c)** Compression isotherms of 500 µl and 1500 µl of PSiFeNPs sample (1 mg·ml^{-1}) at 20 °C and 40 °C performed on a 0.1 M KCl subphase. **d)** Comparison of surface pressure isotherms and corresponding surface compressional moduli of 500 µl of PSiFeNPs sample (1 mg·ml^{-1}) deposited on 0.1 M KCl solution. The author's own figure, previously published in ref.[20] (CC-BY 4.0).

Table 4. Surface area at selected surface pressures for PSiFeNPs films (500 µL) at 40 °C or 20 °C, at water or 0.1 M KCl subphase. Notably, experiments at water were performed with the first batch of PSiFeNPs of higher diameter. Nonetheless, the 0.1 M KCl isotherms were significantly shifted towards higher surface area.

	20 °C			**40 °C**		
	0.3 mN·m^{-1}	**5 mN·m^{-1}**	**10 mN·m^{-1}**	**0.3 mN·m^{-1}**	**5 mN·m^{-1}**	**10 mN·m^{-1}**
water	138 cm^2	48 cm^2	28 cm^2	122 cm^2	45 cm^2	30 cm^2
0.1 M KCl	271 cm^2	171 cm^2	141 cm^2	200 cm^2	103 cm^2	79 cm^2
0.1 M KCl/water	1.96	3.56	5.04	1.64	2.29	2.63

The isotherms were responsible for the temperature, analogously to ultrapure water. The comparable experiments were presented in Figure 18 c) and d). At the HT (40 °C), the isotherms are significantly shifted towards lower surface area. The contradiction of the area occupied by a single nanoparticle was expected because PNIPAM still should fold similarly as at ultra-pure water conditions – the change of LCST due to the salting-out effect is almost negligible even at 0.1 M KCl. The reversed temperature expansion (500 µl PSiFeNPs sample of 1 mg·ml^{-1} deposited on 0.1 M KCl subphase), from 40 °C to 20 °C, resulted in a 66% increase of the area at 5 mN·m^{-1} and 78% increase of the area at 10 mN·m^{-1}. By estimating the maximal difference in PNIPAM shell for the second batch of PSiFeNPs, the area of the film should shrink within the range of 9% to 25%, depending on the assumption (analogously to that for batch I). That means the reversed temperature expansion should be within the range of 10-33%. The estimation limits are based on the theoretical bending of 24-mer PNIPAM according to Tucker and Stevens[297] and no PNIPAM is counted into the size of a nanoparticle. While the reversed thermal expansion was within this range for ultrapure water, the results for 0.1 M KCl solution clearly showed that other factors contributed to the behaviour of the films.

The most surprising results were registered when more PSiFeNPs were deposited at the 0.1 M KCl solution's surface. Figure 18 c) presents that the compression of more (1500 µl) PSiFeNPs sample results in almost the same isotherm. While the isotherms were independent of the amount of nanoparticles, they still depended on temperature. Since at the beginning of the compression the surface pressure was equal to zero, and the fact that the surface pressure did not rise at the initial compression, PSiFeNPs definitely could not have occupied the whole

available area, even after depositing 1500 µl of the sample to the maximal area of the trough (maximally extended barriers). That means the films could not behave like those at the ultrapure water subphase in terms of linear isotherm scaling. Ultrapure water experiments were linearly scalable.

For further evaluation of the films, the surface compressional moduli have been calculated. The surface compressional moduli slightly exceeded 20 $mN \cdot m^{-1}$. That means the film could be classified as being between the low-density liquid phase and the liquid-expanded phase (Table 1) at this point. As in the ultrapure water experiments, surface compressional moduli were lower than this value throughout most of the compression (Figure 18 d)). However, the results for 0.1 M KCl were not monotonous, revealing local maxima. This observation was a hint that nanoparticles could evacuate from the interface due to the rising mechanical compression. Then, PSiFeNPs could be desorbed into the subphase or cause multilayering of the film. Therefore, the abnormal indifference to the amount of the deposited sample could be partially explained by the facilitated collapse of the monolayer.

4.3. Brewster Angle Microscopy

Simultaneously with the compression-decompression cycles, Brewster angle microscopy was registered. Figure 19 presents the comparison of ultrapure water experiments and those performed at 0.01 M KCl and 0.1 M KCl. Cycles performed at 40 °C showed that at ultrapure water, only small, barely visible aggregates were formed during the compression, and they disappeared upon decompression of the film. On the contrary, plenty of aggregates were noticed in 0.01 M KCl and 0.1 M KCl, even before the experiment. At 0.1 M KCl, huge “ice-floes” were observed. Therefore, increasing the ionic force of the subphase facilitated the aggregation of nanoparticles, as expected. Decompressing the films at 40 °C resulted in many irregular 2D aggregates, both at the presented 0.01 M KCl and 0.1 M KCl. The aggregation was even more pronounced for the films compressed at the LT. Worth mentioning, the aggregation was already clearly visible without the salt. Nonetheless, forming a uniform layer was already observed at 0.01 M KCl (including barely visible films, as for ultrapure water). A dense layer of aggregates was clearly visible in 0.1 M KCl, suggesting the presence of 3D aggregates. Decompression of the films at the LT revealed that, interestingly, at 0.01 M KCl the fractal-like structures were dominant (similar to ultrapure water experiments), while at 0.1 M KCl the film broke into oblong pieces (probably due to the one-directional compression-decompression).

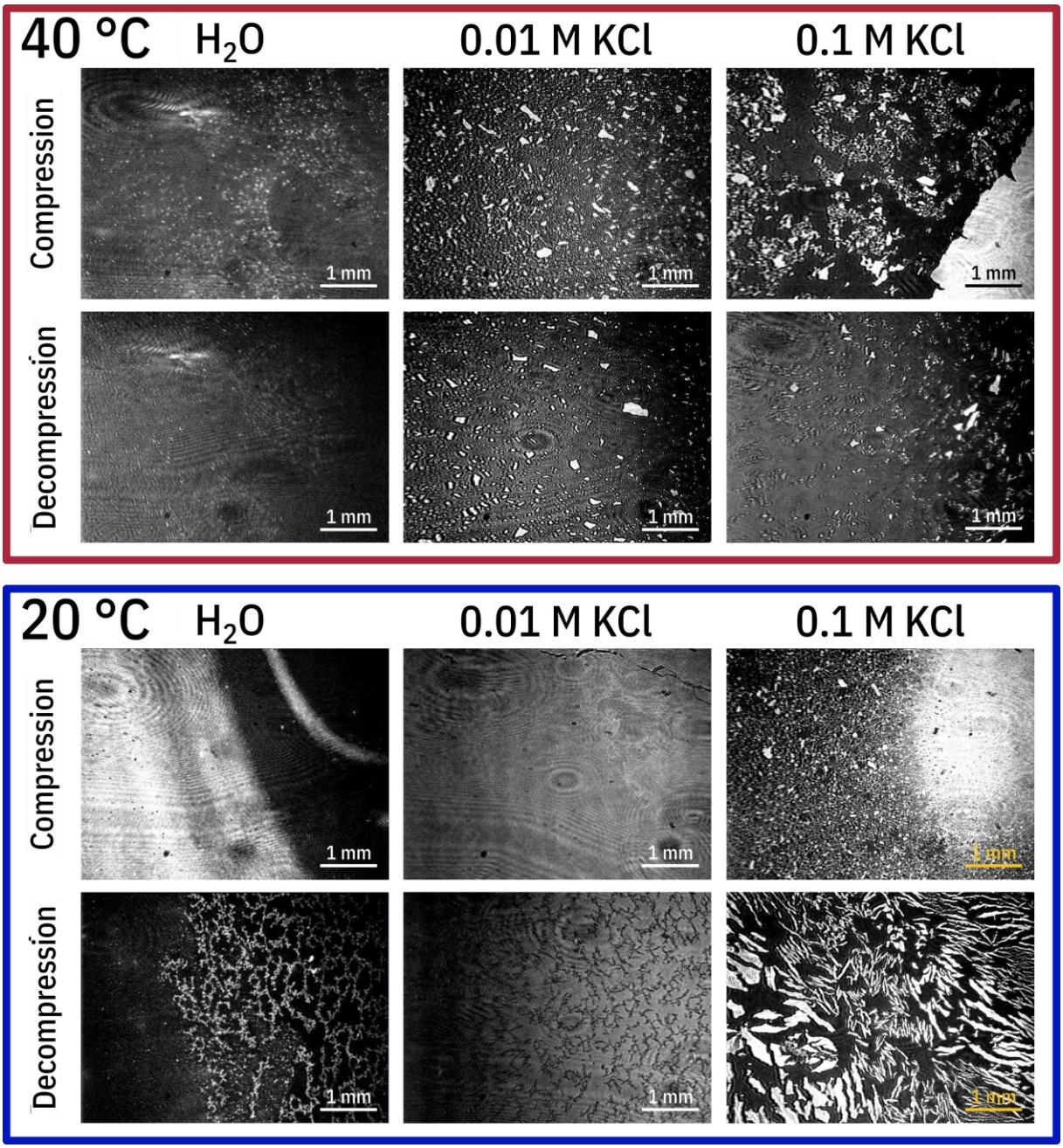

Figure 19. Brewster Angle Microscopy picture comparison between water and KCl solution subphase at 20 °C and 40 °C. The author's own figure, previously published in ref.[20] (CC-BY 4.0).

4.4. PSiFeNPs Films Transferred onto Solid Substrates

The PSiFeNPs films were transferred onto silicon wafers, using the Langmuir-Blodgett technique. Although samples transferred from KCl solutions will be compared with ultrapure water samples, a few differences should be noted for proper interpretation of the analysis. First, the PSiFeNPs of the ultrapure water study are bigger, which is clearly visible in the SEM pictures. Second, the compared films were transferred at very similar, but different surface

pressures (8 $mN \cdot m^{-1}$ vs 9 $mN \cdot m^{-1}$). The difference between these two values, in fact, is negligible. There is no change in this range in terms of isotherm shape; the change in area is minimal, and even with controlled surface pressure, film transfer is usually not ideal and fluctuates around these values (as in this case). The latter has its origin in out-of-equilibrium phenomena. These phenomena are the aftermath of the compromise between the time scale of a single experiment and the deviation from thermodynamic equilibrium. In ideal conditions, after an infinitesimal change in area, the system is left to fully reach equilibrium. However, such an approach is problematic not only in the limited time but also from a technical point of view. Evaporation of water from a relatively large area of the trough and the thin subphase layer, especially at the HT, imposes time constraints. Refilling the system with water, as done for the switching experiment (Figure 12 d)), causes disturbances that can only be partially mitigated by extending the equilibrium time, as shown in the results. An alternative approach to performing the experiment under saturated vapour conditions was attempted by using beakers with evaporating water in the plexiglass box. Nevertheless, this approach was denied. Water condensation, especially during surface-potential measurements, was dangerous to the equipment. There were doubts about whether water condensation would affect the stability of the PSiFeNPs by wetting the PNIPAM layer. In KCl experiments, water evaporation alters the salt concentration in the subphase. However, due to the aforementioned issues, it was more reliable to perform a standard experiment in a reasonable time. Therefore, the conditions implied the speed of the barriers' movement.

As described in Section 4, ultrapure water films at 8 $mN \cdot m^{-1}$ showed differences in the ordered and disordered morphologies of the HT and LT films, respectively. At the HT, there were only small discrepancies in the nanoparticle layer – little voids or point 3D aggregates. The LT films showed areas of local high and low nanoparticle density. Nonetheless, even the aggregated high-density fragments of the film showed small discrepancies as voids and point 3D aggregates.

The films transferred from 0.001 M KCl subphase presented the same morphology as the ultrapure water ones, with an ordered layer at the HT and the presence of voids in the low-density parts of the film and some discrepancies in the structure of the layer in high-density parts of the film at the LT.

Increasing the KCl concentration to 0.01 M changed the morphology of the films. At the HT, the layer of PSiFeNPs was similar to water and 0.001 M KCl, being dense and

well-ordered. However, the layer had fewer defects (small voids and point 3D aggregates). The Langmuir-Blodgett films transferred at the LT were also dense and well-ordered. No low-density parts were detected. Some spaces were observed between particles or some locally closer groups of nanoparticles. Notably, the film was not rinsed after the transfer and was only left to dry (to avoid disturbing the extracted layer). Hence, a typical fractal-like pattern of a semi-transparent layer covered the monolayer of PSiFeNPs at 40 °C. This semi-transparent layer was identified as KCl residues. Similar patterns were found at 20 °C. Despite the patterns seeming similar, they were thinner. A closer look at the structure revealed that, in some parts of this pattern, nanoparticles were aggregated, forming 3D aggregates. Salt crystallisation and solvent evaporation from colloidal liquids containing dissolved salts could slightly modify the structure of the transferred films.[332] Nonetheless, no evidence of modification of the underlying layer was observed. Contact profilometry of the dense fragments of the film showed that the films were almost monolayers at both temperature regimes. The measured film height was consistent with the measured size of PSiFeNPs. Worth noting: on the profilometer path at 40 °C, large KCl residues were observed (visible at much lower magnification). These residues correspond to much higher measurement points registered in profilometry. The profilometry results of 0.01 M KCl films were presented in Figure 20 a).

The films transferred from 0.1 M KCl were similar to those transferred from 0.01 M KCl. The SEM pictures showed a dense layer of nanoparticles at both temperature regimes. In this case, films showed greater discrepancies in breaking two-dimensional structures. Some voids were still noticed at 20 °C. Compared to the previous concentration, the fractal patterns of salt residues were replaced by point, less-ordered and uniformly distributed salt residues. The spots where they were registered, the film of nanoparticles contained more 3D aggregates. As reported by Alipour et al., manipulating salt and colloidal particle concentrations yields various structures.[332] The summary of the SEM pictures of PSiFeNPs films transferred from the different subphases is presented in Figure 20 b).

Taking into account the shapes of the isotherms, the morphology of the films observed under Brewster angle microscopy, and the films transferred onto silicon wafers and analysed under SEM, a constant collapse was observed, analogous to that in ultrapure water experiments. Locally observed multilayers (or rather 3D aggregates), especially in combination with the salt residues, reassemble thin films formed via Stranski-Krastanov epitaxial growth (layers and islands). Nonetheless, the mechanism behind the formation of such structures must have been

different. Dai et al. investigated the collapse of gold nanoparticles trapped at interfaces and laterally compressed. They proposed a crinkle-folding mechanism based on synchrotron experiments (grazing-incidence X-ray off-specular scattering).[333] The observation of the PSiFeNPs films suggests an analogous mechanism as proposed by the authors. However, the interpretation is "blurred" by salt- and/or evaporation-induced aggregation, which leads to discrepancies in the Langmuir-Blodgett films.

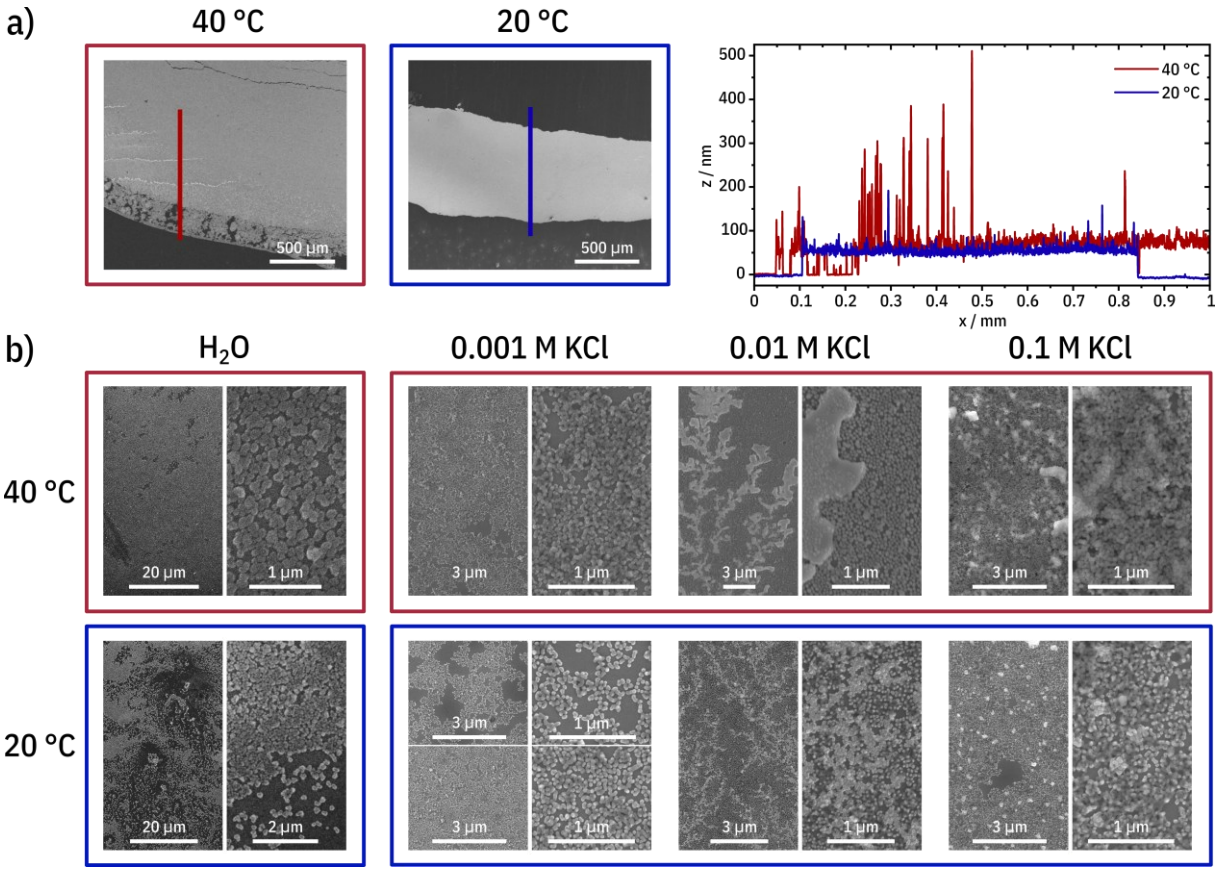

Figure 20. SEM pictures of Langmuir-Blodgett films transferred at different KCl concentrations and profilometry. **a)** low-magnification pictures of PSiFeNPs films transferred at 8 $mN \cdot m^{-1}$ at HT and LT from 0.01 M KCl with the profilometer paths and the related profiles. **b)** SEM images of Langmuir-Blodgett films transferred onto silicon wafers. The H_2O samples correspond to the first system and the related publication,[19] and were transferred at 9 $mN \cdot m^{-1}$. Samples of KCl subphases were transferred at 9 $mN \cdot m^{-1}$.The author's own figure, previously published in ref.[20] (CC-BY 4.0).

4.5. Spacing between Nanoparticles

As mentioned before, SEM images showed that the distance between nanoparticles increased after replacing the ultrapure water subphase with KCl solutions. Since the PSiFeNPs are not monodispersed and two batches differing in size were used, the distances between the edges of the particles were used to evaluate the interactions between nanoparticles. The DLVO

(Derjaguin–Landau–Verwey–Overbeek) theory, the most commonly used approach to nanoparticle aggregation, posits the existence of a distance between nanoparticles at which the energy is minimised.[255] That occurs due to the interplay of the attractive and repulsive forces. The mechanical stress induced by the barriers disrupts the minimum; however, comparing the films at the same surface pressure provides insight into the interplay of forces.

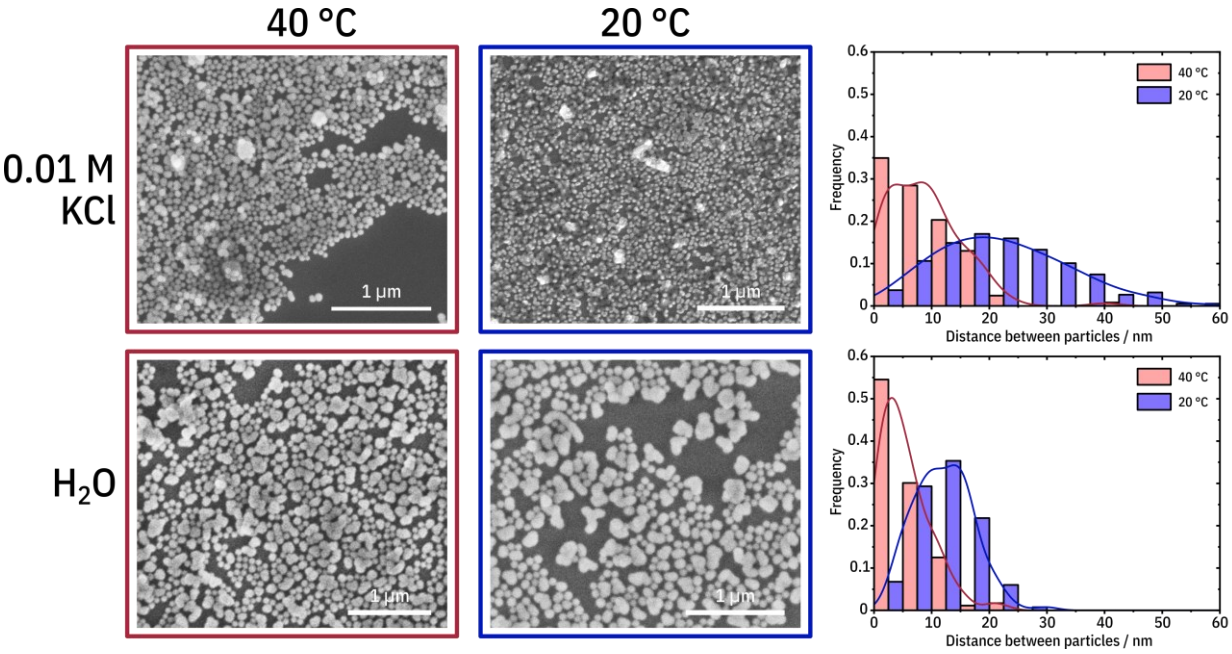

Figure 21. SEM images of PSiFeNPs films transferred onto silicon wafers from ultrapure water and 0.01 M KCl subphases at the HT (40 °C) and the LT (20 °C), and related histograms of distances between nanoparticles. The ultrapure water films were extracted at 9 $mN \cdot m^{-1}$, 0.01 M KCl films were extracted at 8 $mN \cdot m^{-1}$. The plots show distributions (histograms and corresponding kernel density estimation curves) of distances between nanoparticles with thresholds of 40 nm for ultrapure water samples and 60 nm for KCl samples. The author's own figure, previously published in ref.[20] (CC-BY 4.0).

Figure 21 presents pictures of the PSiFeNPs films transferred from ultrapure water and 0.01 M KCl at the HT and the LT. The films, especially those transferred from ultrapure water, were distracted by voids. To standardise measurements of nanoparticle distance, certain limits were introduced. First, only the distances to the closest neighbours were considered (the first-order neighbours, no other particles were between the two analysed particles). Second, since large voids were observed in the pictures, thresholds were arbitrarily established for the shortest distance between two particles (edge to edge). The latter limitation was intended to calculate distances within 2D aggregates, not between aggregates. These structures were especially visible in the ultrapure water sample. The distributions (histograms and related kernel density estimations) are presented in Figure 21.

The distribution of distances between nanoparticles has changed drastically with the change in temperature. First, in ultrapure water and a 0.01 M KCl solution, the difference in distances between nanoparticles at the HT and the LT was significant. For ultrapure water, the average distance was 5.4 ± 4.4 nm at 40 °C and 12.0 ± 5.0 nm at 20 °C. In the case of 0.01 M KCl, the average distance was 8.7 ± 6.4 nm at 40 °C and 22.4 ± 11.3 nm. By considering half of these values, the results for ultrapure water match the theoretical thickness of the PNIPAM layer. The difference with 0.01 M KCl suggests that the distance of the energy minimum in this balance of forces is further away from the surface of a particle. 0.1 M KCl film was already highly aggregated, which was surprising as the surface pressure isotherms were shifted significantly towards larger areas, and 3D aggregation decreases the average area occupied by a nanoparticle at the interface. The high rise in pressure suggests that the 0.1 M KCl layer is strongly trapped at the interface and that the repulsion (the resultant force) is a longer-range interaction, as it was in ultrapure water. Strong entrappement at the interface is possible. PSiFeNPs were negatively charged, so the interface is.[334] In such a case, screening both reduces electrostatic repulsion at the interface and could increase deposition efficiency in these experiments.[335,336]

4.6. Interactions between Nanoparticles

The properties of the PSiFeNPs system have changed significantly as the ionic strength of the subphase is increased (by replacing the subphase with KCl solutions). According to the literature, the Hofmeister effect affects the thermoresponsive properties of hydrogels.[337] However, for PNIPAM in 0.1 M KCl, the expected drop in the LCST is only 1.2 °C (linear).[338] Analogical decrease (approx. 1.2 °C for every 0.1 M KCl) in the LCST was observed by Humphreys et al. for 120 nm SiO_2NPs capped with PNIPAM.[327] According to these works, the LCST of PSiFeNPs should not differ much from 31 °C (32.2 °C for Humphreys' particles in water). Additionally, an attachment of the NIPAM oligomer at the surface of a nanoparticle keeps the LCST on a "bulk", polymeric level, if the oligomer is not shorter than approximately. 18 monomers. The LCST decreases with the shortening of the oligomer.[298] On the contrary, free-standing NIPAM oligomers exhibit a linear rise of the LCST with the shortening of the length of the oligomer below 18N.[298] Since the experiments were performed at two temperatures far from the critical temperature (20 °C and 40 °C), a full transition between "open" (hydrated) and "closed" (dehydrated) states should be observed.

"Closing" of PNIPAM at the PSiFeNPs decreased the overall size of the nanoparticles. That was demonstrated at compression at the Langmuir trough at 20 °C and 40 °C (both at water and KCl solutions), where the onset of the isotherms was shifted towards larger values of surface areas at the LT compared to the HT. Mansfield et al. showed PNIPAM decorated SiO_2NPs, which aggregated above the LCST, as registered in the increase of the measured hydrodynamic radius.[339] On the other hand, others showed that similar particles (AuNPs and SiO_2NPs) did not aggregate above the LCST, and their hydrodynamic radii decreased or remained almost the same.[327,340] Humphreys et al. also showed that PNIPAM-coated particles decreased their hydrodynamic radius in the presence of salt. Their particles' hydrodynamic radii decreased from 290 nm to 165 nm in KCl solution when the temperature was increased from 20 °C to 40 °C. The authors used nanoparticles scaled by a factor of around 2 (120 nm – diameter, 10 nm PNIPAM layer versus 65 nm – diameter and approximately 5-6 nm of PNIPAM layer of PSiFeNPs, batch 2).

In the case of PSiFeNPs, the observed change in hydrodynamic radius was small; it slightly increased at the HT. These differences were repeatable and consistent; however, they fell within the standard deviation range. A significant change was observed only at 0.1 M KCl, and, based on the distribution, it was attributed to aggregation (Table 3, Figure A6.1). The possibility of aggregation was also confirmed in KCl solutions by others.[340] Such a small difference, compared with the particles used by Humphres et al., was enough to observe drastically different behaviour of the particles at the interface.

As shown by Weiss et al., changes in the hydrodynamic radii of nanoparticles result in an increase in the normalised friction coefficient due to higher salt concentration and increased charge. This is caused by so-called electrostatic friction, arising from interactions with water molecules and ions.[341] PSiFeNPs were investigated in these terms as well. Electrophoretic mobilities of PSiFeNPs decreased more than 2 times compared to 0.1 M KCl with ultrapure water (Table 3). These values suggested that an ionic shell surrounded particles and implied considerable extra friction. While this was based on DLS measurements (particles in 3D suspensions), the importance of electrostatic friction at the interface was reported by Gehring et al.[342]

Analysing properties of PSiFeNPs in suspension, which supported an assumption of ionic surroundings of nanoparticles at the interface, was a key hint in the examination of the system. Table 4 compares areas of the films of the same volumes and mass concentrations of

the samples (different batches varying in nanoparticle sizes, however) reached certain surface pressures upon compression. The lift-off area (0.3 $mN \cdot m^{-1}$) was shifted by almost 1.96 times at 20 °C, and 1.64 times at 40 °C, comparing 0.1 M KCl to ultrapure water experiments. With the compression, this difference was more pronounced. At 5 $mN \cdot m^{-1}$ the ratios were equal to 3.56 at 20 °C and 2.29 at 40 °C. At 10 $mN \cdot m^{-1}$ these ratios were 5.04 and 2.63 at the LT and the HT, respectively. The fact that the batch of smaller particles was used in KCl experiments (which effectively increases the occupied area by the same mass of particles) does not explain such huge ratios. That suggested that the distance between PSiFeNPs increased compared to water experiments, even if the Debye length at 0.1 M KCl decreased to only around 1 nm.

The most unusual results were observed with the increase in the amount of the deposited sample at 0.1 M KCl. The graphs presented in Figure 18 c) showed the overlap of the isotherms recorded for 500 µl and 1500 µl. The phenomenon was not observed in ultrapure water. Linear growth was noticed instead.

Figure 22 shows a scheme of a theoretical DLVO-based interaction energy diagram. This is the qualitative assumption based on the distances between nanoparticles and on the ease with which nanoparticles aggregate. The distances separating compressed nanoparticles were larger at the LT than at the HT, and larger on KCl than on the water subphase (Figure 21). Short-range repulsion should be screened with a Debye length decreasing with the rise of the KCl concentration. On the other hand, the aggregation observed at the BAM seems to be facilitated by the increase in salt concentration (Figure 19). These are the reasons behind depicting the interactions this way.

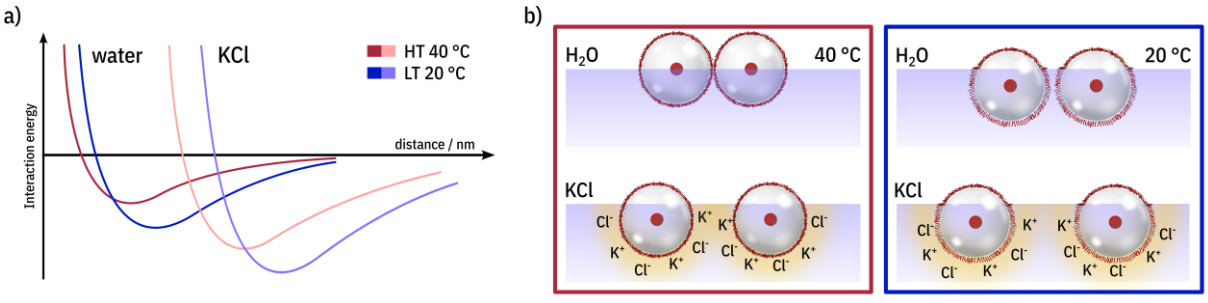

Figure 22. a) Postulated energy diagram scheme postulated according to the results. **b)** Probable conformations and immersions of the particles based on the results. The author's own figure, previously published in ref.[20] (CC-BY 4.0).

One possible explanation for the observed phenomenon (i.e., repulsion at a relatively large distance upon addition of KCl) was derived from a research report describing the repulsion between oppositely charged plates. A local excess of ions surrounding charged surfaces induced

an influx of water, analogous to osmosis. This resulted in a measurable long-distance force acting on the separation, which was much larger than Debye's length.[343] PSiFeNPs formed a similar system, where the chaotropic effect fostered the accumulation of ions close to the PNIPAM chains. Hence, many more ions were in the proximity of the air-water interface than in the bulk. To equilibrate the osmotic pressure, the influx of water effectively separated the nanoparticles. The ionic clouds and their separation were presented in Figure 22 b). Such a hypothesis can justify the distances that are much larger than Debye's length.

An additional repulsive force, as described above, shifted the local energy minimum to larger separations between nanoparticles (Figure 22). However, the overlapping of isotherms of different amounts of the sample (nanoparticles) remains mysterious. Possibly, ionic clouds and the additional repulsive forces made it easier to detach excess nanoparticles from the interface, forming 3D aggregates or desorbing into the subphase. The first option is supported by SEM images, which show more multilayered nanoparticles at the same surface pressures than in water experiments. The latter can be justified by the fact that nanoparticles surrounded by ions are much more hydrophilic, thereby facilitating desorption into the subphase. On the other hand, desorption and resorption of LCST-polymer-capped nanoparticles from the air-water interface were presented and investigated by Stefaniu et al.[241–244,303] Optionally, a continuous collapse of single particles into the water and formation of multilayers can be in accord with both hypotheses. None of them, however, explains exactly the same shape, especially the isotherm offset. The surface pressure was zero during the initial stages of compression, regardless of the amount of sample deposited. In all cases, significant preaggregation was observed immediately after deposition. Reconciling all the aforementioned scenarios, the surface pressure begins to rise only when a critical area is reached, with a constant number of nanoparticles trapped at the interface. Any excessive nanoparticle desorbs from the interface without influencing the surface pressure measurement. What is more, the same particle density at the interface, spread over a larger area, does not yield the same surface pressure, which seems impossible. The unusual experiments were repeated at least twice for each temperature regime and sample volume (500 µl, 1000 µl, and 1500 µl). The isotherms of compression were distorted, suggesting multiple random reorganisations of the film due to temporal out-of-equilibrium stresses originating from the mechanical compression (supported by the derived surface compressional moduli).

Section 3.3 in the Literature Review briefly describes different types of interactions as the most significant drivers of nanoarchitectonics in interfacial systems. Lateral capillary forces can be divided into two types: flotation capillary forces and immersion capillary forces. The flotation capillary forces result from the deformation of the interface under gravity. Immersion capillary forces arise from the deformation of the interface induced by wetting. That type of capillary force is present in the three-phase medium – fluid-fluid-fluid. The thickness of the middle phase has to be smaller than the particle's diameter. Both types of capillary forces can be attractive and repulsive. According to the literature, however, for PSiFeNPs smaller than 5-10 μm, interface deformation is negligible, and the particle's partial immersion is determined directly from its wetting properties.[250,253,254]

Reynaert et al. examined negatively charged polystyrene microbeads (3.1 ± 0.2 μm diameter) entrapped at the decane-water interface.[318] The particles exhibited fractal aggregation due to the dissolving NaCl in the aqueous phase, which screened electrostatic repulsion. Then, based on the theoretical work,[344] the authors explain that lateral capillary forces drove the aggregation. Similar fractal aggregates were observed in the PSiFeNPs system; the nanoparticles were too small to be effectively driven in a similar manner.

For partially immersed nanoparticles at the air-water interface, the capillary interaction energy depends on the contact line radius and the wetting properties. As the temperature transition of PNIPAM affects hydrophobicity, PSiFeNPs likely changed their immersion by exceeding the LCST. Aveyard and Clint discussed theoretical fundamentals of particles at the Langmuir trough, deriving equations relating the wetting angle to the collapse surface pressure.[345] The PNIPAM gels' wetting angle varies from around 45° below LCST to around 90° above the LCST. At the PNIPAM-grafted surface, the values were around 50° below the LCST and around 90° above the LCST.[296] Therefore, PSiFeNPs were expected to behave similarly.

Another type of interaction – van der Waals forces – was found to drive the self-organisation of nanoparticles. Ohara et al. showed that larger gold nanoparticles (5-6 nm) are sufficiently attracted to one another to form a close-packed aggregate, surrounded by smaller ones. Based on Monte Carlo simulations, the authors concluded that minimising the van der Waals energy was the principle of assembly.[346] PSiFeNPs were much less polydisperse than the particles used in that study; nonetheless, van der Waals forces could not be excluded as a potential factor influencing the nanoarchitectonics of the PSiFeNPs system.

Bonn et al. examined Teflon nanoparticles as an example of a system in which van der Waals forces between nanoparticles are expected to decrease to a negligible minimum. In such a system, self-organisation of screened electrostatic repulsion and critical Casimir forces were expected to play a vital role. Such an interplay also resulted in the fractal aggregation.[347] Boniello et al. also described fluctuation forces in an interfacial system composed of microparticles. Counterintuitively, the authors noticed that particles that were more immersed in water (air-water system) moved faster than those that were less immersed. These phenomenon was associated with thermal fluctuations and can interfere with the aggregation.[348]

None of these examples (Reynaert et al., Ohara et al., Bonn et al.) seems to explain the observed phenomena in the PSiFeNPs system. Therefore, the hypothesis of ionic clouds surrounding nanoparticles appears most probable, as it modifies the interplay between electrostatic and van der Waals interactions. That conclusion was supported by a simulation calculated by Dr Asghar Aryanfar, presented in the article on which this work is based. Because I did not participate in this part of the work, I do not include it in the thesis.

4.7. Summary – KCl-Solution-Based System

Introducing KCl into the subphase of the PSiFeNPs system led to unexpected observations. While increased aggregation of nanoparticles was expected due to the screening of electrostatic repulsion, the expanded separation of NPs in the compressed films, as well as the indifference of the registered film to the amount of the sample that was deposited, were surprising. The system still exhibited the thermoresponsiveness, similar to the water experiments. The changes, however, were more pronounced.

The decrease in ζ-potential due to the increased KCl concentration suggested that the nanoparticles were covered with the ions. That is also supported by the decrease in the electrophoretic mobilities, suggesting that despite the fact that the PNIPAM layer changes its conformation between “closed” and “open”, the PSiFeNPs’ diffusion depends almost only on the temperature (kinetics), not on the conformation-based resistance of movement.

The aforementioned bulk observations surprisingly manifested at the interface, with increased nanoparticle separation in the compressed (2D-aggregated) state. This was possibly explained by ionic clouds and osmotic water influx, which kept nanoparticles farther apart. The indifference of the compression isotherms to the amount of PSiFeNPs deposited at the interface

was not yet fully understood. Ionic clouds surrounding the nanoparticles could increase the particle's hydrophilicity, facilitating desorption from the interface.

Summary

The aim of this thesis was to develop the nanoengineering of adaptive colloidal Langmuir films at the air-water interface, particularly in terms of the nanoarchitectonics of thermoresponsive interfacial systems – the vast, barely mapped landscape of modern nanotechnology.

The study focused on filling the gap in the behaviour of nanoparticles capped with short thermoresponsive polymer brushes. The presented system exhibited unique features that could pique interest in the topic and expand knowledge in the field. Each and every chapter of the work introduced new insights into this field of nanotechnology

The literature review provided a brief scientometric and economic summary of current trends in the field, collected and condensed the data, and justified the further development of nanotechnology from a macroscopic perspective. The optimistic, broad view of the field is further challenged by the recently highlighted challenges, showing that there is still plenty of room at the bottom. Future developments will focus on the formation and integration of complex systems, particularly with biological entities. Up-to-date research has laid strong foundations for nanoscience, enabling the transfer of technology to other fields, especially biomedicine and energy storage and harvesting. That makes nanotechnology hard to track. New fields, such as agriculture, are emerging rapidly. New kinds of nanomaterials are also extensively investigated (e.g., MXenes). Nowadays, the implementation of artificial intelligence and machine learning appears as an auxiliary pathway accelerating the design and understanding of complex systems. In the next sections, the chapter recalled my review article on adaptive 2D and pseudo-2D systems, and provided an overview of the subfield of nanotechnology that promisingly addressed a couple of modern nanotechnology challenges. The chapter discussed the terminology of the systems and described the term “adaptive” in the context of current nanotechnological trends. The main principles of the design of these systems were then outlined, with particular focus on molecular, polymeric, and colloidal building blocks. To aid understanding of the next sections, the description of adaptive systems was followed by a discussion of the principles of the Langmuir method. It briefly reviewed the

history of the Langmuir method and described the modern trend of nanoarchitectonics of Langmuir films. Then, the most important physical principles were highlighted.

Then, after defining the main aims of the thesis, a state-of-the-art contextualisation of the research was done in the Experimental chapter. The Materials and Methods section was preceded by a detailed explanation of the nanomaterial design in the study. The key features of short PNIPAM were explained in detail to facilitate discussion of the results.

The experimental sections were divided into two Results and Discussions subchapters corresponding to two research articles on which they were based. The first one considered a nanoparticulate system built on an ultra-pure water surface. The stability and reversibility of Langmuir monolayers of PSiFeNPs were described, with particular attention to their temperature dependence. The system showed an unusual decrease in surface pressure with increasing temperature. Surface rheology experiments showed that the system composed of 90-nm nanoparticles capped with a 5-nm layer of the polymer behaves as if it were composed of rigid spheres rather than soft matter. The aggregation patterns driven by the nanoarchitectonics were discussed. The system exhibited facilitated aggregation of the nanoparticles below the polymer's LCST, which is the opposite of what is usually observed in an LCST-polymer-based system, where LCST polymers dehydrate and aggregate above the LCST. This phenomenon led to a seemingly ordered, mechanically induced two-dimensional aggregation at 40 °C and formation of seemingly disordered structures at 20 °C, again, opposite to typical crystallisation processes.

Replacing ultrapure water with a KCl solution led to several additional phenomena. The system maintained its thermoresponsiveness, manifested in an atypical decrease in surface pressure with increasing temperature or in the disordering of the compressed films at lower temperatures. Additional phenomena seemed to overlap with those, apparently. Spontaneous aggregation just after deposition was facilitated and enhanced by salt, and also observed at 40 °C. This phenomenon was anticipated, as the increase in the ionic strength effectively screened the electrostatic repulsion of negatively charged PSiFeNPs. However, despite reducing the Debye length due to the increased KCl concentration, nanoparticles were more separated from each other when compressed to the same surface pressure (aggregated). The isotherms shifted to larger areas, indicating that nanoparticles were more separated at higher KCl concentrations, as observed under SEM of Langmuir-Blodgett films. The change in the distance at which nanoparticles were in the energy minimum suggested that another

phenomenon occurred, resulting in an increase in repulsion or a decrease in attraction. Osmotic water influx into the ionic clouds surrounding the nanoparticles and, consequently, the separation of nanoparticles were proposed as explanations for the observed results. The system exhibited one more extraordinary feature: the compression isotherm was indifferent to the amount of the deposited sample at 0.1 M KCl. Surrounding the PSiFeNPs with ionic clouds could increase their hydrophilicity, thereby facilitating their desorption from the interface and the formation of 3D aggregates. This hypothesis was supported by observing these aggregates at different KCl concentrations, but at the same surface pressure as the Langmuir-Blodgett films. More aggregates were observed for higher KCl concentrations.

Eventually, the thesis presented an organised introduction to the unexplored topic of 2D and pseudo-2D adaptive colloidal systems and provided a physico-chemical insight into the nanoarchitectonics of Langmuir films composed of relatively large nanoparticles capped with short thermoresponsive polymer brushes at the air-water interface. The thesis presents unexpected phenomena that occurred when KCl was added to the system, having a strong impact on nanoarchitectonics. Langmuir trough experiments allowed for a close look at the interactions between nanoparticles and their properties at the air-water interface, depending on the external stimuli. Taken together, the observations enabled a comprehensive characterisation of the designed adaptive system and provided insight into the underlying mechanisms of the observed phenomena.

Appendix 1

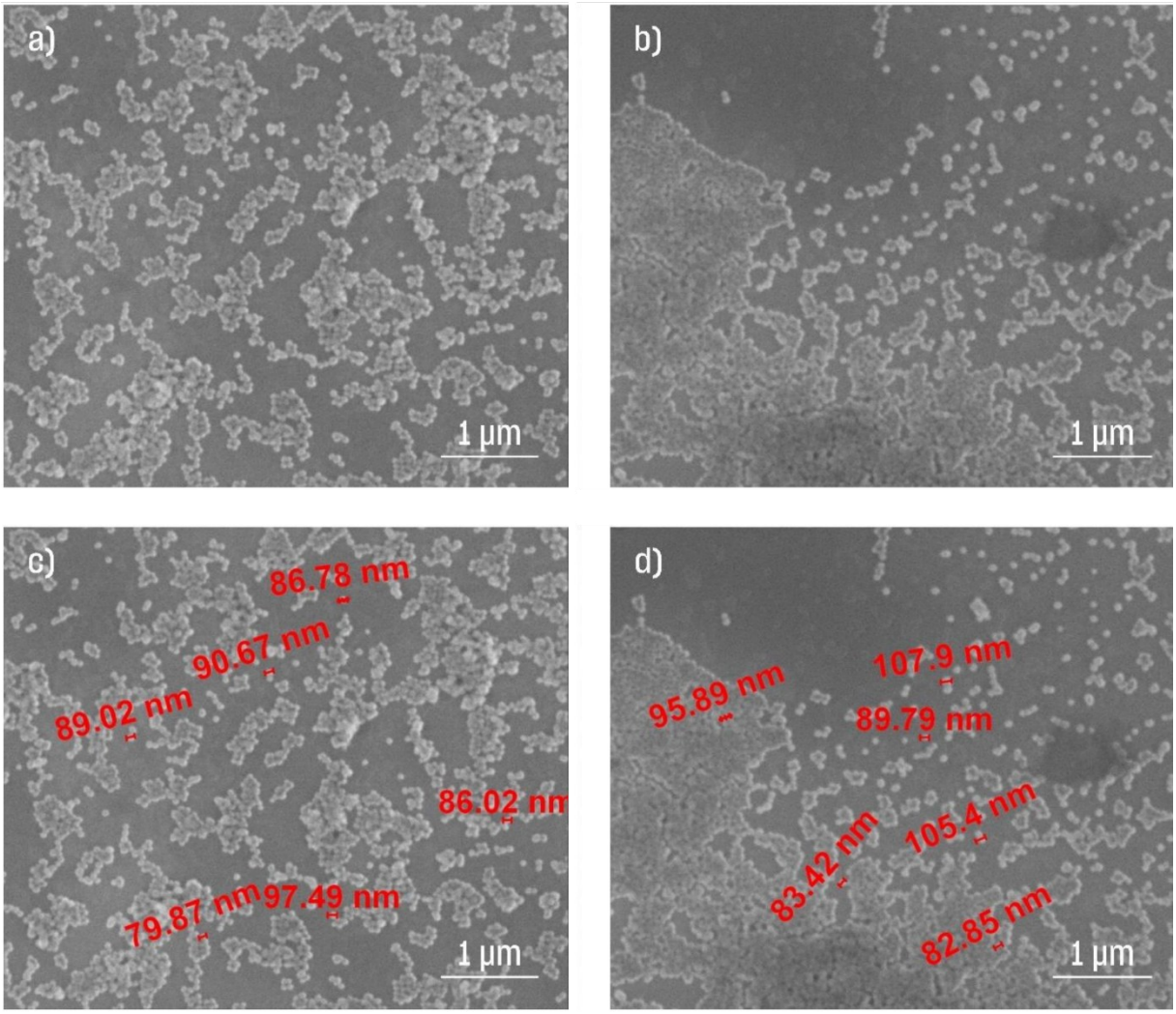

Figure A1.1. SEM pictures of $Fe_xO_y@SiO_2$ nanoparticles without PNIPAM ligands. The figure previously published in ref.[19] (CC-BY 4.0).

Table A1.1. Size distribution parameters of $Fe_xO_y@SiO_2$ nanoparticles without PNIPAM ligands (DLS, room temperature, distribution by volume).

$Fe_xO_y@SiO_2$ NPs			**Hydrodynamic diameter / nm**	**Fraction by volume / %**	**Std Deviation / nm**
Z-Average / nm	93.2	**Peak 1**	86.0	100	24.7
PdI	0.082				

Table A1.2.. Size distribution parameters of PSiFe nanoparticles (DLS, post-synthesis, room temperature, distribution by volume).

Fe_xO_y@SiO_2@PNIPAM NPs			Hydrodynamic diameter / nm	Fraction by volume / %	Std Deviation / nm
Z-Average / nm	130.1	**Peak 1**	114.2	95.5	56.0
PdI	0.216	**Peak 2**	5224	4.5	754

The hydrodynamic diameters of PSiFeNPs at 20 °C and 40 °C also measured the sample diluted to 1 $mg \cdot ml^{-1}$ of PSiFeNPs at 20 °C and 40 °C. The average hydrodynamic diameters (by volume) were 100 nm ± 35 nm at 40 °C and 90 nm ± 31 nm at 20 °C. This may seem to contradict the other data presented in the main manuscript. However, the hydrodynamic diameters are not equal to the sizes and distances of nanoparticles that were analysed in the main text. First, the DLS measurements were done for the suspension, not the interface. Second, the hydrodynamic diameter accounts for water molecules and ions in the vicinity of the particles that can effectively move with them. A bias could unlikely occur in post-processing of DLS data if a certain fraction of PSiFeNPs aggregated at HT, increasing the average size; nonetheless, distribution by numbers and by intensity did not show any evidence for that. Analogous shift in the hydrodynamic diameter was observed in the second batch of nanoparticles. Those results are recalled in Appendix 6, showing that no aggregation was registered in water samples.

ζ-potential of PSiFeNPs in pure water showed a change of the value from -54.62 mV to -41.87 mV with the temperature increase from 20 °C to 40 °C (Table A1.1.).

Table A1.3. ζ -potential measurements of PSiFe nanoparticles (batch I).

Zeta Potential			
20 °C		40 °C	
Zeta Potential	Standard Deviation	Zeta Potential	Standard Deviation
-54.62 mV	13.10 mV	-41.87 mV	15.77 mV

Raman Spectrum of PSiFeNPs

Signals typical for Fe_3O_4 (300-600 cm^{-1} and 670 cm^{-1}) were not expected to appear as the magnetic core was covered by the silica shell.[349] The latter should be noticed as bands around 600, 800, 980, 1060 and 1180 cm^{-1}.[350] CH_3 and CH_2 vibrations of PNIPAM should appear around 1380-1470 cm, and two amide-related bands should be visible within 1500-1600 cm^{-1} and 1600-1700 cm^{-1}.[351,352] A broad band corresponding to the bending of a water molecule should be visible around 1640 cm^{-1}, as the sample was suspended in water. The bands can be shifted due to the PSiFeNPs' structure. According to the literature, the Raman spectrum is shown in Figure A1.2. matches the postulated nanoparticle structure.

The Raman spectrum measurements were supported by MSc. Eng. Patryk Pyrcz.

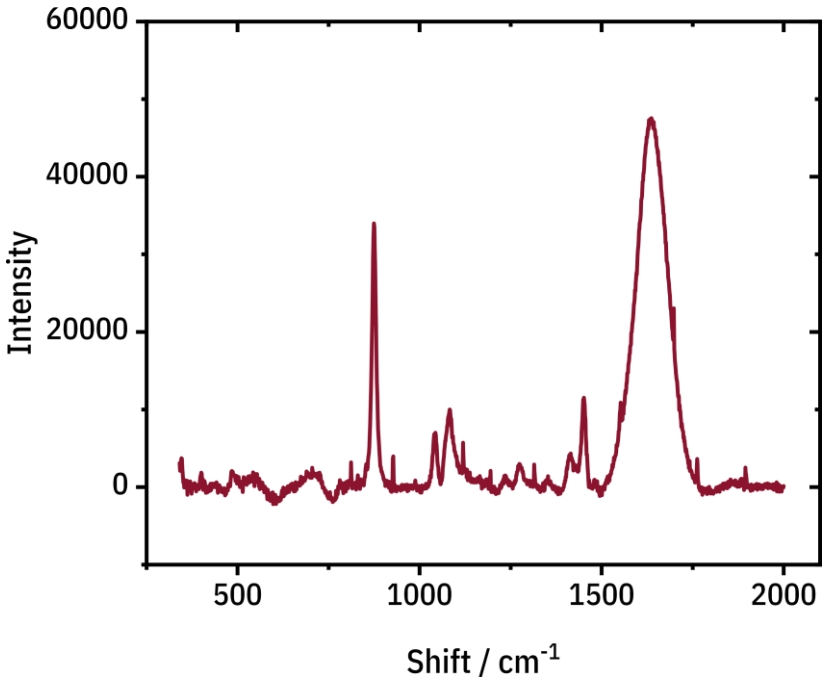

Figure A1.2. Raman spectrum of PSiFeNPs suspended in water (batch II, 5 $mg \cdot ml^{-1}$) measured with 785 nm laser (28.6 mW) at room temperature. The author's own figure, previously published in ref.[20] (CC-BY 4.0).

UV-Vis spectrum of PSiFeNPs

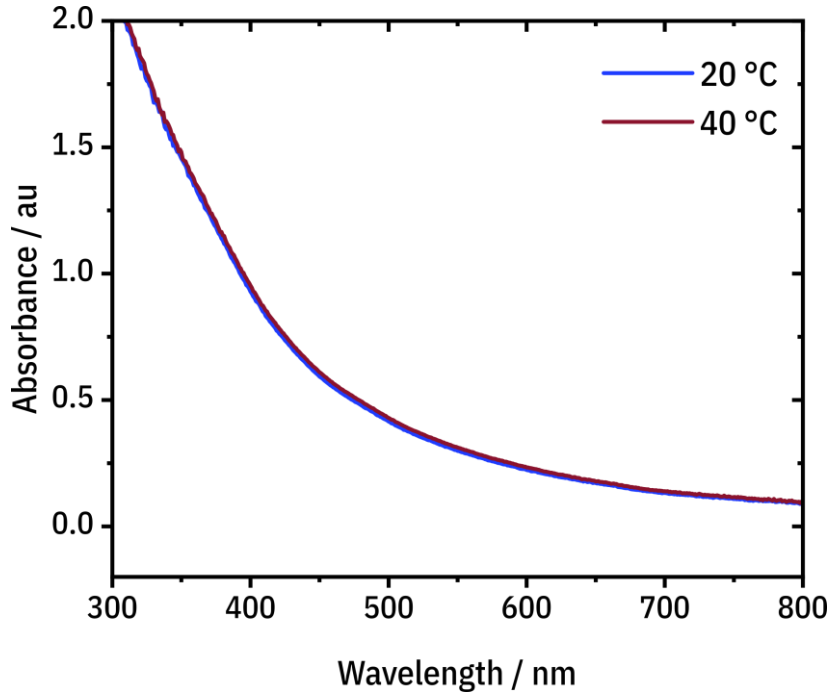

Figure A1.3. UV-Vis spectrum of PSiFeNPs suspended in water (batch II, 5 mg·ml^{-1}) measured at 20 °C and 40 °C. The author's own figure, previously published in ref.[20] (CC-BY 4.0).

X-ray energy-dispersive spectrum

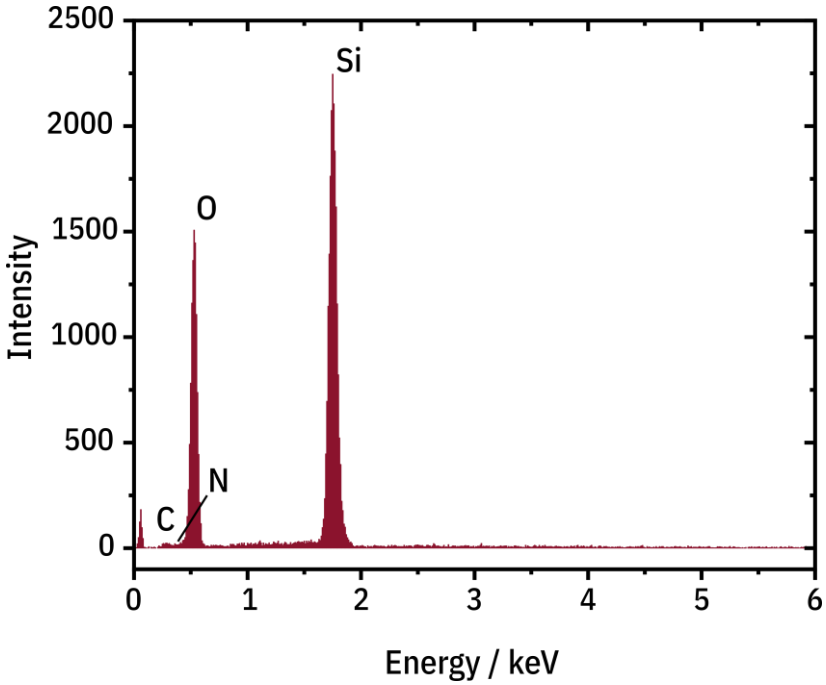

Figure A1.4. X-ray energy-dispersive spectrum of PSiFeNPs. The signal corresponding to nitrogen was not distinguishable from the background. The author's own figure, previously published in ref.[20] (CC-BY 4.0).

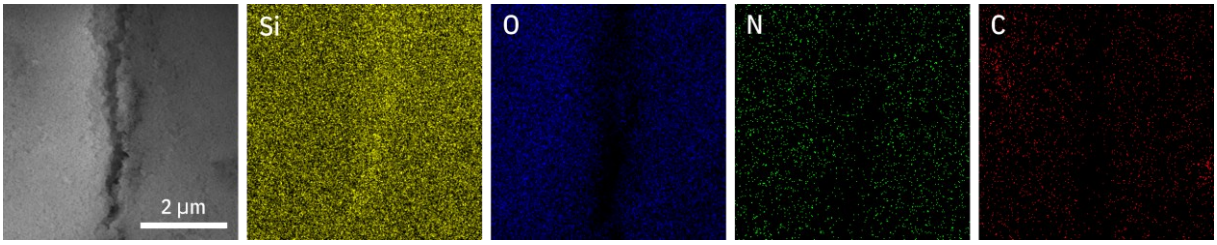

Figure A1.5. X-ray energy-dispersive spectroscopy maps by elements of a thick layer of PSiFeNPs. The author's own figure, previously published in ref.[20] (CC-BY 4.0).

Data presented in Figure A1.4. and Figure A1.5. were collected from the same area of the film. The nanoparticle suspension was drop-cast onto a silicon wafer. The elemental maps present a film with a crack. Observation of the slightly more signals (counts) for Si in the crack region and an analogous drop in signals for other elements confirmed the presence of Si, O, N, and C in PSiFeNPs. The increased signal for Si from the crack corresponds to the substrate (silicon wafer).

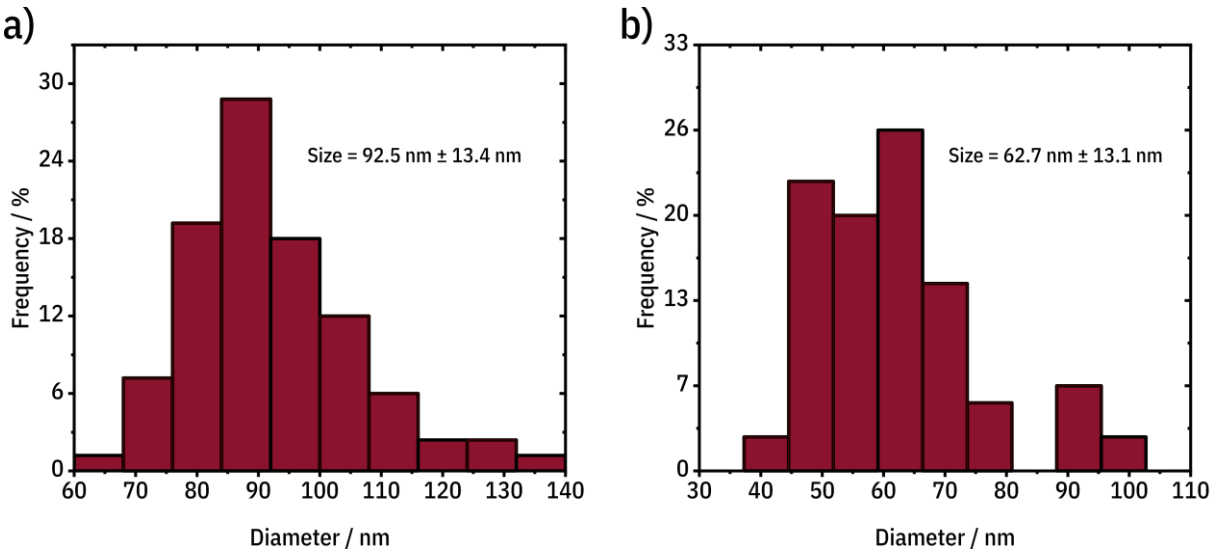

Figure A1.6. Size histograms (diameter) based on the SEM pictures **a)** batch I, **b)** batch II.

Figure A1.6 presents histograms of diameters of PSiFeNPs used in the study. Since the polymer coating of the particle is not visible under SEM, and DLS results in this system are difficult in interpretation, it is hard to assess the size of nanoparticles without any assumptions. Therefore, taking into account DLS, SEM, profilometry and theoretical length of the ligands, batches were described as approximately 90 nm (batch I) and approximately 65 nm (batch II) to simplify the analysis. The values describe diameters of nanoparticles without the capping layer.

Appendix 2

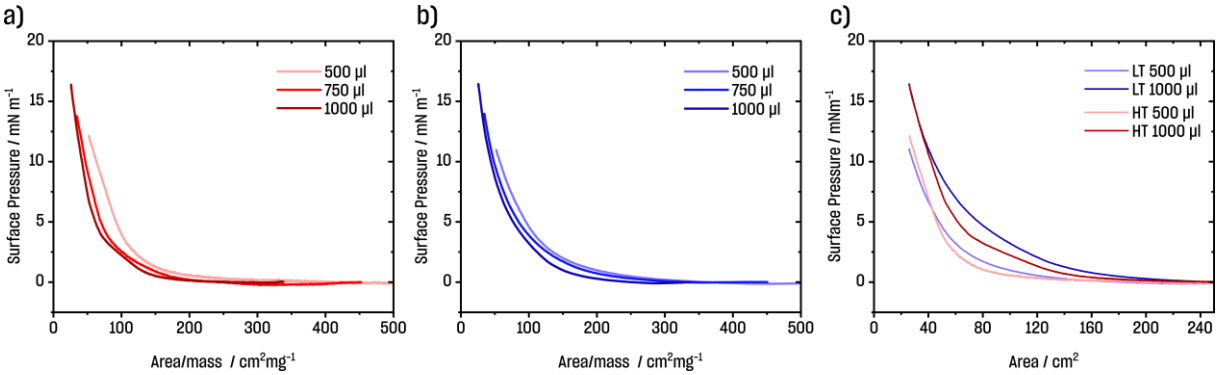

Figure A2.1. a) Normalised (area/mass) stability experiments of the PSiFe nanoparticles at the air-water interface, 40 °C; **b)** Normalised (area/mass) stability experiments of the PSiFe nanoparticles at the air-water interface, 20 °C; **c)** comparison of isotherms (500 µl vs 1000 µl) depending on the temperature regime. The author's own figure, previously published in ref.[19] (CC-BY 4.0).

Appendix 3

SEM picture analysis

Films transferred at 9 $mN \cdot m^{-1}$ were presented. Additional transfers at 5 $mN \cdot m^{-1}$ and 25 $mN \cdot m^{-1}$ are presented below. At 5 $mN \cdot m^{-1}$, PSiFeNPs Langmuir-Blodgett films at both temperature regimes seemed to be similar – single 3D aggregates were visible across large monolayer areas. The dense islands of aggregated nanoparticles were separated with voids. Many more 3D aggregates were observed at 25 $mN \cdot m^{-1}$. Similarly, at 9 $mN \cdot m^{-1}$, the films at the HT were more ordered, whereas those at the LT were more disordered, with irregular aggregates and irregular breaks in the structures. Voids were almost not present at the HT.

Since more of the 3D aggregates were visible with the rising surface pressure(5 $mN \cdot m^{-1}$, 9 $mN \cdot m^{-1}$, 25 $mN \cdot m^{-1}$), the SEM pictures revealed continuous collapse of the layer instead of folding, typical for molecular Langmuir films.

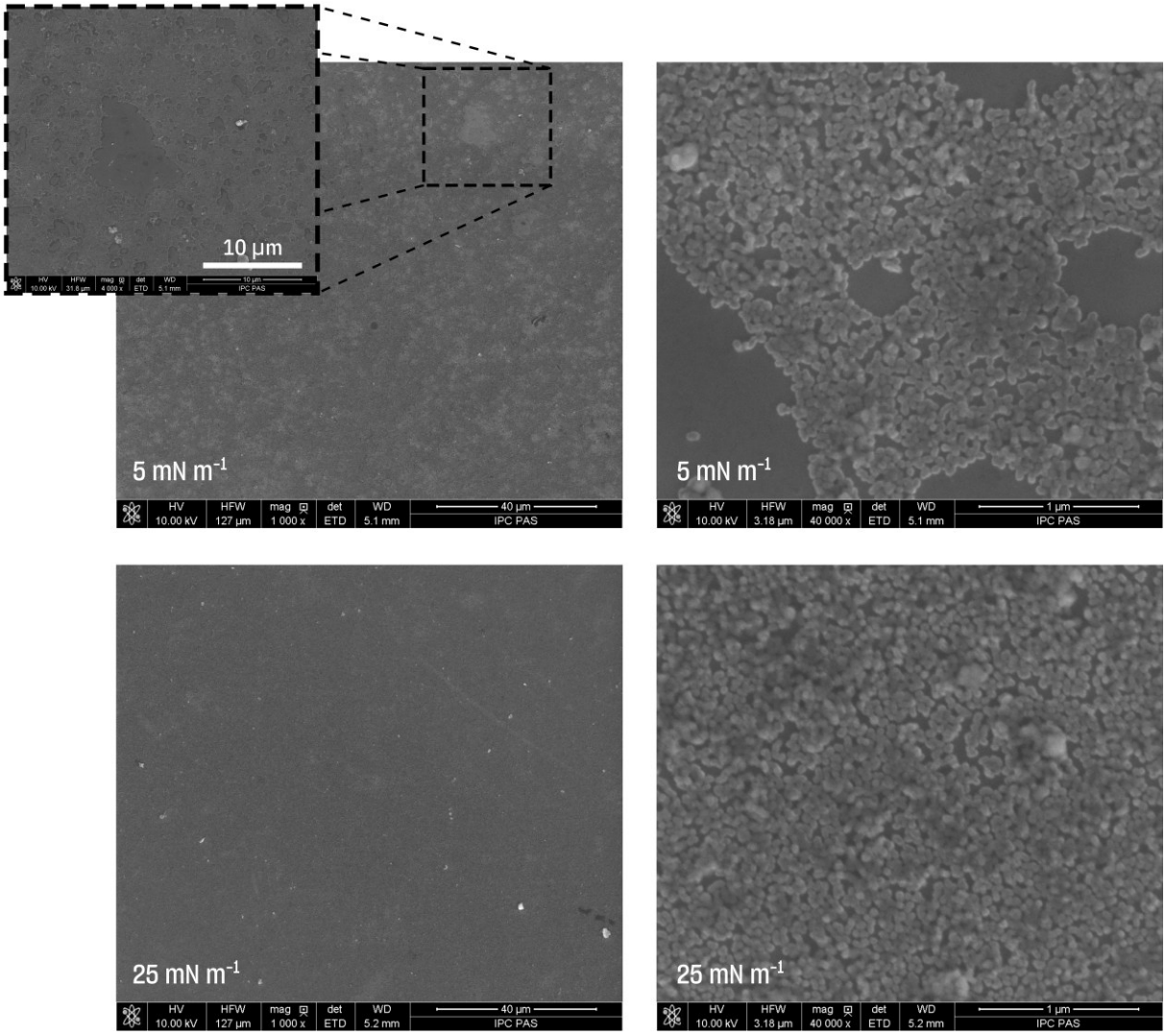

Figure A3.1. SEM pictures of films transferred onto silica wafers at **HT** at 5 mN·m^{-1} and 25 mN·m^{-1}. The author's own figure, previously published in ref.[19] (CC-BY 4.0).

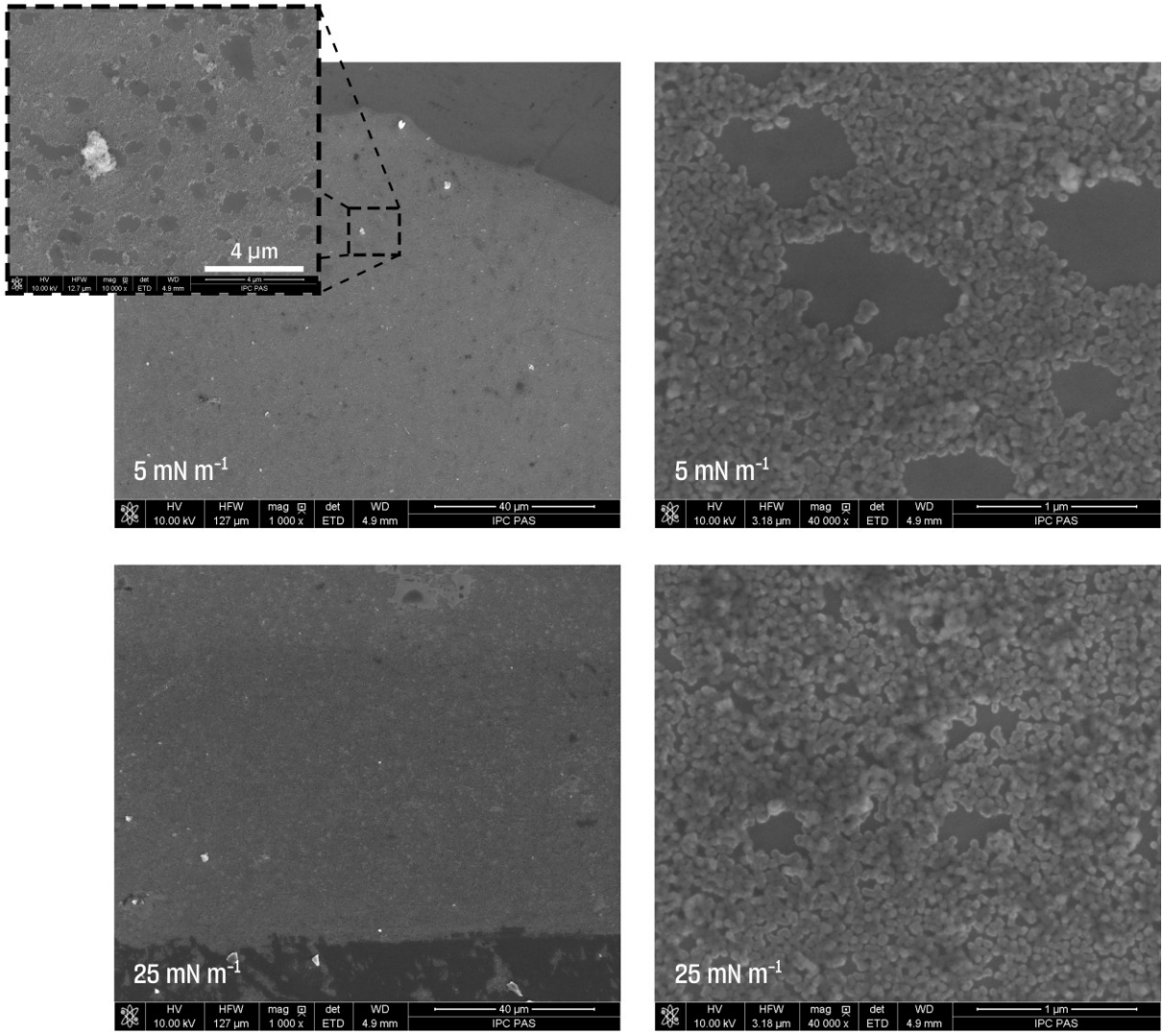

Figure A3.2. SEM pictures of films transferred onto silica wafers at **LT** at 5 $mN \cdot m^{-1}$ and 25 $mN \cdot m^{-1}$. The author's own figure, previously published in ref.[19] (CC-BY 4.0).

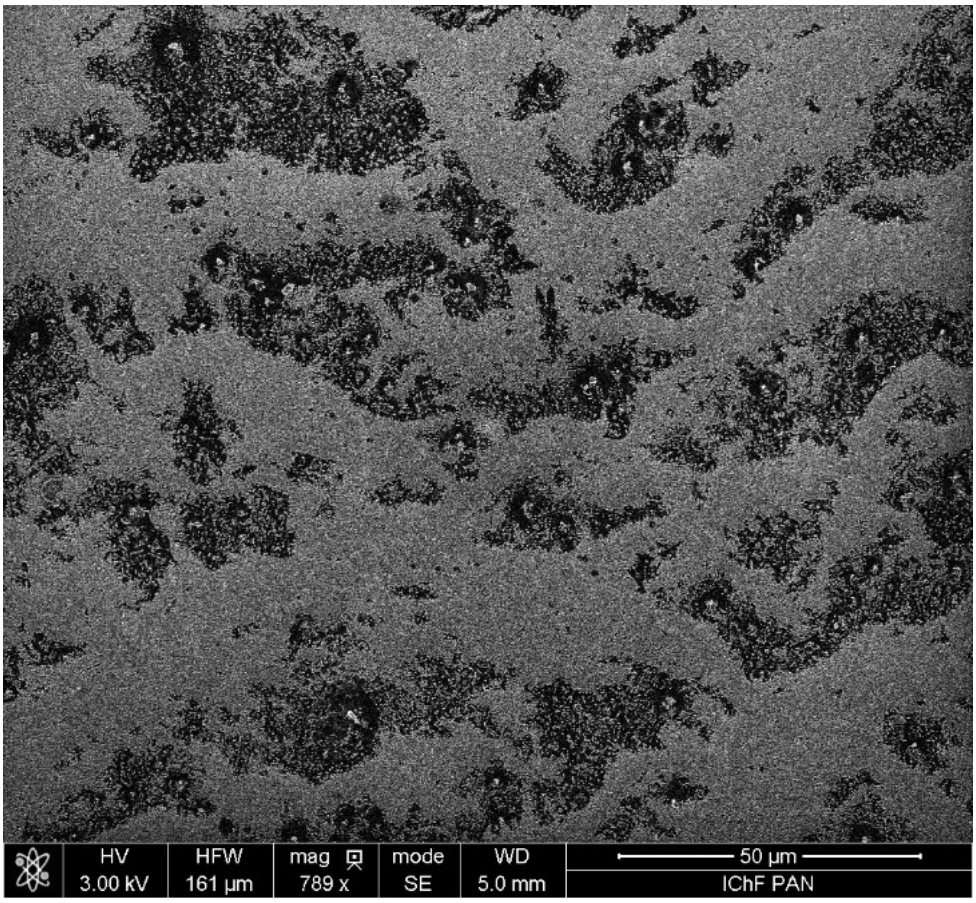

Figure A3.3. The broader picture PSiFeNPs film transferred onto a silicon wafer at 20 °C (**LT**) at 9 $mN \cdot m^{-1}$. The author's own figure, previously published in ref.[19] (CC-BY 4.0).

Appendix 4

Model experiment of thermal expansion (stearic acid)

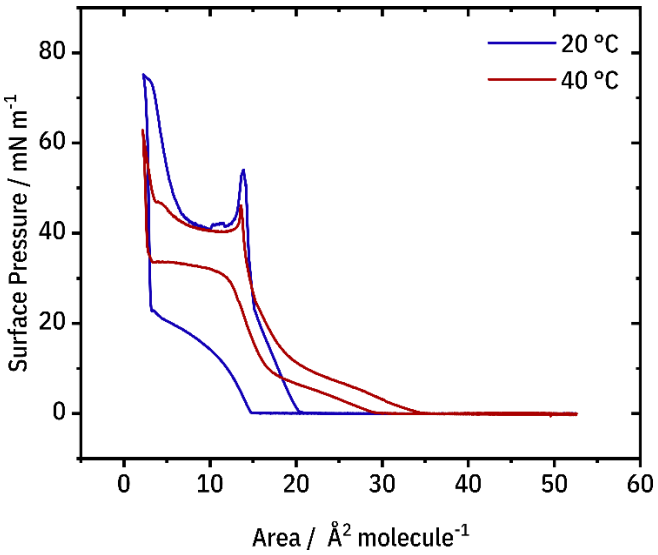

Figure A4.1. The thermal expansion of compression-decompression isotherms of a non-thermoresponsive model compound (stearic acid) at the LT and the HT. The author's own figure, previously published in ref.[19] (CC-BY 4.0).

The isotherms overlap at high surface pressure (solid-phase region up to collapse). The collapse occurs at a lower surface pressure at the HT, as there is more energy (k_BT) that enables the event. At the liquid phase, the thermal expansion is much more pronounced as molecules' mobility causes a rise of the surface pressure in the higher areas.

Appendix 5

This section contains calculations prepared jointly with Jan Paczesny (supervisor), justifying the linear regime of surface rheological measurements within 5-10% changes in area.

Rheological measurements

Figure 15 a) presents the surface compressional modulus that was calculated with regard to the compression isotherms. The values were higher for the LT, as the “closed” conformation of PSiFeNPs was expected to interact less with each other. These results did not reveal an apparent collapse of the layer, allowing the measurement of the film's dynamic properties via barrier oscillations. Rare 3D aggregates visible in the SEM pictures in this surface pressure range were neglected.

Oscillation experiments exhibited a slight drift of the surface pressure values. The possible origins were discussed by Hilles et al., who examined various polymers.[353] Therefore, the drift could come from desorption from the interface and dissolution in the subphase. That explanation was supported by Morioka and Kawaguchi. Another explanation is that the film could deform in the direction perpendicular to the interface. In the case of PSiFeNPs, the drift could also originate from a long relaxation of the compressed film. The 1-hour period dedicated to that could not be sufficient to fully get rid of the relaxation drift, despite the fact that after that time, the effect should be insignificant (Figure 15 e)). For the experiments at 40 °C, where the relaxation is faster, the slight drift comes from the evaporation of the subphase as well; however, this should be negligible for short-time oscillation experiments. For all of the aforementioned reasons, the drift could not have been simply explained by the extrapolation of Hilles et al.’s conclusions.

The linear regime was confirmed accordingly to the method presented by Hilles et al.. Figure A5.1. presents the relationship between the changes in surface pressure and in moduli of changes in area. The results were previously corrected for the drifting trend. Individual cycles were linear without the correction.

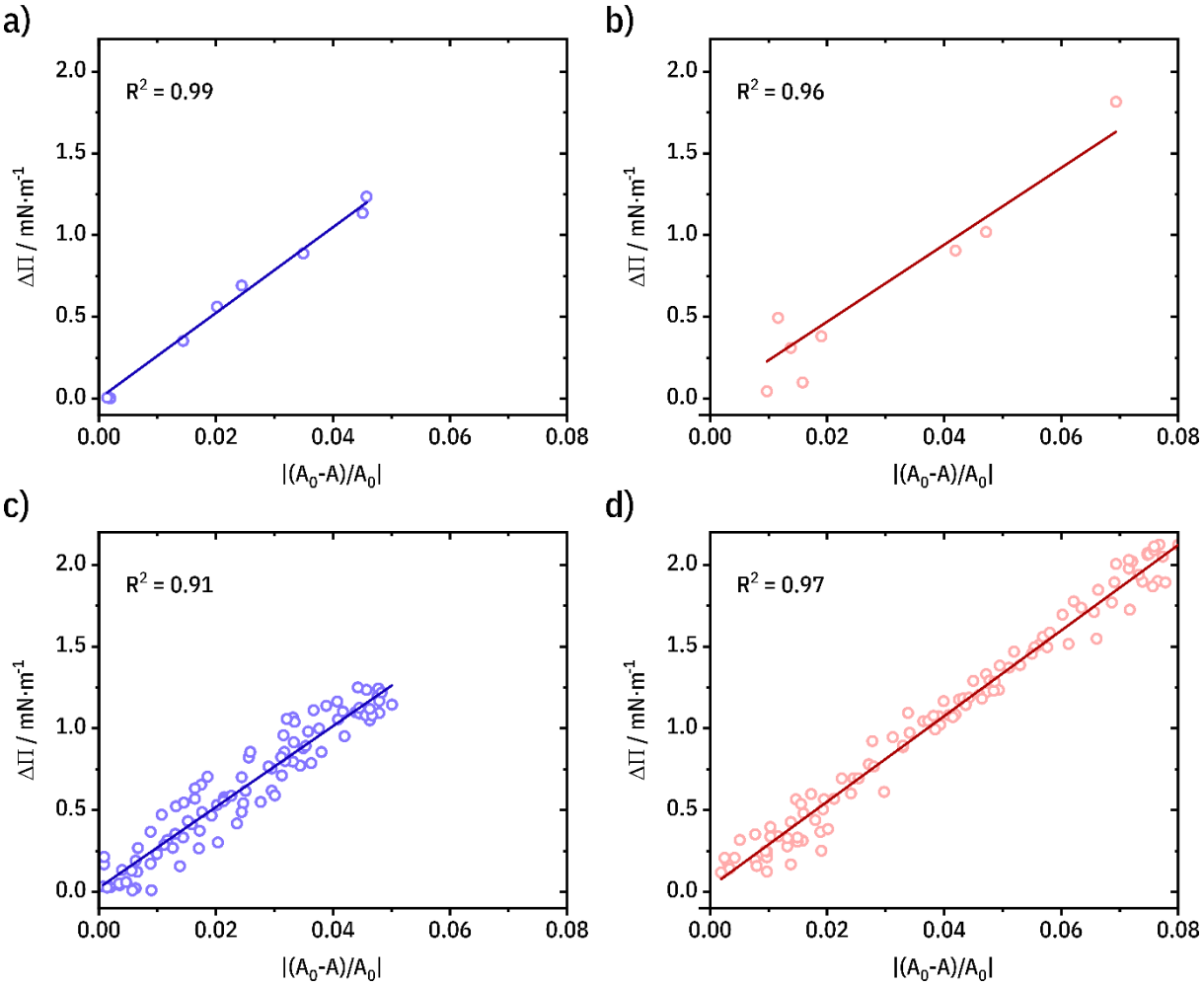

Figure A5.1. The relationship between changes in surface pressure and moduli of relative changes in area. The experiments were conducted with a frequency of 0.10 Hz. **a)** and **b)** show single compression at the LT and the HT, respectively. **c)** and **d)** present data for multiple cycles with the correction of the drift. The author's own figure, based on a previously published one in the ref.[19] (CC-BY 4.0).

Then, following the Guzmán et al. work, the total harmonic distortion parameter was analysed (Figure A5.2).[354] The Fourier transformation was applied to identify fundamental and harmonic frequencies in the surface pressure corresponding to 0.10 Hz oscillation experiments. Total harmonic frequencies were calculated according to the formula:

$$THD = \sqrt{\frac{\sum h_i^2}{f^2}}$$

where h is the harmonic amplitude, and f is the fundamental amplitude.

The values were 0.07 for the LT and 0.12 for the HT. These values were similar to Guzmán et al.'s research on 1,2-dipalmitoyl-sn-glycerol-3-phosphocholine (DPPC) with area changes of 5-10%.[355]

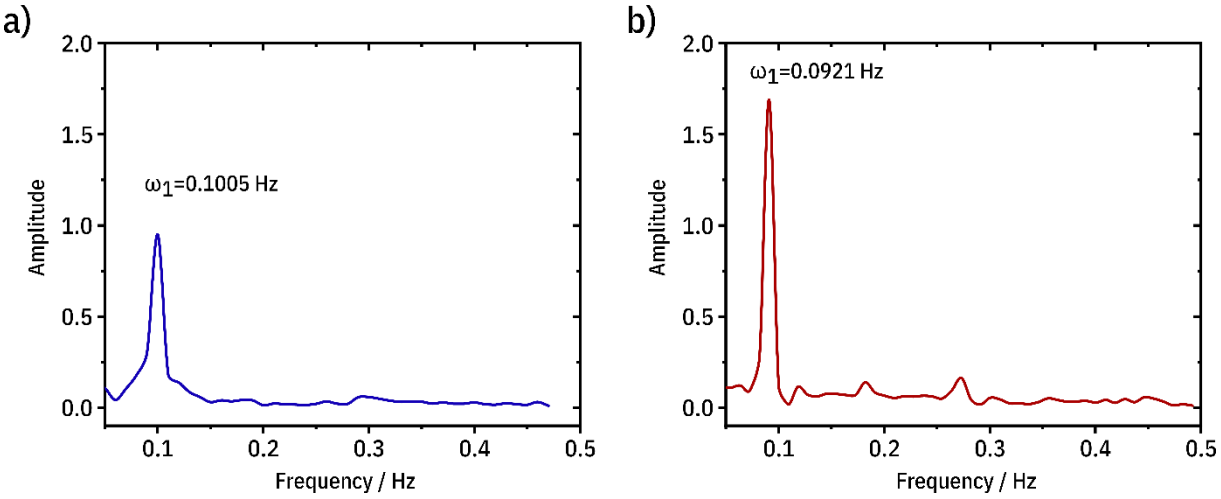

Figure A5.2. FFT spectra of the surface pressure signals corresponding to the oscillation experiments with a frequency of 0.10 Hz **a)** at the LT and **b)** at the HT. The author's own figure, based on a previously published one in ref.[19] (CC-BY 4.0).

Additional Lissajous diagrams for a frequency of 0.05 Hz

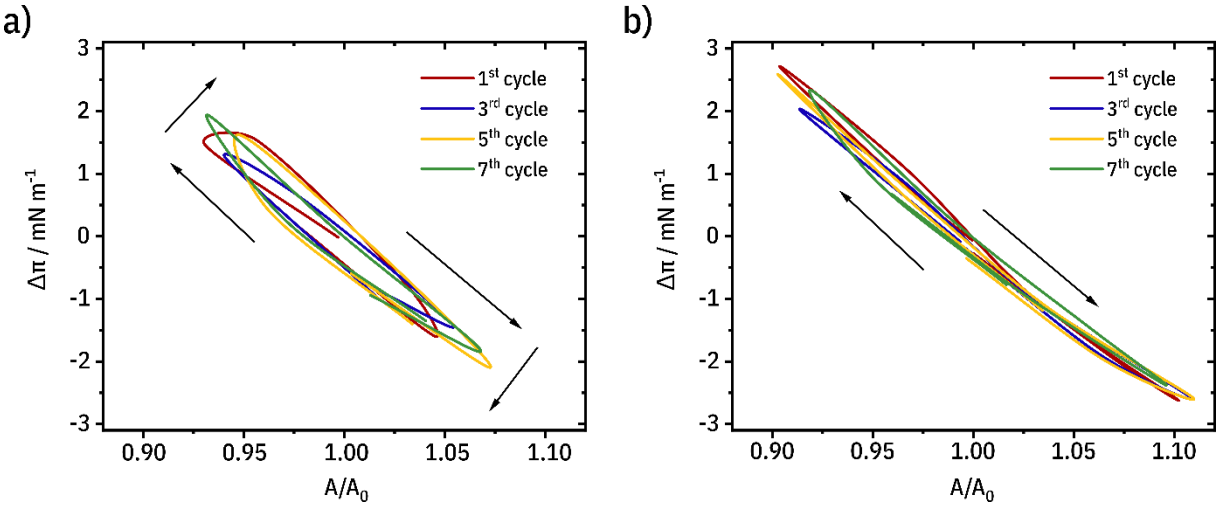

Figure A5.3. Lissajous diagrams for PSiFeNPs films registered with a frequency of 0.05 Hz **a)** at the LT and **b)** at the LT. . The correction of the drift was applied. The author's own figure, based on a previously published one in ref.[19] (CC-BY 4.0).

Appendix 6

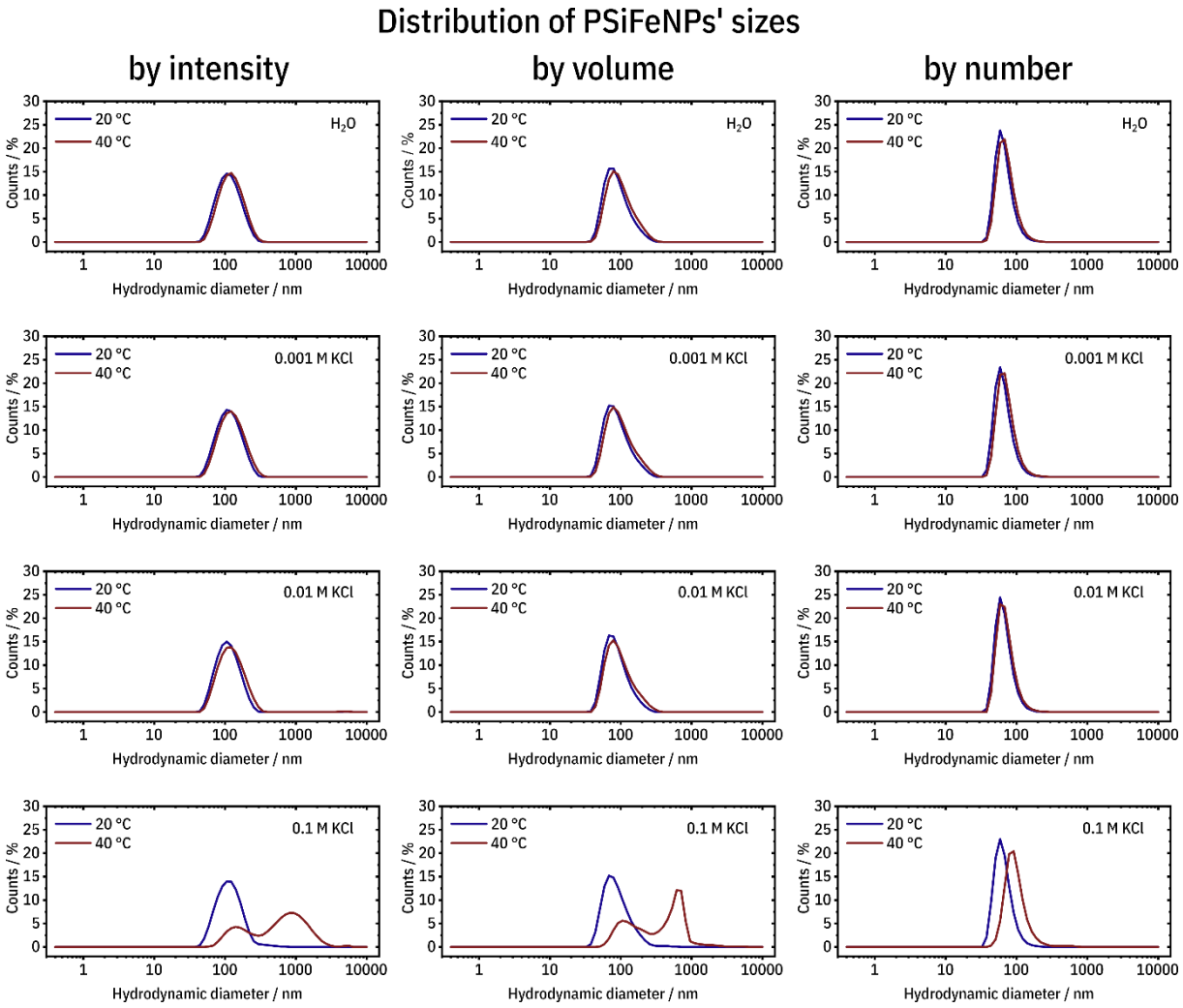

Figure A6.1.. DLS measurements of PSiFeNPs (batch II) in different concentrations of KCl.

All the measurements in this section were conducted with a backscattering at 175° because PSiFeNPs are relatively large and possibly could aggregate. Distributions by intensity and by volume of PSiFeNPs' sizes in 0.1 M KCl reveal that a fraction of nanoparticles aggregated. The author's own figure.

References

(1) Smith, Adam. *An Inquiry into the Nature and Causes of the Wealth of Nations*, (Original work 1776).; MataLibri: Amsterdam, 2007.

(2) Mosini, V. *Equilibrium in Economics: Scope and Limits*; Mosini, V., Ed.; Routledge Taylor & Francis Group, 2008.

(3) Hodgson, G. M. On the Meaning of "Neoclassical Economics." *J. Econ. Issues* **2025**, *59* (4), 1070–1083. https://doi.org/10.1080/00213624.2025.2575654.

(4) Nash, J. F. Equilibrium Points in n -Person Games. *Proceedings of the National Academy of Sciences* **1950**, *36* (1), 48–49. https://doi.org/10.1073/pnas.36.1.48.

(5) Bensaude-Vincent, B.; Mosini, V. Between Economics and Chemistry Lavoisier's and Le Chatelier's Notions of Equilibrium. In *Equilibrium in Economics: Scope and Limits*; Mosini, V., Ed.; Routledge Taylor & Francis Group, 2008.

(6) Merriam Webster. *Le Chatelier's principle*. merriam-webster.com. https://www.merriam-webster.com/medical/Le%20Chatelier's%20principle (accessed 2025-12-22).

(7) Samuelson, P. A. *Foundations of Economic Analysis, by Paul Anthony Samuelson*; Harvard University Press, 1947.

(8) Samuelson, P. A. An Extension of the Le Chatelier Principle. *Econometrica* **1960**, *28* (2), 368. https://doi.org/10.2307/1907727.

(9) Fisher, F. M. . *Disequilibrium Foundations of Equilibrium Economics*; Cambridge University Press, 1989.

(10) Bouchaud, J.-P.; Farmer, J. D.; Lillo, F. How Markets Slowly Digest Changes in Supply and Demand. **2008**.

(11) Taleb, N. Nicholas. *The Black Swan : The Impact of the Highly Improbable*; Random House, 2012.

(12) Hołyst, R.; Bubak, G.; Kalwarczyk, T.; Kwapiszewska, K.; Michalski, J.; Pilz, M. Living Cell as a Self-Synchronized Chemical Reactor. *J. Phys. Chem. Lett.* **2024**, *15* (13), 3559–3570. https://doi.org/10.1021/acs.jpclett.4c00190.

(13) Whitesides, G. M.; Grzybowski, B. Self-Assembly at All Scales. *Science (1979).* **2002**, *295* (5564), 2418–2421. https://doi.org/10.1126/science.1070821.

(14) Grzybowski, B. A.; Stone, H. A.; Whitesides, G. M. Dynamic Self-Assembly of Magnetized, Millimetre-Sized Objects Rotating at a Liquid–Air Interface. *Nature* **2000**, *405* (6790), 1033–1036. https://doi.org/10.1038/35016528.

(15) Mirkin, C. A.; Petrosko, S. H.; Artzi, N.; Aydin, K.; Biaggne, A.; Brinker, C. J.; Bujold, K. E.; Cao, Y. C.; Chan, R. R.; Chen, C.; Chen, P.-C.; Chen, X.; Chevalier, O. J. G. L.;

Choi, C. H. J.; Crooks, R. M.; Dravid, V. P.; Du, J. S.; Ebrahimi, S. B.; Fan, H.; Farha, O. K.; Figg, C. A.; Fink, T. D.; Forsyth, C. M.; Fuchs, H.; Geiger, F. M.; Gianneschi, N. C.; Gibson, K. J.; Ginger, D. S.; Guo, S.; Hanes, J. S.; Hao, L.; Huang, J.; Hunter, B. M.; Huo, F.; Hwang, J.; Jin, R.; Kelley, S. O.; Kempa, T. J.; Kim, Y.; Kudruk, S.; Kumari, S.; Landy, K. M.; Lee, K.-B.; Leon, N. J.; Li, J.; Li, Y.; Li, Z.; Liu, B.; Liu, G.; Liu, X.; Liz-Marzán, L. M.; Lorch, J. H.; Luo, T.; Macfarlane, R. J.; Millstone, J. E.; Mrksich, M.; Murphy, C. J.; Naik, R. R.; Nel, A. E.; Oetheimer, C.; Hedlund Orbeck, J. K.; Park, S.-J.; Partridge, B. E.; Peppas, N. A.; Personick, M. L.; Raj, A.; Ramani, N.; Ross, M. B.; Ross, S. B.; Sargent, E. H.; Sengupta, T.; Schatz, G. C.; Seferos, D. S.; Seideman, T.; Seo, S. E.; Shen, B.; Shim, W.; Shin, D.; Simon, U.; Sinegra, A. J.; Smith, P. T.; Spokoyny, A. M.; Stang, P. J.; Stegh, A. H.; Stoddart, J. F.; Swearer, D. F.; Tan, W.; Teplensky, M. H.; Thaxton, C. S.; Walt, D. R.; Wang, M. X.; Wang, Z.; Wei, W. D.; Weiss, P. S.; Winegar, P. H.; Xia, Y.; Xie, Y.; Xu, X.; Yang, P.; Yang, Y.; Ye, Z.; Yoon, K. R.; Zhang, C.; Zhang, H.; Zhang, K.; Zhang, L.; Zhang, X.; Zhang, Y.; Zheng, Z.; Zhou, W.; Zhu, S.; Zhu, W. 33 Unresolved Questions in Nanoscience and Nanotechnology. *ACS Nano* **2025**, *19* (36), 31933–31968. https://doi.org/10.1021/acsnano.5c12854.

(16) Hughes, K. J.; Ganesan, M.; Tenchov, R.; Iyer, K. A.; Ralhan, K.; Diaz, L. L.; Bird, R. E.; Ivanov, J.; Zhou, Q. A. Nanoscience in Action: Unveiling Emerging Trends in Materials and Applications. *ACS Omega* **2025**, *10* (8), 7530–7548. https://doi.org/10.1021/acsomega.4c10929.

(17) Zbonikowski, R.; Mente, P.; Bończak, B.; Paczesny, J. Adaptive 2D and Pseudo-2D Systems: Molecular, Polymeric, and Colloidal Building Blocks for Tailored Complexity. *Nanomaterials* **2023**, *13* (5), 855. https://doi.org/10.3390/nano13050855.

(18) Oliveira, O. N.; Caseli, L.; Ariga, K. The Past and the Future of Langmuir and Langmuir-Blodgett Films. *Chem. Rev.* **2022**, *122* (6), 6459–6513. https://doi.org/10.1021/acs.chemrev.1c00754.

(19) Zbonikowski, R.; Iwan, M.; Paczesny, J. Stimuli-Responsive Langmuir Films Composed of Nanoparticles Decorated with Poly(N -Isopropyl Acrylamide) (PNIPAM) at the Air/Water Interface. *ACS Omega* **2023**, *8* (26), 23706–23719. https://doi.org/10.1021/acsomega.3c01862.

(20) Zbonikowski, R.; Aryanfar, A.; Iwan, M.; Presselt, M.; Paczesny, J. Langmuir Nanoarchitectonics of Thermoresponsive Adaptive System of PNIPAM-Decorated Nanoparticles Induced by the Ionic Strength of the Subphase. *The Journal of Physical Chemistry C* **2025**. https://doi.org/10.1021/acs.jpcc.5c02555.

(21) Taniguchi, N. On the Basic Concept of Nanotechnology. In *Proceedings of the International Conference on Production Engineering*; 1974; pp 18–23.

(22) Bayda, S.; Adeel, M.; Tuccinardi, T.; Cordani, M.; Rizzolio, F. The History of Nanoscience and Nanotechnology: From Chemical–Physical Applications to Nanomedicine. *Molecules* **2019**, *25* (1), 112. https://doi.org/10.3390/molecules25010112.

(23) Feynmann, R. *There's Plenty of Room at the Bottom: An Invitation to Enter a New Field of Physics*. http://www.phy.pku.edu.cn/~qhcao/resources/class/QM/Feynman%27s-Talk.pdf (accessed 2020-03-16).

(24) Freestone, I.; Meeks, N.; Sax, M.; Higgitt, C. The Lycurgus Cup — A Roman Nanotechnology. *Gold Bull.* **2007**, *40* (4), 270–277. https://doi.org/10.1007/BF03215599.

(25) Kochmann, W.; Reibold, M.; Goldberg, R.; Hauffe, W.; Levin, A. A.; Meyer, D. C.; Stephan, T.; Müller, H.; Belger, A.; Paufler, P. Nanowires in Ancient Damascus Steel. *J. Alloys Compd.* **2004**, *372* (1–2), L15–L19. https://doi.org/10.1016/j.jallcom.2003.10.005.

(26) Padeletti, G.; Fermo, P. How the Masters in Umbria, Italy, Generated and Used Nanoparticles in Art Fabrication during the Renaissance Period. *Appl. Phys. A Mater. Sci. Process.* **2003**, *76* (4), 515–525. https://doi.org/10.1007/s00339-002-1935-1.

(27) *Nano-*. Oxford English Dictionary. https://www.oed.com/ (accessed 2025-12-29).

(28) *Nānus*. Online Latin Dictionary. https://www.online-latin-dictionary.com/ (accessed 2025-12-29).

(29) *νανος*. Biblissima. https://outils.biblissima.fr/fr/ (accessed 2025-12-29).

(30) Boholm, M. The Use and Meaning of Nano in American English: Towards a Systematic Description. *Ampersand* **2016**, *3*, 163–173. https://doi.org/10.1016/j.amper.2016.10.001.

(31) *The International System of Units (SI)*; Sèvres, 2019. https://doi.org/10.59161/AUEZ1291.

(32) *National Nanotechnology Initiative website*. https://www.nano.gov/about-nni/what/funding. (accessed 2025-01-21).

(33) *National Nanotechnology Initiative - about nanotechnology*. https://www.nano.gov/about-nanotechnology. (accessed 2025-01-21).

(34) COMMISSION, E. Commission Recommendation of 10 June 2022 on the Definition of Nanomaterial. *Official Journal of the European Union* **2022**, *36237* (October 2011), 1–5. https://doi.org/10.2788/36237.

(35) Roduner, E. Size Matters: Why Nanomaterials Are Different. *Chem. Soc. Rev.* **2006**, *35* (7), 583. https://doi.org/10.1039/b502142c.

(36) Burda, C.; Chen, X.; Narayanan, R.; El-Sayed, M. A. Chemistry and Properties of Nanocrystals of Different Shapes. *Chem. Rev.* **2005**, *105* (4), 1025–1102. https://doi.org/10.1021/cr030063a.

(37) Alivisatos, A. P. Semiconductor Clusters, Nanocrystals, and Quantum Dots. *Science (1979).* **1996**, *271* (5251), 933–937. https://doi.org/10.1126/science.271.5251.933.

(38) Baig, N.; Kammakakam, I.; Falath, W. Nanomaterials: A Review of Synthesis Methods, Properties, Recent Progress, and Challenges. *Mater. Adv.* **2021**, *2* (6), 1821–1871. https://doi.org/10.1039/D0MA00807A.

(39) Milunovich, S.; Roy, J. The next Small Thing. An Introduction to Nanotechnology. *Merrill Lynch* **2001**.

(40) Westworld. HBO: The United States of America 2016.

(41) Doctor Who. BBC: United Kingdom 1963.

(42) Payal; Pandey, P. Role of Nanotechnology in Electronics: A Review of Recent Developments and Patents. *Recent Pat. Nanotechnol.* **2022**, *16* (1), 45–66. https://doi.org/10.2174/1872210515666210120114504.

(43) Chau, R.; Datta, S.; Doczy, M.; Doyle, B.; Jin, B.; Kavalieros, J.; Majumdar, A.; Metz, M.; Radosavljevic, M. Benchmarking Nanotechnology for High-Performance and Low-Power Logic Transistor Applications. *IEEE Trans. Nanotechnol.* **2005**, *4* (2), 153–158. https://doi.org/10.1109/TNANO.2004.842073.

(44) Wu, J.; Shen, Y.-L.; Reinhardt, K.; Szu, H.; Dong, B. A Nanotechnology Enhancement to Moore's Law. *Applied Computational Intelligence and Soft Computing* **2013**, *2013*, 1–13. https://doi.org/10.1155/2013/426962.

(45) Shu, Y.; Lin, X.; Qin, H.; Hu, Z.; Jin, Y.; Peng, X. Quantum Dots for Display Applications. *Angew. Chem. Int. Ed.* **2020**, *59* (50), 22312–22323. https://doi.org/10.1002/anie.202004857.

(46) Bourzac, K. Quantum Dots Go on Display. *Nature* **2013**, *493* (7432), 283–283. https://doi.org/10.1038/493283a.

(47) Taha, T. B.; Barzinjy, A. A.; Hussain, F. H. S.; Nurtayeva, T. Nanotechnology and Computer Science: Trends and Advances. *Memories - Materials, Devices, Circuits and Systems* **2022**, *2*, 100011. https://doi.org/10.1016/j.memori.2022.100011.

(48) Mimona, M. A.; Mobarak, M. H.; Ahmed, E.; Kamal, F.; Hasan, M. Nanowires: Exponential Speedup in Quantum Computing. *Heliyon* **2024**, *10* (11), e31940. https://doi.org/10.1016/j.heliyon.2024.e31940.

(49) Mehrdel, B.; Nikbakht, A.; Aziz, A. A.; Jameel, M. S.; Dheyab, M. A.; Khaniabadi, P. M. Upconversion Lanthanide Nanomaterials: Basics Introduction, Synthesis Approaches, Mechanism and Application in Photodetector and Photovoltaic Devices. *Nanotechnology* **2022**, *33* (8), 082001. https://doi.org/10.1088/1361-6528/ac37e3.

(50) Wong, K. V.; Perilla, N.; Paddon, A. Nanoscience and Nanotechnology in Solar Cells. *J. Energy Resour. Technol.* **2014**, *136* (1). https://doi.org/10.1115/1.4024715.

(51) Alktranee, M. Applications of Nanotechnology with Hybrid Photovoltaic/Thermal Systems. *Journal of Applied Engineering Science* **2020**, 1–15. https://doi.org/10.5937/jaes0-28760.

(52) Baer, D. R.; Burrows, P. E.; El-Azab, A. A. Enhancing Coating Functionality Using Nanoscience and Nanotechnology. *Prog. Org. Coat.* **2003**, *47* (3–4), 342–356. https://doi.org/10.1016/S0300-9440(03)00127-9.

(53) Zhu, Q.; Chua, M. H.; Ong, P. J.; Cheng Lee, J. J.; Le Osmund Chin, K.; Wang, S.; Kai, D.; Ji, R.; Kong, J.; Dong, Z.; Xu, J.; Loh, X. J. Recent Advances in Nanotechnology-Based Functional Coatings for the Built Environment. *Mater. Today Adv.* **2022**, *15*, 100270. https://doi.org/10.1016/j.mtadv.2022.100270.

(54) Jianrong, C.; Yuqing, M.; Nongyue, H.; Xiaohua, W.; Sijiao, L. Nanotechnology and Biosensors. *Biotechnol. Adv.* **2004**, *22* (7), 505–518. https://doi.org/10.1016/j.biotechadv.2004.03.004.

(55) Ramesh, M.; Janani, R.; Deepa, C.; Rajeshkumar, L. Nanotechnology-Enabled Biosensors: A Review of Fundamentals, Design Principles, Materials, and Applications. *Biosensors (Basel).* **2022**, *13* (1), 40. https://doi.org/10.3390/bios13010040.

(56) Talebian, S.; Wallace, G. G.; Schroeder, A.; Stellacci, F.; Conde, J. Nanotechnology-Based Disinfectants and Sensors for SARS-CoV-2. *Nat. Nanotechnol.* **2020**, *15* (8), 618–621. https://doi.org/10.1038/s41565-020-0751-0.

(57) Tovar-Lopez, F. J. Recent Progress in Micro- and Nanotechnology-Enabled Sensors for Biomedical and Environmental Challenges. *Sensors* **2023**, *23* (12), 5406. https://doi.org/10.3390/s23125406.

(58) Olveira, S.; Forster, S. P.; Seeger, S. Nanocatalysis: Academic Discipline and Industrial Realities. *J. Nanotechnol.* **2014**, *2014*, 1–19. https://doi.org/10.1155/2014/324089.

(59) Malik, S.; Muhammad, K.; Waheed, Y. Nanotechnology: A Revolution in Modern Industry. *Molecules* **2023**, *28* (2), 661. https://doi.org/10.3390/molecules28020661.

(60) van der Meel, R.; Sulheim, E.; Shi, Y.; Kiessling, F.; Mulder, W. J. M.; Lammers, T. Smart Cancer Nanomedicine. *Nat. Nanotechnol.* **2019**, *14* (11), 1007–1017. https://doi.org/10.1038/s41565-019-0567-y.

(61) Germain, M.; Caputo, F.; Metcalfe, S.; Tosi, G.; Spring, K.; Åslund, A. K. O.; Pottier, A.; Schiffelers, R.; Ceccaldi, A.; Schmid, R. Delivering the Power of Nanomedicine to Patients Today. *Journal of Controlled Release* **2020**, *326*, 164–171. https://doi.org/10.1016/j.jconrel.2020.07.007.

(62) Sahu, T.; Ratre, Y. K.; Chauhan, S.; Bhaskar, L. V. K. S.; Nair, M. P.; Verma, H. K. Nanotechnology Based Drug Delivery System: Current Strategies and Emerging Therapeutic Potential for Medical Science. *J. Drug Deliv. Sci. Technol.* **2021**, *63*, 102487. https://doi.org/10.1016/j.jddst.2021.102487.

(63) Malik, S.; Muhammad, K.; Waheed, Y. Emerging Applications of Nanotechnology in Healthcare and Medicine. *Molecules* **2023**, *28* (18), 6624. https://doi.org/10.3390/molecules28186624.

(64) Haleem, A.; Javaid, M.; Singh, R. P.; Rab, S.; Suman, R. Applications of Nanotechnology in Medical Field: A Brief Review. *Global Health Journal* **2023**, *7* (2), 70–77. https://doi.org/10.1016/j.glohj.2023.02.008.

(65) Grand View Research. *Nanotechnology Market Size, Share & Growth Report, 2030*; 2023.

(66) Fortune Business Insights. *Nanotechnology Market Size, Share & Industry Analysis, By Type (Nanodevices and Nanosensors), By Industry (Electronics, Healthcare, Manufacturing, Energy & Power, Automotive, Aerospace & Defense, Food & Beverages, and Others), and Regional Forecast, 2026-2034*; 2026.

(67) Precedence Research. *Nanotechnology Market*; 2024.

(68) Ulucan-Karnak, F.; Kuru, C. I.; Sağin, F. G. Critical Evaluation of Publications and Patents in Nanobiotechnology-Based Research in the Last Decade. *Turkish Journal of Biochemistry* **2023**, *48* (6), 606–619. https://doi.org/10.1515/tjb-2023-0144.

(69) *National Nanotechnology Initiative*. www.nano.gov. (accessed 2025-12-29).

(70) Tang, Z.; Shi, X.; Ren, H.; Guo, L.; Ma, H.; Feng, Q. *White Paper: Nanotechnology Industry China (2025) - Global Leadership and Technological Breaktrough*; 2025.

(71) StatNano. *Nanotechnology Patents in EPO*. https://statnano.com/report/s102 (accessed 2025-12-29).

(72) StatNano. *Nanotechnology Patents in USPTO*. **2025**. https://statnano.com/report/s103 (accessed 2025-12-29).

(73) OECD. *Patents in OECD selected technologies*. https://data-explorer.oecd.org/vis?lc=en&df[ds]=dsDisseminateFinalDMZ&df[id]=DSD_PATENTS%40DF_PATENTS_OECDSPECIFIC&df[ag]=OECD.STI.PIE&dq=.A.....&pd=%2C&to[TIME_PERIOD]=false (accessed 2025-12-29).

(74) El-Showk, S. *Saudi Arabia draws on new reserves*. Nature. https://www.nature.com/nature-index/news/saudi-arabia-draws-on-new-reserves (accessed 2026-03-17).

(75) StatNano. *Nanotechnology Publications*. https://statnano.com/report/s29 (accessed 2025-11-20).

(76) Tao, H.; Wu, T.; Aldeghi, M.; Wu, T. C.; Aspuru-Guzik, A.; Kumacheva, E. Nanoparticle Synthesis Assisted by Machine Learning. *Nat. Rev. Mater.* **2021**, *6* (8), 701–716. https://doi.org/10.1038/s41578-021-00337-5.

(77) Walker, N.; Lee, S.; Dagdelen, J.; Cruse, K.; Gleason, S.; Dunn, A.; Ceder, G.; Alivisatos, A. P.; Persson, K. A.; Jain, A. Extracting Structured Seed-Mediated Gold Nanorod Growth Procedures from Scientific Text with LLMs. *Digital Discovery* **2023**, *2* (6), 1768–1782. https://doi.org/10.1039/D3DD00019B.

(78) Lee, S.; Cruse, K.; Gleason, S. P.; Alivisatos, A. P.; Ceder, G.; Jain, A. Data-Driven Analysis of Text-Mined Seed-Mediated Syntheses of Gold Nanoparticles. *Digital Discovery* **2025**, *4* (1), 93–104. https://doi.org/10.1039/D4DD00158C.

(79) Dubrovsky, I.; Dmitrenko, A.; Dmitrenko, A.; Serov, N.; Vinogradov, V. Unveiling the Potential of AI for Nanomaterial Morphology Prediction. **2024**.

(80) Jiang, Y.; Salley, D.; Sharma, A.; Keenan, G.; Mullin, M.; Cronin, L. An Artificial Intelligence Enabled Chemical Synthesis Robot for Exploration and Optimization of Nanomaterials. *Sci. Adv.* **2022**, *8* (40). https://doi.org/10.1126/sciadv.abo2626.

(81) Odobesku, R.; Romanova, K.; Mirzaeva, S.; Zagorulko, O.; Sim, R.; Khakimullin, R.; Razlivina, J.; Dmitrenko, A.; Vinogradov, V. Agent-Based Multimodal Information Extraction for Nanomaterials. *NPJ Comput. Mater.* **2025**, *11* (1), 194. https://doi.org/10.1038/s41524-025-01674-7.

(82) Stoddart, J. F. The Chemistry of the Mechanical Bond. *Chem. Soc. Rev.* **2009**, *38* (6), 1802. https://doi.org/10.1039/b819333a.

(83) Sauvage, J.-P. Transition Metal-Containing Rotaxanes and Catenanes in Motion: Toward Molecular Machines and Motors. *Acc. Chem. Res.* **1998**, *31* (10), 611–619. https://doi.org/10.1021/ar960263r.

(84) Browne, W. R.; Feringa, B. L. Making Molecular Machines Work. *Nat. Nanotechnol.* **2006**, *1* (1), 25–35. https://doi.org/10.1038/nnano.2006.45.

(85) Ju, X.; Chen, C.; Oral, C. M.; Sevim, S.; Golestanian, R.; Sun, M.; Bouzari, N.; Lin, X.; Urso, M.; Nam, J. S.; Cho, Y.; Peng, X.; Landers, F. C.; Yang, S.; Adibi, A.; Taz, N.; Wittkowski, R.; Ahmed, D.; Wang, W.; Magdanz, V.; Medina-Sánchez, M.; Guix, M.; Bari, N.; Behkam, B.; Kapral, R.; Huang, Y.; Tang, J.; Wang, B.; Morozov, K.; Leshansky, A.; Abbasi, S. A.; Choi, H.; Ghosh, S.; Borges Fernandes, B.; Battaglia, G.; Fischer, P.; Ghosh, A.; Jurado Sánchez, B.; Escarpa, A.; Martinet, Q.; Palacci, J.; Lauga, E.; Moran, J.; Ramos-Docampo, M. A.; Städler, B.; Herrera Restrepo, R. S.; Yossifon, G.; Nicholas, J. D.; Ignés-Mullol, J.; Puigmartí-Luis, J.; Liu, Y.; Zarzar, L. D.; Shields, C. W.; Li, L.; Li, S.; Ma, X.; Gracias, D. H.; Velev, O.; Sánchez, S.; Esplandiu, M. J.; Simmchen, J.; Lobosco, A.; Misra, S.; Wu, Z.; Li, J.; Kuhn, A.; Nourhani, A.; Maric, T.; Xiong, Z.; Aghakhani, A.; Mei, Y.; Tu, Y.; Peng, F.; Diller, E.; Sakar, M. S.; Sen, A.; Law, J.; Sun, Y.; Pena-Francesch, A.; Villa, K.; Li, H.; Fan, D. E.; Liang, K.; Huang, T. J.; Chen, X.-Z.; Tang, S.; Zhang, X.; Cui, J.; Wang, H.; Gao, W.; Kumar Bandari, V.; Schmidt, O. G.; Wu, X.; Guan, J.; Sitti, M.; Nelson, B. J.; Pané, S.; Zhang, L.; Shahsavan, H.; He, Q.; Kim, I.-D.; Wang, J.; Pumera, M. Technology Roadmap of Micro/Nanorobots. *ACS Nano* **2025**, *19* (27), 24174–24334. https://doi.org/10.1021/acsnano.5c03911.

(86) Uzoma, P. C.; Hu, H.; Khadem, M.; Penkov, O. V. Tribology of 2D Nanomaterials: A Review. *Coatings* **2020**, *10* (9), 897. https://doi.org/10.3390/coatings10090897.

(87) *MoS_2*; Wang, Z. M., Ed.; Springer International Publishing: Cham, 2014; Vol. 21. https://doi.org/10.1007/978-3-319-02850-7.

(88) Geim, A. K. Graphene: Status and Prospects. *Science (1979).* **2009**, *324* (5934), 1530–1534. https://doi.org/10.1126/science.1158877.

(89) COMMISSION, E. Commission Recommendation of 10 June 2022 on the Definition of Nanomaterial. *Official Journal of the European Union* **2022**, *36237* (October 2011), 1–5. https://doi.org/10.2788/36237.

(90) Ariga, K. Chemistry of Materials Nanoarchitectonics for Two-Dimensional Films: Langmuir–Blodgett, Layer-by-Layer Assembly, and Newcomers. *Chemistry of Materials* **2023**, *35* (14), 5233–5254. https://doi.org/10.1021/acs.chemmater.3c01291.

(91) Yujun, W. S.; Zhang. *Inorganic and Organic Thin Films, Chapters 1-2*; Song, Y., Ed.; Wiley, 2021. https://doi.org/10.1002/9783527344987.

(92) Whitesides, G. M.; Grzybowski, B. Self-Assembly at All Scales. *Science (1979).* **2002**, *295* (5564), 2418–2421. https://doi.org/10.1126/science.1070821.

(93) Zbonikowski, R.; Mente, P.; Bończak, B.; Paczesny, J. Adaptive 2D and Pseudo-2D Systems: Molecular, Polymeric, and Colloidal Building Blocks for Tailored Complexity. *Nanomaterials* **2023**, *13* (5), 855. https://doi.org/10.3390/nano13050855.

(94) Klajn, R.; Wesson, P. J.; Bishop, K. J. M.; Grzybowski, B. A. Writing Self-Erasing Images Using Metastable Nanoparticle "Inks." *Angew. Chem. Int. Ed.* **2009**, *48* (38), 7035–7039. https://doi.org/10.1002/anie.200901119.

(95) He, X.; Aizenberg, M.; Kuksenok, O.; Zarzar, L. D.; Shastri, A.; Balazs, A. C.; Aizenberg, J. Synthetic Homeostatic Materials with Chemo-Mechano-Chemical Self-Regulation. *Nature* **2012**, *487* (7406), 214–218. https://doi.org/10.1038/nature11223.

(96) Kaspar, C.; Ravoo, B. J.; van der Wiel, W. G.; Wegner, S. V.; Pernice, W. H. P. The Rise of Intelligent Matter. *Nature* **2021**, *594* (7863), 345–355. https://doi.org/10.1038/s41586-021-03453-y.

(97) Kang, S. H. Dynamically Adaptive Materials. *MRS Bull.* **2024**, *49* (11), 1121–1126. https://doi.org/10.1557/s43577-024-00798-3.

(98) Walther, A. Viewpoint: From Responsive to Adaptive and Interactive Materials and Materials Systems: A Roadmap. *Advanced Materials* **2020**, *32* (20). https://doi.org/10.1002/adma.201905111.

(99) Lehn, J. Perspectives in Chemistry—Aspects of Adaptive Chemistry and Materials. *Angew. Chem. Int. Ed.* **2015**, *54* (11), 3276–3289. https://doi.org/10.1002/anie.201409399.

(100) Yang, J.; Zhang, X.; Zhang, X.; Wang, L.; Feng, W.; Li, Q. Beyond the Visible: Bioinspired Infrared Adaptive Materials. *Advanced Materials* **2021**, *33* (14). https://doi.org/10.1002/adma.202004754.

(101) Samanta, S.; Kim, S.; Saito, T.; Sokolov, A. P. Polymers with Dynamic Bonds: Adaptive Functional Materials for a Sustainable Future. *J. Phys. Chem. B* **2021**, *125* (33), 9389–9401. https://doi.org/10.1021/acs.jpcb.1c03511.

(102) Zhang, X.; Chen, L.; Lim, K. H.; Gonuguntla, S.; Lim, K. W.; Pranantyo, D.; Yong, W. P.; Yam, W. J. T.; Low, Z.; Teo, W. J.; Nien, H. P.; Loh, Q. W.; Soh, S. The Pathway to Intelligence: Using Stimuli-Responsive Materials as Building Blocks for Constructing Smart and Functional Systems. *Advanced Materials* **2019**, *31* (11), 1804540. https://doi.org/10.1002/adma.201804540.

(103) Ashley, C. E.; Carnes, E. C.; Phillips, G. K.; Padilla, D.; Durfee, P. N.; Brown, P. A.; Hanna, T. N.; Liu, J.; Phillips, B.; Carter, M. B.; Carroll, N. J.; Jiang, X.; Dunphy, D. R.; Willman, C. L.; Petsev, D. N.; Evans, D. G.; Parikh, A. N.; Chackerian, B.; Wharton, W.; Peabody, D. S.; Brinker, C. J. The Targeted Delivery of Multicomponent Cargos to Cancer Cells by Nanoporous Particle-Supported Lipid Bilayers. *Nat. Mater.* **2011**, *10* (5), 389–397. https://doi.org/10.1038/nmat2992.

(104) Trachootham, D.; Alexandre, J.; Huang, P. Targeting Cancer Cells by ROS-Mediated Mechanisms: A Radical Therapeutic Approach? *Nat. Rev. Drug Discov.* **2009**, *8* (7), 579–591. https://doi.org/10.1038/nrd2803.

(105) Ferris, D. P.; Zhao, Y.-L.; Khashab, N. M.; Khatib, H. A.; Stoddart, J. F.; Zink, J. I. Light-Operated Mechanized Nanoparticles. *J. Am. Chem. Soc.* **2009**, *131* (5), 1686–1688. https://doi.org/10.1021/ja807798g.

(106) Guan, Y.; Zhang, Y. PNIPAM Microgels for Biomedical Applications: From Dispersed Particles to 3D Assemblies. *Soft Matter* **2011**, *7* (14), 6375. https://doi.org/10.1039/c0sm01541e.

(107) Jiang, Y.; Lee, A.; Chen, J.; Cadene, M.; Chait, B. T.; MacKinnon, R. The Open Pore Conformation of Potassium Channels. *Nature* **2002**, *417* (6888), 523–526. https://doi.org/10.1038/417523a.

(108) Fang, Y.; Tan, J.; Lim, S.; Soh, S. Rupturing Cancer Cells by the Expansion of Functionalized Stimuli-Responsive Hydrogels. *NPG Asia Mater.* **2018**, *10* (2), e465–e465. https://doi.org/10.1038/am.2017.232.

(109) Shiraki, T.; Dawn, A.; Le, T. N. L.; Tsuchiya, Y.; Tamaru, S.; Shinkai, S. Heat and Light Dual Switching of a Single-Walled Carbon Nanotube/Thermo-Responsive Helical Polysaccharide Complex: A New Responsive System Applicable to Photodynamic Therapy. *Chemical Communications* **2011**, *47* (25), 7065. https://doi.org/10.1039/c1cc11288k.

(110) Gong, C. B.; Lam, M. H. -W.; Yu, H. X. The Fabrication of a Photoresponsive Molecularly Imprinted Polymer for the Photoregulated Uptake and Release of Caffeine. *Adv. Funct. Mater.* **2006**, *16* (13), 1759–1767. https://doi.org/10.1002/adfm.200500907.

(111) Lee, J.; Ku, K. H.; Kim, M.; Shin, J. M.; Han, J.; Park, C. H.; Yi, G.; Jang, S. G.; Kim, B. J. Stimuli-Responsive, Shape-Transforming Nanostructured Particles. *Advanced Materials* **2017**, *29* (29). https://doi.org/10.1002/adma.201700608.

(112) Andres, C. M.; Zhu, J.; Shyu, T.; Flynn, C.; Kotov, N. A. Shape-Morphing Nanocomposite Origami. *Langmuir* **2014**, *30* (19), 5378–5385. https://doi.org/10.1021/la404955s.

(113) Tariq, A.; Arif, Z. U.; Khalid, M. Y.; Hossain, M.; Rasool, P. I.; Umer, R.; Ramakrishna, S. Recent Advances in the Additive Manufacturing of Stimuli-Responsive Soft Polymers. *Adv. Eng. Mater.* **2023**, *25* (21). https://doi.org/10.1002/adem.202301074.

(114) Mazur, T.; Mazur, Ł.; Lachowicz, D.; Piasecki, A.; Giżyński, K.; Szuwarzyński, M. Synergistic Co-Assembly of Nanoparticles on Patterned Polyelectrolyte Surfaces via

Magnetic and Electrostatic Interactions. *J. Mol. Liq.* **2025**, *433*, 127959. https://doi.org/10.1016/j.molliq.2025.127959.

(115) Klajn, R.; Wesson, P. J.; Bishop, K. J. M.; Grzybowski, B. A. Writing Self-Erasing Images Using Metastable Nanoparticle "Inks." *Angew. Chem. Int. Ed.* **2009**, *48* (38), 7035–7039. https://doi.org/10.1002/anie.200901119.

(116) Wang, Q.; Cai, Y.; Teng, P.; Zhang, S.; Wu, S.; Li, Y.; Zhang, F.; Wang, S. Strategies for Continuous Responsive Motion in a Constant Environment. *Advanced Materials* **2025**, *37* (39). https://doi.org/10.1002/adma.202502926.

(117) Moulin, E.; Faour, L.; Carmona-Vargas, C. C.; Giuseppone, N. From Molecular Machines to Stimuli-Responsive Materials. *Advanced Materials* **2020**, *32* (20). https://doi.org/10.1002/adma.201906036.

(118) Dreyfus, R.; Baudry, J.; Roper, M. L.; Fermigier, M.; Stone, H. A.; Bibette, J. Microscopic Artificial Swimmers. *Nature* **2005**, *437* (7060), 862–865. https://doi.org/10.1038/nature04090.

(119) Giménez, C.; Climent, E.; Aznar, E.; Martínez-Máñez, R.; Sancenón, F.; Marcos, M. D.; Amorós, P.; Rurack, K. Towards Chemical Communication between Gated Nanoparticles. *Angew. Chem. Int. Ed.* **2014**, *53* (46), 12629–12633. https://doi.org/10.1002/anie.201405580.

(120) Ventura, J.; Llopis-Lorente, A.; Abdelmohsen, L. K. E. A.; van Hest, J. C. M.; Martínez-Máñez, R. Models of Chemical Communication for Micro/Nanoparticles. *Acc. Chem. Res.* **2024**, *57* (6), 815–830. https://doi.org/10.1021/acs.accounts.3c00619.

(121) Tai, W.; Mo, R.; Di, J.; Subramanian, V.; Gu, X.; Buse, J. B.; Gu, Z. Bio-Inspired Synthetic Nanovesicles for Glucose-Responsive Release of Insulin. *Biomacromolecules* **2014**, *15* (10), 3495–3502. https://doi.org/10.1021/bm500364a.

(122) Gu, Z.; Dang, T. T.; Ma, M.; Tang, B. C.; Cheng, H.; Jiang, S.; Dong, Y.; Zhang, Y.; Anderson, D. G. Glucose-Responsive Microgels Integrated with Enzyme Nanocapsules for Closed-Loop Insulin Delivery. *ACS Nano* **2013**, *7* (8), 6758–6766. https://doi.org/10.1021/nn401617u.

(123) Yoshida, R. Creation of Softmaterials Based on Self-Oscillating Polymer Gels. *Polym. J.* **2022**, *54* (7), 827–849. https://doi.org/10.1038/s41428-022-00638-8.

(124) Kumar, K.; Knie, C.; Bléger, D.; Peletier, M. A.; Friedrich, H.; Hecht, S.; Broer, D. J.; Debije, M. G.; Schenning, A. P. H. J. A Chaotic Self-Oscillating Sunlight-Driven Polymer Actuator. *Nat. Commun.* **2016**, *7* (1), 11975. https://doi.org/10.1038/ncomms11975.

(125) Chen, I. C.; Kuksenok, O.; Yashin, V. V.; Balazs, A. C.; Van Vliet, K. J. Mechanical Resuscitation of Chemical Oscillations in Belousov–Zhabotinsky Gels. *Adv. Funct. Mater.* **2012**, *22* (12), 2535–2541. https://doi.org/10.1002/adfm.201103036.

(126) Soozanipour, A.; Sohrabi, H.; Abazar, F.; Khataee, A.; Noorbakhsh, A.; Asadnia, M.; Taheri-Kafrani, A.; Majidi, M. R.; Razmjou, A. Ion Selective Nanochannels: From

Critical Principles to Sensing and Biosensing Applications. *Adv. Mater. Technol.* **2021**, *6* (10). https://doi.org/10.1002/admt.202000765.

(127) Zhang, M.; Hou, X.; Wang, J.; Tian, Y.; Fan, X.; Zhai, J.; Jiang, L. Light and PH Cooperative Nanofluidic Diode Using a Spiropyran-Functionalized Single Nanochannel. *Advanced Materials* **2012**, *24* (18), 2424–2428. https://doi.org/10.1002/adma.201104536.

(128) Siwy, Z.; Apel, P.; Baur, D.; Dobrev, D. D.; Korchev, Y. E.; Neumann, R.; Spohr, R.; Trautmann, C.; Voss, K.-O. Preparation of Synthetic Nanopores with Transport Properties Analogous to Biological Channels. *Surf. Sci.* **2003**, *532–535*, 1061–1066. https://doi.org/10.1016/S0039-6028(03)00448-5.

(129) Zhao, W.; Yang, S.; Yang, J.; Li, J.; Zheng, J.; Qing, Z.; Yang, R. Visual Biopsy by Hydrogen Peroxide-Induced Signal Amplification. *Anal. Chem.* **2016**, *88* (21), 10728–10735. https://doi.org/10.1021/acs.analchem.6b03330.

(130) Kurup, C. P.; Mohd-Naim, N. F.; Ahmed, M. U. Recent Trends in Nanomaterial-Based Signal Amplification in Electrochemical Aptasensors. *Crit. Rev. Biotechnol.* **2022**, *42* (5), 794–812. https://doi.org/10.1080/07388551.2021.1960792.

(131) Yang, L.; Zhang, S.; Liu, X.; Tang, Y.; Zhou, Y.; Wong, D. K. Y. Detection Signal Amplification Strategies at Nanomaterial-Based Photoelectrochemical Biosensors. *J. Mater. Chem. B* **2020**, *8* (35), 7880–7893. https://doi.org/10.1039/D0TB01191F.

(132) Zhou, F.; Li, B. Exonuclease III-Assisted Target Recycling Amplification Coupled with Liposome-Assisted Amplification: One-Step and Dual-Amplification Strategy for Highly Sensitive Fluorescence Detection of DNA. *Anal. Chem.* **2015**, *87* (14), 7156–7162. https://doi.org/10.1021/acs.analchem.5b00993.

(133) Chagri, S.; Ng, D. Y. W.; Weil, T. Designing Bioresponsive Nanomaterials for Intracellular Self-Assembly. *Nat. Rev. Chem.* **2022**, *6* (5), 320–338. https://doi.org/10.1038/s41570-022-00373-x.

(134) Thorkelsson, K.; Bai, P.; Xu, T. Self-Assembly and Applications of Anisotropic Nanomaterials: A Review. *Nano Today* **2015**, *10* (1), 48–66. https://doi.org/10.1016/j.nantod.2014.12.005.

(135) Lin, Z.; Gao, C.; Chen, M.; Lin, X.; He, Q. Collective Motion and Dynamic Self-Assembly of Colloid Motors. *Curr. Opin. Colloid Interface Sci.* **2018**, *35*, 51–58. https://doi.org/10.1016/j.cocis.2018.01.006.

(136) Grzybowski, B. A.; Fitzner, K.; Paczesny, J.; Granick, S. From Dynamic Self-Assembly to Networked Chemical Systems. *Chem. Soc. Rev.* **2017**, *46* (18), 5647–5678. https://doi.org/10.1039/c7cs00089h.

(137) Hasanzadeh, A.; Saeedi, S.; Dastanpour, L.; Biabanaki, Z. S.; Asadi, L.; Noori, H.; Hamblin, M. R.; Liu, Y.; Karimi, M. Self-Replicating Nanomaterials as a New Generation of Smart Nanostructures. *Biotechnol. Adv.* **2025**, *81*, 108565. https://doi.org/10.1016/j.biotechadv.2025.108565.

(138) Dadon, Z.; Samiappan, M.; Safranchik, E. Y.; Ashkenasy, G. Light-Induced Peptide Replication Controls Logic Operations in Small Networks. *Chemistry – A European Journal* **2010**, *16* (40), 12096–12099. https://doi.org/10.1002/chem.201001488.

(139) Xie, P.; Li, D.; Yip, S.; Ho, J. C. Emerging Optoelectronic Artificial Synapses and Memristors Based on Low-Dimensional Nanomaterials. *Appl. Phys. Rev.* **2024**, *11* (1). https://doi.org/10.1063/5.0173547.

(140) Kausar, A. Shape Memory Polyester-Based Nanomaterials: Cutting-Edge Advancements. *Polymer-Plastics Technology and Materials* **2020**, *59* (7), 765–779. https://doi.org/10.1080/25740881.2019.1695268.

(141) Yu, J.; Luo, M.; Lv, Z.; Huang, S.; Hsu, H.-H.; Kuo, C.-C.; Han, S.-T.; Zhou, Y. Recent Advances in Optical and Optoelectronic Data Storage Based on Luminescent Nanomaterials. *Nanoscale* **2020**, *12* (46), 23391–23423. https://doi.org/10.1039/D0NR06719A.

(142) Hager, M. D.; Bode, S.; Weber, C.; Schubert, U. S. Shape Memory Polymers: Past, Present and Future Developments. *Prog. Polym. Sci.* **2015**, *49–50*, 3–33. https://doi.org/10.1016/j.progpolymsci.2015.04.002.

(143) Tregubov, A. A.; Nikitin, P. I.; Nikitin, M. P. Advanced Smart Nanomaterials with Integrated Logic-Gating and Biocomputing: Dawn of Theranostic Nanorobots. *Chem. Rev.* **2018**, *118* (20), 10294–10348. https://doi.org/10.1021/acs.chemrev.8b00198.

(144) Luo, C.; He, L.; Chen, F.; Fu, T.; Zhang, P.; Xiao, Z.; Liu, Y.; Tan, W. Stimulus-Responsive Nanomaterials Containing Logic Gates for Biomedical Applications. *Cell Rep. Phys. Sci.* **2021**, *2* (2), 100350. https://doi.org/10.1016/j.xcrp.2021.100350.

(145) Angelos, S.; Yang, Y.-W.; Khashab, N. M.; Stoddart, J. F.; Zink, J. I. Dual-Controlled Nanoparticles Exhibiting AND Logic. *J. Am. Chem. Soc.* **2009**, *131* (32), 11344–11346. https://doi.org/10.1021/ja9042752.

(146) Qian, L.; Winfree, E.; Bruck, J. Neural Network Computation with DNA Strand Displacement Cascades. *Nature* **2011**, *475* (7356), 368–372. https://doi.org/10.1038/nature10262.

(147) Hadke, S.; Kang, M.-A.; Sangwan, V. K.; Hersam, M. C. Two-Dimensional Materials for Brain-Inspired Computing Hardware. *Chem. Rev.* **2025**, *125* (2), 835–932. https://doi.org/10.1021/acs.chemrev.4c00631.

(148) Jiang, X.; Ng, D. K. P. Sequential Logic Operations with a Molecular Keypad Lock with Four Inputs and Dual Fluorescence Outputs. *Angew. Chem. Int. Ed.* **2014**, *53* (39), 10481–10484. https://doi.org/10.1002/anie.201406002.

(149) Merindol, R. M.; Walther, A. Materials Learning from Life: Concepts for Active, Adaptive and Autonomous Molecular Systems. *Chem. Soc. Rev* **2017**, *5588*, 5588. https://doi.org/10.1039/c6cs00738d.

(150) Grzelczak, M.; Liz-Marzán, L. M.; Klajn, R. Stimuli-Responsive Self-Assembly of Nanoparticles. *Chem. Soc. Rev.* **2019**, *48* (5), 1342–1361. https://doi.org/10.1039/c8cs00787j.

(151) Van Ravensteijn, B. G. P.; Voets, I. K.; Kegel, W. K.; Eelkema, R. Out-of-Equilibrium Colloidal Assembly Driven by Chemical Reaction Networks. *Langmuir* **2020**, *36* (36), 10639–10656. https://doi.org/10.1021/acs.langmuir.0c01763.

(152) Van Rossum, S. A. P.; Tena-Solsona, M.; Van Esch, J. H.; Eelkema, R.; Boekhoven, J. Dissipative Out-of-Equilibrium Assembly of Man-Made Supramolecular Materials. *Chem. Soc. Rev.* **2017**, *46* (18), 5519–5535. https://doi.org/10.1039/c7cs00246g.

(153) Szaciłowski, K. Digital Information Processing in Molecular Systems. *Chem. Rev.* **2008**, *108* (9), 3481–3548. https://doi.org/10.1021/cr068403q.

(154) Steeno, R.; Minoia, A.; Gimenez-Lopez, M. C.; Blunt, M. O.; Champness, N. R.; Lazzaroni, R.; Mali, K. S.; De Feyter, S. Molecular Dopant Determines the Structure of a Physisorbed Self-Assembled Molecular Network. *Chemical Communications* **2021**, *57* (12), 1454–1457. https://doi.org/10.1039/d0cc07338e.

(155) Li, Y.; Liu, T.; Liu, H.; Tian, M.-Z.; Li, Y. Self-Assembly of Intramolecular Charge-Transfer Compounds into Functional Molecular Systems. *Acc. Chem. Res.* **2014**, *47* (4), 1186–1198. https://doi.org/10.1021/ar400264e.

(156) Zhou, W.; Chen, D.; Li, J.; Xu, J.; Lv, J.; Liu, H.; Li, Y. Photoisomerization of Spiropyran for Driving a Molecular Shuttle. *Org. Lett.* **2007**, *9* (20), 3929–3932. https://doi.org/10.1021/ol7015862.

(157) Schultz, T.; Quenneville, J.; Levine, B.; Toniolo, A.; Martínez, T. J.; Lochbrunner, S.; Schmitt, M.; Shaffer, J. P.; Zgierski, M. Z.; Stolow, A. Mechanism and Dynamics of Azobenzene Photoisomerization. *J. Am. Chem. Soc.* **2003**, *125* (27), 8098–8099. https://doi.org/10.1021/ja021363x.

(158) Abdel-Mottaleb, M. M. S.; Gomar-Nadal, E.; Surin, M.; Uji-i, H.; Mamdouh, W.; Veciana, J.; Lemaur, V.; Rovira, C.; Cornil, J.; Lazzaroni, R.; Amabilino, D. B.; De Feyter, S.; De Schryver, F. C. Self-Assembly of Tetrathiafulvalene Derivatives at a Liquid/Solid Interface—Compositional and Constitutional Influence on Supramolecular Ordering. *J. Mater. Chem.* **2005**, *15* (43), 4601–4615. https://doi.org/10.1039/B509336H.

(159) Fameau, A. L.; Arnould, A.; Saint-Jalmes, A. Responsive Self-Assemblies Based on Fatty Acids. *Curr. Opin. Colloid Interface Sci.* **2014**, *19* (5), 471–479. https://doi.org/10.1016/J.COCIS.2014.08.005.

(160) Sauvage, J. P. From Chemical Topology to Molecular Machines (Nobel Lecture). *Angew. Chem. Int. Ed.* **2017**, *56* (37), 11080–11093. https://doi.org/10.1002/anie.201702992.

(161) Moulin, E.; Faour, L.; Carmona-Vargas, C. C.; Giuseppone, N. From Molecular Machines to Stimuli-Responsive Materials. *Advanced Materials* **2020**, *32* (20), 1–26. https://doi.org/10.1002/adma.201906036.

(162) Patel, D.; Mamtora, D.; Kamath, A.; Shukla, A. Rogue One: A Plastic Story. *Mar. Pollut. Bull.* **2022**, *177*. https://doi.org/10.1016/J.MARPOLBUL.2022.113509.

(163) Gauthier, M. A.; Gibson, M. I.; Klok, H. A. Synthesis of Functional Polymers by Post-Polymerization Modification. *Angew. Chem. Int. Ed.* **2009**, *48* (1), 48–58. https://doi.org/10.1002/ANIE.200801951.

(164) Pious, C. V.; Thomas, S. Polymeric Materials—Structure, Properties, and Applications. In *Printing on Polymers*; Elsevier, 2016; pp 21–39. https://doi.org/10.1016/B978-0-323-37468-2.00002-6.

(165) Wesley, R. D.; Dreiss, C. A.; Cosgrove, T.; Armes, S. P.; Thompson, L.; Baines, F. L.; Billingham, N. C. Structure of a Hydrophilic-Hydrophobic Block Copolymer and Its Interactions with Salt and an Anionic Surfactant. *Langmuir* **2005**, *21* (11), 4856–4861. https://doi.org/10.1021/la046830y.

(166) Flemming, P.; Münch, A. S.; Fery, A.; Uhlmann, P. Constrained Thermoresponsive Polymers - New Insights into Fundamentals and Applications. *Beilstein Journal of Organic Chemistry*. Beilstein-Institut Zur Forderung der Chemischen Wissenschaften 2021, pp 2123–2163. https://doi.org/10.3762/bjoc.17.138.

(167) Wei, M.; Gao, Y.; Li, X.; Serpe, M. J. Stimuli-Responsive Polymers and Their Applications. *Polym. Chem.* **2016**, *8* (1), 127–143. https://doi.org/10.1039/C6PY01585A.

(168) Kaloni, T. P.; Giesbrecht, P. K.; Schreckenbach, G.; Freund, M. S. Polythiophene: From Fundamental Perspectives to Applications. *Chemistry of Materials* **2017**, *29* (24), 10248–10283. https://doi.org/10.1021/acs.chemmater.7b03035.

(169) Lamontagne, H. R.; Lessard, B. H. Nitroxide-Mediated Polymerization: A Versatile Tool for the Engineering of Next Generation Materials. *ACS Appl. Polym. Mater.* **2020**, *2* (12), 5327–5344. https://doi.org/10.1021/acsapm.0c00888.

(170) Matyjaszewski, K.; Xia, J. Atom Transfer Radical Polymerization. *Chem. Rev.* **2001**, *101* (9), 2921–2990. https://doi.org/10.1021/cr940534g.

(171) Perrier, S. 50th Anniversary Perspective : RAFT Polymerization—A User Guide. *Macromolecules* **2017**, *50* (19), 7433–7447. https://doi.org/10.1021/acs.macromol.7b00767.

(172) Kuwabara, J.; Tsuchida, W.; Guo, S.; Hu, Z.; Yasuda, T.; Kanbara, T. Synthesis of Conjugated Polymers via Direct C–H/C–Cl Coupling Reactions Using a Pd/Cu Binary Catalytic System. *Polym. Chem.* **2019**, *10* (18), 2298–2304. https://doi.org/10.1039/C9PY00232D.

(173) Suresh, D.; Goh, P. S.; Ismail, A. F.; Hilal, N. Surface Design of Liquid Separation Membrane through Graft Polymerization: A State of the Art Review. *Membranes (Basel).* **2021**, *11* (11), 832. https://doi.org/10.3390/membranes11110832.

(174) Roy, D.; Brooks, W. L. A.; Sumerlin, B. S. New Directions in Thermoresponsive Polymers. *Chem. Soc. Rev.* **2013**, *42* (17), 7214–7243. https://doi.org/10.1039/c3cs35499g.

(175) Schattling, P.; Jochum, F. D.; Theato, P. Multi-Stimuli Responsive Polymers-the All-in-One Talents. *Polym. Chem.* **2014**, *5* (1), 25–36. https://doi.org/10.1039/c3py00880k.

(176) Murad Bhayo, A.; Yang, Y.; He, X. Polymer Brushes: Synthesis, Characterization, Properties and Applications. *Prog. Mater. Sci.* **2022**, *130*, 101000. https://doi.org/10.1016/J.PMATSCI.2022.101000.

(177) Dienstmaier, J. F.; Medina, D. D.; Dogru, M.; Knochel, P.; Bein, T.; Heckl, W. M.; Lackinger, M. Isoreticular Two-Dimensional Covalent Organic Frameworks Synthesized by On-Surface Condensation of Diboronic Acids. *ACS Nano* **2012**, *6* (8), 7234–7242. https://doi.org/10.1021/nn302363d.

(178) Patil, R. R.; Turgman-Cohen, S.; Šrogl, J.; Kiserow, D.; Genzer, J. On-Demand Degrafting and the Study of Molecular Weight and Grafting Density of Poly(Methyl Methacrylate) Brushes on Flat Silica Substrates. *Langmuir* **2015**, *31* (8), 2372–2381. https://doi.org/10.1021/la5044766.

(179) Colson, J. W.; Dichtel, W. R. Rationally Synthesized Two-Dimensional Polymers. *Nature Chemistry 2013 5:6* **2013**, *5* (6), 453–465. https://doi.org/10.1038/nchem.1628.

(180) Zhuang, X.; Mai, Y.; Wu, D.; Zhang, F.; Feng, X. Two-Dimensional Soft Nanomaterials: A Fascinating World of Materials. *Advanced Materials* **2015**, *27* (3), 403–427. https://doi.org/10.1002/ADMA.201401857.

(181) Uhlmann, P.; Ionov, L.; Houbenov, N.; Nitschke, M.; Grundke, K.; Motornov, M.; Minko, S.; Stamm, M. Surface Functionalization by Smart Coatings: Stimuli-Responsive Binary Polymer Brushes. *Prog. Org. Coat.* **2006**, *55* (2), 168–174. https://doi.org/10.1016/j.porgcoat.2005.09.014.

(182) Koberstein, J. T. Molecular Design of Functional Polymer Surfaces. *J. Polym. Sci. B Polym. Phys.* **2004**, *42* (16), 2942–2956. https://doi.org/10.1002/polb.20157.

(183) Guvendiren, M.; Yang, S.; Burdick, J. A. Swelling-Induced Surface Patterns in Hydrogels with Gradient Crosslinking Density. *Adv. Funct. Mater.* **2009**, *19* (19), 3038–3045. https://doi.org/10.1002/ADFM.200900622.

(184) Chung, J. Y.; Nolte, A. J.; Stafford, C. M. Diffusion-Controlled, Self-Organized Growth of Symmetric Wrinkling Patterns. *Advanced Materials* **2009**, *21* (13), 1358–1362. https://doi.org/10.1002/ADMA.200803209.

(185) Lei, X.; Ye, D.; Chen, J.; Tang, S.; Sun, P.; Chen, L.; Lu, A.; Du, Y.; Zhang, L. Customizable Multidimensional Self-Wrinkling Structure Constructed via Modulus Gradient in Chitosan Hydrogels. *Chemistry of Materials* **2019**, *31* (24), 10032–10039. https://doi.org/10.1021/acs.chemmater.9b02812.

(186) Bae, W. G.; Kim, H. N.; Kim, D.; Park, S. H.; Jeong, H. E.; Suh, K. Y. 25th Anniversary Article: Scalable Multiscale Patterned Structures Inspired by Nature: The Role of Hierarchy. *Advanced Materials* **2014**, *26* (5), 675–700. https://doi.org/10.1002/ADMA.201303412.

(187) Hou, H.; Yin, J.; Jiang, X. Smart Patterned Surface with Dynamic Wrinkles. *Acc. Chem. Res.* **2019**, *52* (4), 1025–1035. https://doi.org/10.1021/acs.accounts.8b00623.

(188) Hou, H.; Li, F.; Su, Z.; Yin, J.; Jiang, X. Light-Reversible Hierarchical Patterns by Dynamic Photo-Dimerization Induced Wrinkles. *J. Mater. Chem. C Mater.* **2017**, *5* (34), 8765–8773. https://doi.org/10.1039/C7TC02569F.

(189) Hou, H.; Yin, J.; Jiang, X. Reversible Diels–Alder Reaction To Control Wrinkle Patterns: From Dynamic Chemistry to Dynamic Patterns. *Advanced Materials* **2016**, *28* (41), 9126–9132. https://doi.org/10.1002/ADMA.201602105.

(190) Zeng, S.; Li, R.; Freire, S. G.; M Garbellotto, V. M.; Huang, E. Y.; Smith, A. T.; Hu, C.; T Tait, W. R.; Bian, Z.; Zheng, G.; Zhang, D.; Sun, L.; Zeng, S.; Freire, S. G.; M Garbellotto, V. M.; Huang, E. Y.; Smith, A. T.; Hu, C.; T Tait, W. R.; Sun, L.; Li, R.; Zhang, D.; Bian, Z.; Zheng, G. Moisture-Responsive Wrinkling Surfaces with Tunable Dynamics. *Advanced Materials* **2017**, *29* (24), 1700828. https://doi.org/10.1002/ADMA.201700828.

(191) Seuring, J.; Agarwal, S. Polymers with Upper Critical Solution Temperature in Aqueous Solution: Unexpected Properties from Known Building Blocks. *ACS Macro Lett.* **2013**, *2* (7), 597–600. https://doi.org/10.1021/mz400227y.

(192) Flory, P. J. Thermodynamics of High Polymer Solutions. *J. Chem. Phys.* **1942**, *10* (1), 51–61. https://doi.org/10.1063/1.1723621.

(193) Huggins, M. L. Some Properties of Solutions of Long-Chain Compounds. *J. Phys. Chem.* **1942**, *46* (1), 151–158. https://doi.org/10.1021/j150415a018.

(194) Gnesotto, F. S.; Mura, F.; Gladrow, J.; Broedersz, C. P. Broken Detailed Balance and Non-Equilibrium Dynamics in Living Systems: A Review. *Reports on Progress in Physics* **2018**, *81* (6). https://doi.org/10.1088/1361-6633/aab3ed.

(195) Hess, H.; Ross, J. L. Non-Equilibrium Assembly of Microtubules: From Molecules to Autonomous Chemical Robots. *Chem. Soc. Rev.* **2017**, *46* (18), 5570–5587. https://doi.org/10.1039/c7cs00030h.

(196) Bera, D.; Qian, L.; Tseng, T. K.; Holloway, P. H. Quantum Dots and Their Multimodal Applications: A Review. *Materials* **2010**, *3* (4), 2260–2345. https://doi.org/10.3390/ma3042260.

(197) Wood, V.; Bulović, V. Colloidal Quantum Dot Light-Emitting Devices. *Nano Rev.* **2010**, *1* (1), 5202. https://doi.org/10.3402/nano.v1i0.5202.

(198) Haase, M.; Schäfer, H. Upconverting Nanoparticles. *Angew. Chem. Int. Ed.* **2011**, *50* (26), 5808–5829. https://doi.org/10.1002/anie.201005159.

(199) Wilhelm, S. Perspectives for Upconverting Nanoparticles. *ACS Nano* **2017**, *11* (11), 10644–10653. https://doi.org/10.1021/acsnano.7b07120.

(200) Chan, E. M.; Levy, E. S.; Cohen, B. E. Rationally Designed Energy Transfer in Upconverting Nanoparticles. *Advanced Materials* **2015**, *27* (38), 5753–5761. https://doi.org/10.1002/adma.201500248.

(201) Chen, G.; Qiu, H.; Prasad, P. N.; Chen, X. Upconversion Nanoparticles: Design, Nanochemistry, and Applications in Theranostics. *Chem. Rev.* **2014**, *114* (10), 5161–5214. https://doi.org/10.1021/cr400425h.

(202) Frey, N. A.; Peng, S.; Cheng, K.; Sun, S. Magnetic Nanoparticles: Synthesis, Functionalization, and Applications in Bioimaging and Magnetic Energy Storage. *Chem. Soc. Rev.* **2009**, *38* (9), 2532–2542. https://doi.org/10.1039/b815548h.

(203) Willard, M. A.; Kurihara, L. K.; Carpenter, E. E.; Calvin, S.; Harris, V. G. Chemically Prepared Magnetic Nanoparticles. *International Materials Reviews* **2004**, *49* (3–4), 125–170. https://doi.org/10.1179/095066004225021882.

(204) Kittel, C. Theory of the Structure of Ferromagnetic Domains in Films and Small Particles. *Physical Review* **1946**, *70* (11–12), 965–971. https://doi.org/10.1103/PhysRev.70.965.

(205) Brown, W. F. Thermal Fluctuations of a Single-Domain Particle. *Physical Review* **1963**, *130* (5), 1677–1686. https://doi.org/10.1103/PhysRev.130.1677.

(206) Li, Q.; Kartikowati, C. W.; Horie, S.; Ogi, T.; Iwaki, T.; Okuyama, K. Correlation between Particle Size/Domain Structure and Magnetic Properties of Highly Crystalline Fe3O4 Nanoparticles. *Sci. Rep.* **2017**, *7* (1). https://doi.org/10.1038/s41598-017-09897-5.

(207) Zhong, C. J.; Maye, M. M. Core-Shell Assembled Nanoparticles as Catalysts. *Advanced Materials* **2001**, *13* (19), 1507–1511. https://doi.org/10.1002/1521-4095(200110)13:19<1507::aid-adma1507>3.0.co;2-%23.

(208) Mohanty, A.; Garg, N.; Jin, R. A Universal Approach to the Synthesis of Noble Metal Nanodendrites and Their Catalytic Properties. *Angewandte Chemie* **2010**, *122* (29), 5082–5086. https://doi.org/10.1002/ange.201000902.

(209) Amendola, V.; Pilot, R.; Frasconi, M.; Maragò, O. M.; Iatì, M. A. Surface Plasmon Resonance in Gold Nanoparticles: A Review. *Journal of Physics Condensed Matter* **2017**, *29* (20). https://doi.org/10.1088/1361-648X/aa60f3.

(210) Ammari, H.; Deng, Y.; Millien, P. Surface Plasmon Resonance of Nanoparticles and Applications in Imaging. *Arch. Ration. Mech. Anal.* **2016**, *220* (1), 109–153. https://doi.org/10.1007/s00205-015-0928-0.

(211) Rycenga, M.; Langille, M. R.; Personick, M. L.; Ozel, T.; Mirkin, C. A. Chemically Isolating Hot Spots on Concave Nanocubes. *Nano Lett.* **2012**, *12* (12), 6218–6222. https://doi.org/10.1021/nl3032235.

(212) Ghosh Chaudhuri, R.; Paria, S. Core/Shell Nanoparticles: Classes, Properties, Synthesis Mechanisms, Characterization, and Applications. *Chem. Rev.* **2012**, *112* (4), 2373–2433. https://doi.org/10.1021/cr100449n.

(213) Ghosh Chaudhuri, R.; Paria, S. Core/Shell Nanoparticles: Classes, Properties, Synthesis Mechanisms, Characterization, and Applications. *Chem. Rev.* **2012**, *112* (4), 2373–2433. https://doi.org/10.1021/cr100449n.

(214) Virkki, K.; Demir, S.; Lemmetyinen, H.; Tkachenko, N. V. Photoinduced Electron Transfer in CdSe/ZnS Quantum Dot-Fullerene Hybrids. *Journal of Physical Chemistry C* **2015**, *119* (31), 17561–17572. https://doi.org/10.1021/acs.jpcc.5b04251.

(215) Bang, J. H.; Kamat, P. V. CdSe Quantum Dot-Fullerene Hybrid Nanocomposite for Solar Energy Conversion: Electron Transfer and Photoelectrochemistry. *ACS Nano* **2011**, *5* (12), 9421–9427. https://doi.org/10.1021/nn204350w.

(216) Bończak, B.; Lisowski, W.; Kamińska, A.; Hołdyński, M.; Fiałkowski, M. Gold Nanoparticles Functionalized with Fully Conjugated Fullerene C60 Derivatives as a Material with Exceptional Capability of Absorbing Electrons. *The Journal of Physical Chemistry C* **2019**, *123* (10), 6229–6240. https://doi.org/10.1021/acs.jpcc.8b10842.

(217) Zhang, X.; Fu, Q.; Duan, H.; Song, J.; Yang, H. Janus Nanoparticles: From Fabrication to (Bio)Applications. *ACS Nano* **2021**, *15* (4), 6147–6191. https://doi.org/10.1021/acsnano.1c01146.

(218) Zhang, J.; Grzybowski, B. A.; Granick, S. Janus Particle Synthesis, Assembly, and Application. *Langmuir* **2017**, *33* (28), 6964–6977. https://doi.org/10.1021/acs.langmuir.7b01123.

(219) Liu, Z.; McClements, D. J.; Shi, A.; Zhi, L.; Tian, Y.; Jiao, B.; Liu, H.; Wang, Q. Janus Particles: A Review of Their Applications in Food and Medicine. *Crit. Rev. Food Sci. Nutr.* **2023**, *63* (29), 10093–10104. https://doi.org/10.1080/10408398.2022.2067831.

(220) Hartley, G. S. The Cis-Form of Azobenzene. *Nature* **1937**, *140* (3537), 281–281. https://doi.org/10.1038/140281a0.

(221) Klajn, R.; Bishop, K. J. M.; Grzybowski, B. A. Light-Controlled Self-Assembly of Reversible and Irreversible Nanoparticle Suprastructures. *Proc. Natl. Acad. Sci. U. S. A.* **2007**, *104* (25), 10305–10309. https://doi.org/10.1073/pnas.0611371104.

(222) Klajn, R.; Stoddart, J. F.; Grzybowski, B. A. Nanoparticles Functionalised with Reversible Molecular and Supramolecular Switches. *Chem. Soc. Rev.* **2010**, *39* (6), 2203–2237. https://doi.org/10.1039/b920377j.

(223) Klajn, R. Immobilized Azobenzenes for the Construction of Photoresponsive Materials. *Pure and Applied Chemistry* **2010**, *82* (12), 2247–2276. https://doi.org/10.1351/PAC-CON-10-09-04.

(224) Chu, Z.; Han, Y.; Bian, T.; De, S.; Král, P.; Klajn, R. Supramolecular Control of Azobenzene Switching on Nanoparticles. *J. Am. Chem. Soc.* **2019**, *141* (5), 1949–1960. https://doi.org/10.1021/jacs.8b09638.

(225) Szewczyk, M.; Sobczak, G.; Sashuk, V. Photoswitchable Catalysis by a Small Swinging Molecule Confined on the Surface of a Colloidal Particle. *ACS Catal.* **2018**, *8* (4), 2810–2814. https://doi.org/10.1021/acscatal.8b00328.

(226) Wang, M.; Wang, T.; Wang, D.; Jiang, W.; Fu, J. Acid and Light Stimuli-Responsive Mesoporous Silica Nanoparticles for Controlled Release. *J. Mater. Sci.* **2019**, *54* (8), 6199–6211. https://doi.org/10.1007/s10853-019-03325-x.

(227) Cardoso Dos Santos, M.; Algar, W. R.; Medintz, I. L.; Hildebrandt, N. Quantum Dots for Förster Resonance Energy Transfer (FRET). *TrAC - Trends in Analytical Chemistry* **2020**, *125*, 115819. https://doi.org/10.1016/j.trac.2020.115819.

(228) Xiao, L.; Chen, X.; Yang, X.; Sun, J.; Geng, J. Recent Advances in Polymer-Based Photothermal Materials for Biological Applications. *ACS Appl. Polym. Mater.* **2020**, *2* (10), 4273–4288. https://doi.org/10.1021/acsapm.0c00711.

(229) Pallavicini, P.; Chirico, G.; Taglietti, A. Harvesting Light To Produce Heat: Photothermal Nanoparticles for Technological Applications and Biomedical Devices. *Chemistry - A European Journal* **2021**, *27* (62), 15361–15374. https://doi.org/10.1002/chem.202102123.

(230) Grzybowski, B. A.; Fitzner, K.; Paczesny, J.; Granick, S. From Dynamic Self-Assembly to Networked Chemical Systems. *Chem. Soc. Rev.* **2017**, *46* (18), 5647–5678. https://doi.org/10.1039/c7cs00089h.

(231) Weißenfels, M.; Gemen, J.; Klajn, R. Dissipative Self-Assembly: Fueling with Chemicals versus Light. *Chem* **2021**, *7* (1), 23–37. https://doi.org/10.1016/j.chempr.2020.11.025.

(232) Guzmán, E.; Martínez-Pedrero, F.; Calero, C.; Maestro, A.; Ortega, F.; Rubio, R. G. A Broad Perspective to Particle-Laden Fluid Interfaces Systems: From Chemically Homogeneous Particles to Active Colloids. *Adv. Colloid Interface Sci.* **2022**, *302* (February), 102620. https://doi.org/10.1016/j.cis.2022.102620.

(233) Vialetto, J.; Anyfantakis, M.; Rudiuk, S.; Morel, M.; Baigl, D. Photoswitchable Dissipative Two-Dimensional Colloidal Crystals. *Angew. Chem. Int. Ed.* **2019**, *58* (27), 9145–9149. https://doi.org/10.1002/anie.201904093.

(234) Anyfantakis, M.; Baigl, D. Dynamic Photocontrol of the Coffee-Ring Effect with Optically Tunable Particle Stickiness. *Angew. Chem. Int. Ed.* **2014**, *53* (51), 14077–14081. https://doi.org/10.1002/anie.201406903.

(235) Vialetto, J.; Anyfantakis, M. Exploiting Additives for Directing the Adsorption and Organization of Colloid Particles at Fluid Interfaces. *Langmuir* **2021**, *37* (31), 9302–9335. https://doi.org/10.1021/acs.langmuir.1c01029.

(236) Bończak, B.; Fiałkowski, M. Donor–Acceptor Stenhouse Adducts for Stimuli-Responsive Self-Assembly of Gold Nanoparticles into Semiconducting Thin Films. *The Journal of Physical Chemistry C* **2022**. https://doi.org/10.1021/acs.jpcc.2c00084.

(237) Sashuk, V.; Hołyst, R.; Wojciechowski, T.; Fiałkowski, M. Close-Packed Monolayers of Charged Janus-Type Nanoparticles at the Air–Water Interface. *J. Colloid Interface Sci.* **2012**, *375* (1), 180–186. https://doi.org/10.1016/j.jcis.2012.02.057.

(238) Montelongo, Y.; Sikdar, D.; Ma, Y.; McIntosh, A. J. S.; Velleman, L.; Kucernak, A. R.; Edel, J. B.; Kornyshev, A. A. Electrotunable Nanoplasmonic Liquid Mirror. *Nat. Mater.* **2017**, *16* (11), 1127–1135. https://doi.org/10.1038/NMAT4969.

(239) Rezende, C. A.; Shan, J.; Lee, L. T.; Zalczer, G.; Tenhu, H. Tuning the Structure of Thermosensitive Gold Nanoparticle Monolayers. *Journal of Physical Chemistry B* **2009**, *113* (29), 9786–9794. https://doi.org/10.1021/jp9019393.

(240) Shan, J.; Chen, J.; Nuopponen, M.; Viitala, T.; Jiang, H.; Peltonen, J.; Kauppinen, E.; Tenhu, H. Optical Properties of Thermally Responsive Amphiphilic Gold Nanoparticles Protected with Polymers. *Langmuir* **2006**, *22* (2), 794–801. https://doi.org/10.1021/la052579q.

(241) Stefaniu, C.; Brezesinski, G.; Möhwald, H. Polymer-Capped Magnetite Nanoparticles Change the 2D Structure of DPPC Model Membranes. *Soft Matter* **2012**, *8* (30), 7952–7959. https://doi.org/10.1039/c2sm25773d.

(242) Stefaniu, C.; Chanana, M.; Ahrens, H.; Wang, D.; Brezesinski, G.; Möhwald, H. Conformational Induced Behaviour of Copolymer-Capped Magnetite Nanoparticles at the Air/Water Interface. *Soft Matter* **2011**, *7* (9), 4267–4275. https://doi.org/10.1039/c0sm01370f.

(243) Stefaniu, C.; Chanana, M.; Wang, D.; Brezesinski, G.; Möhwald, H. Stimuli-Responsive Magnetite Nanoparticle Monolayers. *Journal of Physical Chemistry C* **2011**, *115* (13), 5478–5484. https://doi.org/10.1021/jp111374f.

(244) Stefaniu, C.; Chanana, M.; Wang, D.; Novikov, D. V.; Brezesinski, G.; Möhwald, H. Langmuir and Gibbs Magnetite NP Layers at the Air/Water Interface. *Langmuir* **2011**, *27* (3), 1192–1199. https://doi.org/10.1021/la1039464.

(245) Stefaniu, C.; Chanana, M.; Ahrens, H.; Wang, D.; Brezesinski, G.; Möhwald, H. Conformational Induced Behaviour of Copolymer-Capped Magnetite Nanoparticles at the Air/Water Interface. *Soft Matter* **2011**, *7* (9), 4267–4275. https://doi.org/10.1039/c0sm01370f.

(246) Bresme, F.; Oettel, M. Nanoparticles at Fluid Interfaces. *Journal of Physics: Condensed Matter* **2007**, *19* (41), 413101. https://doi.org/10.1088/0953-8984/19/41/413101.

(247) Pieranski, P. Two-Dimensional Interfacial Colloidal Crystals. *Phys. Rev. Lett.* **1980**, *45* (7), 569–572. https://doi.org/10.1103/PhysRevLett.45.569.

(248) Davies, G. B.; Krüger, T.; Coveney, P. V.; Harting, J. Detachment Energies of Spheroidal Particles from Fluid-Fluid Interfaces. *J. Chem. Phys.* **2014**, *141* (15). https://doi.org/10.1063/1.4898071.

(249) Guzmán, E.; Ortega, F.; Rubio, R. G. Forces Controlling the Assembly of Particles at Fluid Interfaces. *Langmuir* **2022**, *38* (44), 13313–13321. https://doi.org/10.1021/acs.langmuir.2c02038.

(250) Kralchevsky, P. A.; Denkov, N. D.; Paunov, V. N.; Velev, O. D.; Ivanov, I. B.; Yoshimura, H.; Nagayama, K. Formation of Two-Dimensional Colloid Crystals in Liquid Films under the Action of Capillary Forces. *J. Phys.: Condens. Matter* **1994**, *6* (A395).

(251) Petkov, P. V.; Danov, K. D.; Kralchevsky, P. A. Monolayers of Charged Particles in a Langmuir Trough: Could Particle Aggregation Increase the Surface Pressure? *J. Colloid Interface Sci.* **2016**, *462*, 223–234. https://doi.org/10.1016/j.jcis.2015.09.075.

(252) Danov, K. D.; Kralchevsky, P. A. Forces Acting on Dielectric Colloidal Spheres at a Water/Nonpolar-Fluid Interface in an External Electric Field. 1. Uncharged Particles. *J. Colloid Interface Sci.* **2013**, *405*, 278–290. https://doi.org/10.1016/j.jcis.2013.05.020.

(253) Kralchevsky, P. A.; Denkov, N. D. Capillary Forces and Structuring in Layers of Colloid Particles. *Curr. Opin. Colloid Interface Sci.* **2001**, *6* (4), 383–401. https://doi.org/10.1016/S1359-0294(01)00105-4.

(254) Kralchevsky, P. A.; Nagayama, K. Capillary Interactions between Particles Bound to Interfaces, Liquid Films and Biomembranes. *Adv. Colloid Interface Sci.* **2000**, *85* (2), 145–192. https://doi.org/10.1016/S0001-8686(99)00016-0.

(255) Lyklema, J.; van Leeuwen, H. P.; Minor, M. DLVO-Theory, a Dynamic Re-Interpretation. *Adv. Colloid Interface Sci.* **1999**, *83* (1–3), 33–69. https://doi.org/10.1016/S0001-8686(99)00011-1.

(256) Bhattacharjee, S.; Elimelech, M.; Borkovec, M. DLVO Interaction between Colloidal Particles: Beyond Derjaguin's Approximation. *Croatica Chemica Acta* **1998**, *71* (4), 883–903.

(257) Agmo Hernández, V. An Overview of Surface Forces and the DLVO Theory. *ChemTexts* **2023**, *9* (4), 1–16. https://doi.org/10.1007/s40828-023-00182-9.

(258) Pockels, A. Surface Tension. *Nature* **1891**, *43* (1115), 437–439. https://doi.org/10.1038/043437c0.

(259) Langmuir, I. The Constitution and Fundamental Properties of Solids and Liquids. II. Liquids. *J. Am. Chem. Soc.* **1917**, *39* (9), 1848–1906. https://doi.org/10.1021/ja02254a006.

(260) Blodgett, K. B. Monomolecular Films of Fatty Acids on Glass. *J. Am. Chem. Soc.* **1934**, *56* (2), 495. https://doi.org/10.1021/ja01317a513.

(261) Blodgett, K. B. Films Built by Depositing Successive Monomolecular Layers on a Solid Surface. *J. Am. Chem. Soc.* **1935**, *57* (6), 1007–1022. https://doi.org/10.1021/ja01309a011.

(262) Langmuir, I.; Schaefer, V. J. Activities of Urease and Pepsin Monolayers. *J. Am. Chem. Soc.* **1938**, *60* (6), 1351–1360. https://doi.org/10.1021/ja01273a023.

(263) Ariga, K.; Li, J.; Fei, J.; Ji, Q.; Hill, J. P. Nanoarchitectonics for Dynamic Functional Materials from Atomic-/Molecular-Level Manipulation to Macroscopic Action. *Advanced Materials* **2016**, *28* (6), 1251–1286. https://doi.org/10.1002/adma.201502545.

(264) Ariga, K. Chemistry of Materials Nanoarchitectonics for Two-Dimensional Films: Langmuir–Blodgett, Layer-by-Layer Assembly, and Newcomers. *Chemistry of Materials* **2023**, *35* (14), 5233–5254. https://doi.org/10.1021/acs.chemmater.3c01291.

(265) Ariga, K. Don't Forget Langmuir-Blodgett Films 2020: Interfacial Nanoarchitectonics with Molecules, Materials, and Living Objects. *Langmuir* **2020**, *36* (26), 7158–7180. https://doi.org/10.1021/acs.langmuir.0c01044.

(266) Dotor, L.; García-Pinilla, J. M.; Martín, S.; Cea, P. Langmuir and Langmuir–Blodgett Technologies as Nanoarchitectonic Tools for the Incorporation of Curcumin in Membrane Systems. *Nanoscale* **2023**, *15* (6), 2891–2903. https://doi.org/10.1039/D2NR06631A.

(267) Ariga, K. Langmuir–Blodgett Nanoarchitectonics, Out of the Box. *Acc. Mater. Res.* **2022**, *3* (4), 404–410. https://doi.org/10.1021/accountsmr.1c00240.

(268) Ariga, K. Thin Film Nanoarchitectonics via Langmuir–Blodgett and Layer-by-Layer Methods. In *Materials Nanoarchitectonics*; Elsevier, 2024; pp 241–254. https://doi.org/10.1016/B978-0-323-99472-9.00005-5.

(269) Tian, Y.; Li, X.; Bian, P.; Li, A.; Jiao, T. Application of Langmuir-Blodgett Films in Optoelectronic Sensing Devices: Nanoarchitectonics of Functional Interfaces and Advanced Usages. *J. Environ. Chem. Eng.* **2025**, *13* (6), 120234. https://doi.org/10.1016/j.jece.2025.120234.

(270) Pockels, A. On the Relative Contamination of the Water-Surface by Equal Quantities of Different Substances. *Nature* **1892**, *46* (1192), 418–419. https://doi.org/10.1038/046418e0.

(271) Pockels, A. Relations Between the Surface-Tension and Relative Contamination of Water Surfaces. *Nature* **1893**, *48* (1233), 152–154. https://doi.org/10.1038/048152a0.

(272) Pockels, A. On the Spreading of Oil upon Water. *Nature* **1894**, *50* (1288), 223–224. https://doi.org/10.1038/050223a0.

(273) Kraack, H.; Ocko, B. M.; Pershan, P. S.; Sloutskin, E.; Deutsch, M. Langmuir Films of Normal-Alkanes on the Surface of Liquid Mercury. *J. Chem. Phys.* **2003**, *119* (19), 10339–10349. https://doi.org/10.1063/1.1618211.

(274) Kent, M. S.; Majewski, J.; Smith, G. S.; Lee, L. T.; Satija, S. Tethered Chains in Poor Solvent Conditions: An Experimental Study Involving Langmuir Diblock Copolymer Monolayers. *J. Chem. Phys.* **1999**, *110* (7), 3553–3565. https://doi.org/10.1063/1.478223.

(275) Zasadzinski, J. A.; Viswanathan, R.; Madsen, L.; Garnaes, J.; Schwartz, D. K. Langmuir-Blodgett Films. *Science (1979).* **1994**, *263* (5154), 1726–1733. https://doi.org/10.1126/science.8134836.

(276) Kaganer, V. M.; Möhwald, H.; Dutta, P. Structure and Phase Transitions in Langmuir Monolayers. *Rev. Mod. Phys.* **1999**, *71* (3), 779–819. https://doi.org/10.1103/RevModPhys.71.779.

(277) Mampallil, D.; Eral, H. B. A Review on Suppression and Utilization of the Coffee-Ring Effect. *Adv. Colloid Interface Sci.* **2018**, *252*, 38–54. https://doi.org/10.1016/j.cis.2017.12.008.

(278) Oliveira, O. N.; Caseli, L.; Ariga, K. The Past and the Future of Langmuir and Langmuir-Blodgett Films. *Chem. Rev.* **2022**, *122* (6), 6459–6513. https://doi.org/10.1021/acs.chemrev.1c00754.

(279) Harkins, W. D.; Young, T. F.; Boyd, E. The Thermodynamics of Films: Energy and Entropy of Extension and Spreading of Insoluble Monolayers. *J. Chem. Phys.* **1940**, *8* (12), 954–965. https://doi.org/10.1063/1.1750610.

(280) Dervichian, D. G. Changes of Phase and Transformations of Higher Order in Monolayers. *J. Chem. Phys.* **1939**, *7* (10), 931–948. https://doi.org/10.1063/1.1750347.

(281) Davies, J. T.; Rideal, E. K. *Interfacian Phenomena*; Academic Press: London, 1961. https://doi.org/10.1002/ange.19650770625.

(282) Lucassen, J.; Van Den Tempel, M. Dynamic Measurements of Dilational Properties of a Liquid Interface. *Chem. Eng. Sci.* **1972**, *27* (6), 1283–1291. https://doi.org/10.1016/0009-2509(72)80104-0.

(283) Miller, R.; Ferri, J. K.; Javadi, A.; Krägel, J.; Mucic, N.; Wüstneck, R. Rheology of Interfacial Layers. *Colloid Polym. Sci.* **2010**, *288* (9), 937–950. https://doi.org/10.1007/s00396-010-2227-5.

(284) Lucero Caro, A.; Rodríguez Niño, M. R.; Rodríguez Patino, J. M. The Effect of PH on Surface Dilatational and Shear Properties of Phospholipid Monolayers. *Colloids Surf. A Physicochem. Eng. Asp.* **2008**, *327* (1–3), 79–89. https://doi.org/10.1016/j.colsurfa.2008.06.007.

(285) Oliveira, O. N.; Bonardi, C. The Surface Potential of Langmuir Monolayers Revisited. *Langmuir* **1997**, *13* (22), 5920–5924. https://doi.org/10.1021/la970272o.

(286) Hénon, S.; Meunier, J. Microscope at the Brewster Angle: Direct Observation of First-Order Phase Transitions in Monolayers. *Review of Scientific Instruments* **1991**, *62* (4), 936–939. https://doi.org/10.1063/1.1142032.

(287) Hönig, D.; Möbius, D. Direct Visualization of Monolayers at the Air-Water Interface by Brewster Angle Microscopy. *Journal of Physical Chemistry* **1991**, *95* (12), 4590–4592. https://doi.org/10.1021/j100165a003.

(288) Roldán-Carmona, C.; Giner-Casares, J. J.; Pérez-Morales, M.; Martín-Romero, M. T.; Camacho, L. Revisiting the Brewster Angle Microscopy: The Relevance of the Polar Headgroup. *Adv. Colloid Interface Sci.* **2012**, *173*, 12–22. https://doi.org/10.1016/j.cis.2012.02.002.

(289) Daear, W.; Mahadeo, M.; Prenner, E. J. Applications of Brewster Angle Microscopy from Biological Materials to Biological Systems. *Biochimica et Biophysica Acta (BBA) - Biomembranes* **2017**, *1859* (10), 1749–1766. https://doi.org/10.1016/j.bbamem.2017.06.016.

(290) Mendelsohn, R.; Mao, G.; Flach, C. R. Infrared Reflection–Absorption Spectroscopy: Principles and Applications to Lipid–Protein Interaction in Langmuir Films. *Biochimica et Biophysica Acta (BBA) - Biomembranes* **2010**, *1798* (4), 788–800. https://doi.org/10.1016/j.bbamem.2009.11.024.

(291) Cristofolini, L. Synchrotron X-Ray Techniques for the Investigation of Structures and Dynamics in Interfacial Systems. *Curr. Opin. Colloid Interface Sci.* **2014**, *19* (3), 228–241. https://doi.org/10.1016/j.cocis.2014.03.006.

(292) Caselli, L.; Nylander, T.; Malmsten, M. Neutron Reflectometry as a Powerful Tool to Elucidate Membrane Interactions of Drug Delivery Systems. *Adv. Colloid Interface Sci.* **2024**, *325*, 103120. https://doi.org/10.1016/j.cis.2024.103120.

(293) Teng, Y.; Pong, P. W. T. Magnetic Thermally Sensitive Interpenetrating Polymer Network (IPN) Nanogels: IPN-PNIPAm@Fe2O3-SiO2. *RSC Adv.* **2020**, *10* (63), 38287–38293. https://doi.org/10.1039/d0ra04696e.

(294) Lien, Y. H.; Wu, J. H.; Liao, J. W.; Wu, T. M. In Vitro Evaluation of the Thermosensitive and Magnetic Nanoparticles for the Controlled Drug Delivery of Vitamin D3. *Macromol. Res.* **2013**, *21* (5), 511–518. https://doi.org/10.1007/s13233-013-1047-0.

(295) Zhang, J.; Pelton, R.; Deng, Y. Temperature-Dependent Contact Angles of Water on Poly(N-Isopropylacrylamide) Gels. *Langmuir* **1995**, *11* (6), 2301–2302. https://doi.org/10.1021/la00006a071.

(296) Takei, Y. G.; Aoki, T.; Sanui, K.; Ogata, N.; Sakurai, Y.; Okano, T. Dynamic Contact Angle Measurement of Temperature-Responsive Surface Properties for Poly(N-Isopropylacrylamide) Grafted Surfaces. *Macromolecules* **1994**, *27* (21), 6163–6166. https://doi.org/10.1021/ma00099a035.

(297) Tucker, A. K.; Stevens, M. J. Study of the Polymer Length Dependence of the Single Chain Transition Temperature in Syndiotactic Poly(n -Isopropylacrylamide) Oligomers in Water. *Macromolecules* **2012**, *45* (16), 6697–6703. https://doi.org/10.1021/ma300729z.

(298) Shan, J.; Zhao, Y.; Granqvist, N.; Tenhu, H. Thermoresponsive Properties of N-Isopropylacrylamide Oligomer Brushes Grafted to Gold Nanoparticles: Effects of Molar Mass and Gold Core Size. *Macromolecules* **2009**, *42* (7), 2696–2701. https://doi.org/10.1021/ma802482e.

(299) Jones, S. T.; Walsh-Korb, Z.; Barrow, S. J.; Henderson, S. L.; Del Barrio, J.; Scherman, O. A. The Importance of Excess Poly(N-Isopropylacrylamide) for the Aggregation of Poly(N-Isopropylacrylamide)-Coated Gold Nanoparticles. *ACS Nano* **2016**, *10* (3), 3158–3165. https://doi.org/10.1021/acsnano.5b04083.

(300) Greenwood, N. N.; Earnshaw, A. *Chemistry of the Elements*, 2nd editio.; Butterworth-Heinemann: Oxford, 1997.

(301) Heinz, H.; Pramanik, C.; Heinz, O.; Ding, Y.; Mishra, R. K.; Marchon, D.; Flatt, R. J.; Estrela-Lopis, I.; Llop, J.; Moya, S.; Ziolo, R. F. Nanoparticle Decoration with Surfactants: Molecular Interactions, Assembly, and Applications. *Surf. Sci. Rep.* **2017**, *72* (1), 1–58. https://doi.org/10.1016/j.surfrep.2017.02.001.

(302) Paczesny, J.; Wolska-Pietkiewicz, M.; Binkiewicz, I.; Wadowska, M.; Wróbel, Z.; Matuła, K.; Nogala, W.; Lewiński, J.; Hołyst, R. Photoactive Langmuir–Blodgett, Freely Suspended and Free Standing Films of Carboxylate Ligand-Coated ZnO Nanocrystals. *ACS Appl. Mater. Interfaces* **2016**, *8* (21), 13532–13541. https://doi.org/10.1021/acsami.6b03579.

(303) Stefaniu, C.; Chanana, M.; Wang, D.; Novikov, D. V.; Brezesinski, G.; Möhwald, H. Biocompatible Magnetite Nanoparticles Trapped at the Air/Water Interface. *ChemPhysChem* **2010**, *11* (17), 3585–3588. https://doi.org/10.1002/cphc.201000783.

(304) Liu, M.; Wan, X.; Yang, M.; Wang, Z.; Bao, H.; Dai, B.; Liu, H.; Wang, S. Thermo-Responsive Jamming of Nanoparticle Dense Suspensions towards Macroscopic Liquid-Solid Switchable Materials. *Angew. Chem. Int. Ed.* **2021**. https://doi.org/10.1002/anie.202114602.

(305) Pathirana, S. T.; Barbaree, J.; Chin, B. A.; Hartell, M. G.; Neely, W. C.; Vodyanoy, V. Rapid and Sensitive Biosensor for Salmonella. *Biosens. Bioelectron.* **2000**, *15* (3–4), 135–141. https://doi.org/10.1016/S0956-5663(00)00067-1.

(306) Guzmán, E.; Martínez-Pedrero, F.; Calero, C.; Maestro, A.; Ortega, F.; Rubio, R. G. A Broad Perspective to Particle-Laden Fluid Interfaces Systems: From Chemically Homogeneous Particles to Active Colloids. *Adv. Colloid Interface Sci.* **2022**, *302*. https://doi.org/10.1016/j.cis.2022.102620.

(307) Shi, S.; Russell, T. P. Nanoparticle Assembly at Liquid–Liquid Interfaces: From the Nanoscale to Mesoscale. *Advanced Materials* **2018**, *30* (44), 1–22. https://doi.org/10.1002/adma.201800714.

(308) Aveyard, R.; Clint, J. H. Liquid Droplets and Solid Particles at Surfactant Solution Interfaces. *Journal of the Chemical Society, Faraday Transactions* **1995**, *91* (17), 2681–2697. https://doi.org/10.1039/FT9959102681.

(309) Vargaftik, N. B.; Volkov, B. N.; Voljak, L. D. International Tables of the Surface Tension of Water. *Journal of Physical and Chemical Reference Data*. 1983, pp 817–820. https://doi.org/10.1063/1.555688.

(310) Razavi, S.; Cao, K. D.; Lin, B.; Lee, K. Y. C.; Tu, R. S.; Kretzschmar, I. Collapse of Particle-Laden Interfaces under Compression: Buckling vs Particle Expulsion. *Langmuir* **2015**, *31* (28), 7764–7775. https://doi.org/10.1021/acs.langmuir.5b01652.

(311) Garbin, V. Collapse Mechanisms and Extreme Deformation of Particle-Laden Interfaces. *Curr. Opin. Colloid Interface Sci.* **2019**, *39*, 202–211. https://doi.org/10.1016/j.cocis.2019.02.007.

(312) Nakahara, H.; Lee, S.; Sugihara, G.; Chang, C.-H.; Shibata, O. Langmuir Monolayer of Artificial Pulmonary Surfactant Mixtures with an Amphiphilic Peptide at the Air/Water Interface: Comparison of New Preparations with Surfacten (Surfactant TA). *Langmuir* **2008**, *24* (7), 3370–3379. https://doi.org/10.1021/la703180x.

(313) Morioka, T.; Kawaguchi, M. Surface Dilational Moduli of Polymer and Blended Polymer Monolayers Spread at Air-Water Interfaces. *Adv. Colloid Interface Sci.* **2014**, *214*, 1–16. https://doi.org/10.1016/j.cis.2014.10.003.

(314) Hilles, H. M.; Ortega, F.; Rubio, R. G.; Monroy, F. Long-Time Relaxation Dynamics of Langmuir Films of a Glass-Forming Polymer: Evidence of Glasslike Dynamics in Two Dimensions. *Phys. Rev. Lett.* **2004**, *92* (25 I), 1–4. https://doi.org/10.1103/PhysRevLett.92.255503.

(315) Zang, D. Y.; Rio, E.; Delon, G.; Langevin, D.; Wei, B.; Binks, B. P. Influence of the Contact Angle of Silica Nanoparticles at the Air–Water Interface on the Mechanical Properties of the Layers Composed of These Particles. *Mol. Phys.* **2011**, *109* (7–10), 1057–1066. https://doi.org/10.1080/00268976.2010.542778.

(316) Maestro, A.; Guzmán, E. Colloids at Fluid Interfaces. *Processes* **2019**, *7* (12), 1–19. https://doi.org/10.3390/PR7120942.

(317) Yang, M.; Liu, C.; Zhao, K. Concentration Dependent Phase Behavior and Collapse Dynamics of PNIPAM Microgel by Dielectric Relaxation. *Physical Chemistry Chemical Physics* **2017**, *19* (23), 15433–15443. https://doi.org/10.1039/C7CP01378G.

(318) Reynaert, S.; Moldenaers, P.; Vermant, J. Control over Colloidal Aggregation in Monolayers of Latex Particles at the Oil-Water Interface. *Langmuir* **2006**, *22* (11), 4936–4945. https://doi.org/10.1021/la060052n.

(319) Kumar, S.; Saha, D.; Kohlbrecher, J.; Aswal, V. K. Interplay of Interactions for Different Pathways of the Fractal Aggregation of Nanoparticles. *Chem. Phys. Lett.* **2022**, *803*, 139808. https://doi.org/10.1016/j.cplett.2022.139808.

(320) Flores-Tandy, L. M.; García-Monjaraz, A. V.; van Nierop, E. A.; Vázquez-Martínez, E. A.; Ruiz-Garcia, J.; Mejía-Rosales, S. Fractal Aggregates Formed by Ellipsoidal Colloidal Particles at the Air/Water Interface. *Colloids Surf. A Physicochem. Eng. Asp.* **2020**, *590*, 124477. https://doi.org/10.1016/j.colsurfa.2020.124477.

(321) Witten, T. A.; Sander, L. M. Diffusion-Limited Aggregation. *Phys. Rev. B* **1983**, *27* (9), 5686–5697. https://doi.org/10.1103/PhysRevB.27.5686.

(322) Meakin, P. Diffusion-Limited Aggregation in Three Dimensions: Results from a New Cluster-Cluster Aggregation Model. *J. Colloid Interface Sci.* **1984**, *102* (2), 491–504. https://doi.org/10.1016/0021-9797(84)90252-2.

(323) Jungblut, S.; Joswig, J.-O.; Eychmüller, A. Diffusion- and Reaction-Limited Cluster Aggregation Revisited. *Physical Chemistry Chemical Physics* **2019**, *21* (10), 5723–5729. https://doi.org/10.1039/C9CP00549H.

(324) Polimeno, M.; Kim, C.; Blanchette, F. Toward a Realistic Model of Diffusion-Limited Aggregation: Rotation, Size-Dependent Diffusivities, and Settling. *ACS Omega* **2022**, *7* (45), 40826–40835. https://doi.org/10.1021/acsomega.2c03547.

(325) Antonsson, J.; Hamngren Blomqvist, C.; Olsson, E.; Gebäck, T.; Särkkä, A. Modeling Colloidal Particle Aggregation Using Cluster Aggregation with Multiple Particle Interactions. *J. Phys. Chem. B* **2024**, *128* (18), 4513–4524. https://doi.org/10.1021/acs.jpcb.3c07992.

(326) Freitag, R.; Garret-Flaudy, F. Salt Effects on the Thermoprecipitation of Poly-(N -Isopropylacrylamide) Oligomers from Aqueous Solution. *Langmuir* **2002**, *18* (9), 3434–3440. https://doi.org/10.1021/la0106440.

(327) Humphreys, B. A.; Wanless, E. J.; Webber, G. B. Effect of Ionic Strength and Salt Identity on Poly(N-Isopropylacrylamide) Brush Modified Colloidal Silica Particles. *J. Colloid Interface Sci.* **2018**, *516*, 153–161. https://doi.org/10.1016/j.jcis.2018.01.058.

(328) von Smoluchowski, M. Contribution à La Théorie de l'endosmose Électrique et de Quelques Phénomènes Corrélatifs. *Bulletin International de L'Académie des Sciences de Cracovie* **1903**, *8*, 182–200.

(329) von Smoluchowski, M. Przyczynek Do Teorji Endosmozy Elektrycznej i Kilku Pokrewnych Zjawisk. *Rozprawy wydziału matematyczno-przyrodniczego Akademji Umiejętności w Krakowie* **1903**, 110–127.

(330) French, R. A.; Jacobson, A. R.; Kim, B.; Isley, S. L.; Penn, R. L.; Baveye, P. C. Influence of Ionic Strength, PH, and Cation Valence on Aggregation Kinetics of Titanium Dioxide Nanoparticles. *Environ. Sci. Technol.* **2009**, *43* (5), 1354–1359. https://doi.org/10.1021/es802628n.

(331) Winkler, K.; Paszewski, M.; Kalwarczyk, T.; Kalwarczyk, E.; Wojciechowski, T.; Gorecka, E.; Pociecha, D.; Holyst, R.; Fialkowski, M. Ionic Strength-Controlled Deposition of Charged Nanoparticles on a Solid Substrate. *The Journal of Physical Chemistry C* **2011**, *115* (39), 19096–19103. https://doi.org/10.1021/jp206704s.

(332) Alipour, A.; Abedi, M.; Habibi, M. Controlling Salt Crystallization in Evaporating Thin Films of Colloidal Liquids. *Colloids Surf. A Physicochem. Eng. Asp.* **2022**, *636*, 128094. https://doi.org/10.1016/j.colsurfa.2021.128094.

(333) Dai, Y.; Lin, B.; Meron, M.; Kim, K.; Leahy, B.; Witten, T. A.; Shpyrko, O. G. Synchrotron X-Ray Studies of Rapidly Evolving Morphology of Self-Assembled Nanoparticle Films under Lateral Compression. *Langmuir* **2013**, *29* (46), 14050–14056. https://doi.org/10.1021/la403252d.

(334) Flury, M.; Aramrak, S. Role of Air-water Interfaces in Colloid Transport in Porous Media: A Review. *Water Resour. Res.* **2017**, *53* (7), 5247–5275. https://doi.org/10.1002/2017WR020597.

(335) Kang, D. W.; Lim, J. H.; Park, B. J. Heterogeneous Interface Adsorption of Colloidal Particles. *Soft Matter* **2017**, *13* (36), 6234–6242. https://doi.org/10.1039/C7SM00618G.

(336) Kang, D. W.; Park, B. G.; Choi, K. H.; Lim, J. H.; Lee, S. J.; Park, B. J. Geometric Effects of Colloidal Particles on Stochastic Interface Adsorption. *Langmuir* **2018**, *34* (30), 8839–8847. https://doi.org/10.1021/acs.langmuir.8b01124.

(337) Wei, W. Hofmeister Effects Shine in Nanoscience. *Advanced Science* **2023**, *10* (22), 1–18. https://doi.org/10.1002/advs.202302057.

(338) Heyda, J.; Dzubiella, J. Thermodynamic Description of Hofmeister Effects on the LCST of Thermosensitive Polymers. *Journal of Physical Chemistry B* **2014**, *118* (37), 10979–10988. https://doi.org/10.1021/jp5041635.

(339) Mansfield, E. D. H.; Filippov, S. K.; de la Rosa, V. R.; Cook, M. T.; Grillo, I.; Hoogenboom, R.; Williams, A. C.; Khutoryanskiy, V. V. Understanding the Temperature Induced Aggregation of Silica Nanoparticles Decorated with Temperature-Responsive Polymers: Can a Small Step in the Chemical Structure Make a Giant Leap for a Phase Transition? *J. Colloid Interface Sci.* **2021**, *590* (January), 249–259. https://doi.org/10.1016/j.jcis.2021.01.044.

(340) Yusa, S. I.; Fukuda, K.; Yamamoto, T.; Iwasaki, Y.; Watanabe, A.; Akiyoshi, K.; Morishima, Y. Salt Effect on the Heat-Induced Association Behavior of Gold Nanoparticles Coated with Poly(N-Isopropylacrylamide) Prepared via Reversible Addition-Fragmentation Chain Transfer (RAFT) Radical Polymerization. *Langmuir* **2007**, *23* (26), 12842–12848. https://doi.org/10.1021/la702741q.

(341) Weiss, L. B.; Dahirel, V.; Marry, V.; Jardat, M. Computation of the Hydrodynamic Radius of Charged Nanoparticles from Nonequilibrium Molecular Dynamics. *Journal of Physical Chemistry B* **2018**, *122* (22), 5940–5950. https://doi.org/10.1021/acs.jpcb.8b01153.

(342) Gehring, T.; Fischer, T. M. Diffusion of Nanoparticles at an Air/Water Interface Is Not Invariant under a Reversal of the Particle Charge. *The Journal of Physical Chemistry C* **2011**, *115* (48), 23677–23681. https://doi.org/10.1021/jp2061738.

(343) Richter, Ł.; Żuk, P. J.; Szymczak, P.; Paczesny, J.; Bąk, K. M.; Szymborski, T.; Garstecki, P.; Stone, H. A.; Hołyst, R.; Drummond, C. Ions in an AC Electric Field: Strong Long-Range Repulsion between Oppositely Charged Surfaces. *Phys. Rev. Lett.* **2020**, *125* (5), 056001. https://doi.org/10.1103/PhysRevLett.125.056001.

(344) Stamou, D.; Duschl, C.; Johannsmann, D. Long-Range Attraction between Colloidal Spheres at the Air-Water Interface: The Consequence of an Irregular Meniscus. *Phys. Rev. E* **2000**, *62* (4), 5263–5272. https://doi.org/10.1103/PhysRevE.62.5263.

(345) Aveyard, R.; Clint, J. H. Particle Wettability and Line Tension. *Journal of the Chemical Society - Faraday Transactions* **1996**, *92* (1), 85–89. https://doi.org/10.1039/ft9969200085.

(346) Ohara, P. C.; Leff, D. V; Heath, J. R.; Gelbart, W. M. Crystallization of Opals from Polydisperse Nanoparticles. *Phys. Rev. Lett.* **1995**, *75* (19), 3466–3469. https://doi.org/10.1103/PhysRevLett.75.3466.

(347) Bonn, D.; Otwinowski, J.; Sacanna, S.; Guo, H.; Wegdam, G.; Schall, P. Direct Observation of Colloidal Aggregation by Critical Casimir Forces. *Phys. Rev. Lett.* **2009**, *103* (15), 1–4. https://doi.org/10.1103/PhysRevLett.103.156101.

(348) Boniello, G.; Blanc, C.; Fedorenko, D.; Medfai, M.; Mbarek, N. Ben; In, M.; Gross, M.; Stocco, A.; Nobili, M. Brownian Diffusion of a Partially Wetted Colloid. *Nat. Mater.* **2015**, *14* (9), 908–911. https://doi.org/10.1038/nmat4348.

(349) Sparavigna, A. C. Raman Spectroscopy of the Iron Oxides in the Form of Minerals, Particles and Nanoparticles. September 12, 2023. https://doi.org/10.26434/chemrxiv-2023-22kh4-v2.

(350) Alessi, A.; Agnello, S.; Buscarino, G.; Gelardi, F. M. Structural Properties of Core and Surface of Silica Nanoparticles Investigated by Raman Spectroscopy. *Journal of Raman Spectroscopy* **2013**, *44* (6), 810–816. https://doi.org/10.1002/jrs.4292.

(351) Dybal, J.; Trchová, M.; Schmidt, P. The Role of Water in Structural Changes of Poly(N-Isopropylacrylamide) and Poly(N-Isopropylmethacrylamide) Studied by FTIR, Raman

Spectroscopy and Quantum Chemical Calculations. *Vib. Spectrosc.* **2009**, *51* (1), 44–51. https://doi.org/10.1016/j.vibspec.2008.10.003.

(352) Horiba. *Raman Spectroscopy for Analysis and Monitoring*. https://static.horiba.com/fileadmin/Horiba/Technology/Measurement_Techniques/Molecular_Spectroscopy/Raman_Spectroscopy/Raman_Academy/Raman_Tutorial/Raman_bands.pdf?utm_source=uhw&utm_medium=301&utm_campaign=uhw-redirect (accessed 2025-06-18).

(353) Hilles, H.; Monroy, F.; Bonales, L. J.; Ortega, F.; Rubio, R. G. Fourier-Transform Rheology of Polymer Langmuir Monolayers: Analysis of the Non-Linear and Plastic Behaviors. *Adv. Colloid Interface Sci.* **2006**, *122* (1–3), 67–77. https://doi.org/10.1016/j.cis.2006.06.013.

(354) Guzmán, E.; Liggieri, L.; Santini, E.; Ferrari, M.; Ravera, F. DPPC-DOPC Langmuir Monolayers Modified by Hydrophilic Silica Nanoparticles: Phase Behaviour, Structure and Rheology. *Colloids Surf. A Physicochem. Eng. Asp.* **2012**, *413*, 174–183. https://doi.org/10.1016/j.colsurfa.2011.12.059.

(355) Guzmán, E.; Liggieri, L.; Santini, E.; Ferrari, M.; Ravera, F. Effect of Hydrophilic and Hydrophobic Nanoparticles on the Surface Pressure Response of DPPC Monolayers. *Journal of Physical Chemistry C* **2011**, *115* (44), 21715–21722. https://doi.org/10.1021/jp207713x.